NASA TECHNICAL MEMORANDUM

NASA TM X-1758

NASA TM X-1758

WIND-TUNNEL DATA FROM A 0.16-SCALE V/STOL MODEL WITH DIRECT-LIFT AND LIFT-CRUISE JETS

by Matthew M. Winston

Langley Research Center

Langley Station, Hampton, Va.

NATIONAL AERONAUTICS AND SPACE ADMINISTRATION • WASHINGTON, D. C. • MARCH 1969

NASA TM X-1758

WIND-TUNNEL DATA FROM A 0.16-SCALE V/STOL MODEL WITH DIRECT-LIFT AND LIFT-CRUISE JETS

By Matthew M. Winston

Langley Research Center
Langley Station, Hampton, Va.

NATIONAL AERONAUTICS AND SPACE ADMINISTRATION

For sale by the Clearinghouse for Federal Scientific and Technical Information
Springfield, Virginia 22151 – CFSTI price $3.00

WIND-TUNNEL DATA FROM A 0.16-SCALE V/STOL MODEL WITH DIRECT-LIFT AND LIFT-CRUISE JETS

By Matthew M. Winston
Langley Research Center

SUMMARY

The investigation was conducted on a 0.16-scale V/STOL model in the 17-foot (5.18-meter) test section of the Langley 300-mph 7- by 10-foot tunnel. Six cold-air ejectors were used to simulate four direct-lift and two lift-cruise jet engines. Longitudinal and lateral-directional aerodynamic characteristics were investigated for various model configurations, forward speeds, and power conditions in the transition and cruise flight ranges. In addition to control-effectiveness studies, the effects of power variations for different lift-nozzle settings and the effects of height above the ground were investigated. The data are presented without analysis.

INTRODUCTION

The National Aeronautics and Space Administration is actively engaged in the study of aircraft having vertical and short take-off and landing (V/STOL) capability. One of the primary areas of the NASA support to the aircraft industry and military services is the provision of wind-tunnel studies of specific V/STOL aircraft configurations prior to and during the developmental stages. References 1 to 3, for example, report studies of a propeller-driven V/STOL configuration. Recently, increased effort has been focused on aircraft employing jet engines either for lift augmentation or direct lift. (See, for example, refs. 4 and 5.)

The present investigation was undertaken to provide data from a model of a jet V/STOL research airplane which employs four direct-lift engines and two lift-cruise engines. Longitudinal and lateral-directional aerodynamic and control characteristics and jet interference effects were investigated for various power conditions and airspeeds simulating transition and cruise flight. These data are presented herein without analysis.

SYMBOLS

The data are presented in the stability-axis system with moments taken about the moment center shown in figure 1. Physical quantities defined in this section are given both in the U.S. Customary Units and in the International System of Units (SI). Factors relating the two systems are given in reference 6.

b wing span, feet (meters)

C_D drag coefficient, $\frac{\text{Drag}}{qS}$

C_L lift coefficient, $\frac{\text{Lift}}{qS}$

C_l rolling-moment coefficient, $\frac{\text{Rolling moment}}{qSb}$

C_m pitching-moment coefficient, $\frac{\text{Pitching moment}}{qS\bar{c}}$

C_n yawing-moment coefficient, $\frac{\text{Yawing moment}}{qSb}$

C_T thrust coefficient, $\frac{\text{Thrust}}{qS}$

C_Y side-force coefficient, $\frac{\text{Side force}}{qS}$

$\bar{c}$ wing mean aerodynamic chord, feet (meters)

D drag, pounds (newtons)

ΔD drag increment due to jet interference, pounds (newtons)

d effective diameter, diameter of a circle having same area as total cross-sectional area of all operating nozzles of a multijet configuration, feet (meters)

h height of model center of gravity above ground plane, feet (meters)

i_t tail incidence angle, positive when leading edge up, degrees

L lift, pounds (newtons)

ΔL lift increment due to jet interference, pounds (newtons)

M	pitching moment, foot-pounds (meter-newtons)
ΔM	pitching-moment increment due to jet interference, foot-pounds (meter-newtons)
q	free-stream dynamic pressure, $\frac{1}{2}\rho_\infty V_\infty^2$, pounds/foot^2 (newtons/meter^2)
S	wing area, feet^2 (meters^2)
T	thrust, pounds (newtons)
V	velocity, feet/second (meters/second)
α	angle of attack, degrees
β	angle of sideslip, degrees
δ	deflection of control surface or nozzle, degrees
ρ	mass density of air, slugs/foot^3 (kilograms/meter^3)

Subscripts:

e	elevator
f	flap
j	jet
n	exit nozzle
r	rudder
∞	free stream

MODEL, APPARATUS, AND INSTRUMENTATION

The model used in this investigation was a 0.16-scale model of a jet V/STOL research airplane powered by four direct-lift and two lift-cruise engines. Sketches and geometric characteristics of the model are presented in figure 1, and photographs of the

model installed in the 17-foot (5.18-meter) test section of the Langley 300-mph 7- by 10-foot tunnel are shown in figure 2. The fuselage is an aluminum structure covered with fiber glass. The solid aluminum wing incorporates single-slotted flaps which extend from 35 percent to 78 percent of the wing semispan. Flap chord is 30 percent of the wing chord. The flaps can be set at either 0° or 40° deflection with respect to the wing-chord line. The horizontal and vertical tails are also made of aluminum. Horizontal-tail incidence is manually adjustable from -10° to 15° in 5° increments. The full-span elevator is manually adjustable from -30° to 30° in 10° increments, and the rudder can be set from -10° to 20° in 10° increments. Boundary-layer transition was fixed on the wing, horizontal tail, and vertical tail by strips of No. 70 carborundum grit at 0.10 local chord on these surfaces.

The model was powered by six cold-air ejectors, four ejectors simulating direct-lift engines and two ejectors simulating lift-cruise engines. A complete description of an ejector similar to those used on this model is given in reference 7. Compressed air was fed through the model support sting to a plenum chamber within the model and was distributed to each ejector from a plenum manifold. Secondary air from the free stream was entrained through the model inlets (on the upper surface of the fuselage and in the nacelles) and was ducted to the ejector faces. The combined primary and secondary air passing through the ejectors was then ducted through the exit nozzles and passed to the free stream.

The forward, center, and aft pairs of exit nozzles were variably inclined in the longitudinal plane, so that the resultant of the thrust vectors passed through a common point at an inclination 10° forward of the vertical axis. On the full-scale airplane, this arrangement provides a basic hovering attitude of 10° (nose up). This nozzle configuration is designated herein as $\delta_n = 0^{\circ}$. The nozzle pairs could also be deflected to two other positions which rotated the resultant thrust vector 10° farther forward of the basic setting to a 20° total inclination or 10° aft of the basic setting to a 0° inclination; these deflections are designated as $\delta_n = 10^{\circ}$ and $\delta_n = -10^{\circ}$, respectively. All nozzles were inclined 10° away from the plane of symmetry.

The model was mounted on a six-component strain-gage balance and was supported on a sting which contained an internal air-supply line to power the ejector units. The sting was supported by a telescoping strut, so that the model could be driven through a range of pitch and yaw angles and heights. For the tests in ground effect, the telescoping strut permitted operation of the model at various heights above the variable-speed ground plane described in reference 8.

Forces and moments were measured with the six-component balance, pitch angles were measured with an electronic gravity-sensing device, and the sideslip angles were measured with a calibrated gearing arrangement on the support drive mechanism.

Ejector-operating variables, such as pressures and mass flows, were measured with standard types of pressure transducers and flowmeters.

TESTS AND CORRECTIONS

The model was investigated in the 17-foot (5.18-meter) test section of the Langley 300-mph 7- by 10-foot tunnel. The tests were generally conducted at nominal free-stream dynamic pressures of 2.0, 6.5, and 11.0 lb/ft^2 (95.76, 311.22, and 526.68 N/m^2). Other test variables were angles of attack and sideslip, engine thrust, and height above the ground. Model variables were control-surface deflections and exit-nozzle settings. The various thrust levels were obtained by setting the primary air-supply pressure at the entrance to the support sting in accordance with a previously determined relationship between sting pressure and model thrust.

The investigation focused primarily on the model aerodynamic characteristics for simulated transition between vertical and cruise flight. The low-speed portion of the transition was simulated with the six ejector nozzles thrusting vertically as direct-lift engines, and the high-speed portion was simulated with four nozzles thrusting vertically and two nozzles thrusting longitudinally. All transition data (out of ground effect) were obtained at a flap setting of 40° with the nozzle doors on the underside of the fuselage open and the landing gear removed. During tests in ground effect over the moving ground plane, the landing gear was installed.

In addition, a limited amount of investigation was conducted with the model in the cruise configuration. During these tests, flap settings of both 0° and 40° were used, the exit-nozzle doors were closed, and the landing gear was removed. Power for this configuration was supplied by the two nacelle-mounted ejectors thrusting longitudinally.

A test run consisted of a variation in either angle of attack, angle of sideslip, thrust, or dynamic pressure with all other conditions fixed. At each test point during a given run, electrical signals from the six-component balance, pitch-angle sensor, pressure transducers, and fixed tunnel instrumentation were fed into a digital readout and recording system. Other variables, such as sideslip angle and model height, were "hand-fed" into the recording system. The data have been corrected for deadweight tares, for the loads exerted on the balance by the air supply-line installation, and for the effects of varying air pressure on the balance. No corrections to the data have been made to account for the wind-tunnel wall effects, since these effects are believed to be small for a model of this size in the 17-foot (5.18-meter) test section. (See ref. 9.)

PRESENTATION OF DATA

The data from this investigation are presented in two major groups. The longitudinal aerodynamic characteristics over a range of angles of attack and effective velocity ratios are presented first, followed by the longitudinal and lateral-directional aerodynamic characteristics in sideslip. Within these two groups, the data are presented according to the following flight modes:

1. Cruise mode
2. Transition with six nozzles in lift mode
3. Transition with four nozzles in lift mode and two nozzles in cruise mode

Longitudinal Aerodynamic Characteristics

Cruise.- Cruise characteristics with and without power are given in figures 3 and 4. Data for flap deflections of 0° and 40° are included. The gross thrust components have been removed from the data given in figure 4; however, the data contain both the jet exit interference effects and the effects of inlet mass flow. These data are presented in conventional coefficient form.

Transition with six lift nozzles.- The investigation of the model in transition with six lift nozzles operating included studies of horizontal-tail, elevator, and exit-nozzle effectiveness at various thrust coefficients. Where thrust coefficients are compared, the data are also identified by the effective velocity ratio $\sqrt{\rho_{\infty}V_{\infty}^2/\rho_j V_j^2}$. The relationship between the thrust coefficient and the effective velocity ratio is

$$\sqrt{\frac{\rho_{\infty}V_{\infty}^2}{\rho_j V_j^2}} = \sqrt{\frac{2(\text{Nozzle exit area})}{C_T S}}$$

A plot showing this relationship for the model with six nozzles operating in the lift mode is presented in figure 5.

The effects of thrust coefficient and horizontal-tail incidence at the three exit-nozzle settings are shown in figures 6 and 7, respectively. The effects of elevator deflection at three thrust coefficients are shown in figure 8. The longitudinal aerodynamic characteristics over a range of effective velocity ratios for a small portion of the transition range near hover at three angles of attack and the three exit-nozzle settings are shown in figure 9. These data are presented as forces divided by the thrust or as moments divided by the product of thrust and wing mean aerodynamic chord.

Jet interference effects are given in figure 10. The ratios of the interference increment to the thrust were computed from the following equations:

$$\frac{\Delta L}{T} = \frac{L_{measured}}{T} - \frac{L'}{T} - \frac{C_{L,\,power\text{-}off}}{C_T}$$

$$\frac{\Delta D}{T} = \frac{D_{measured}}{T} - \frac{D'}{T} - \frac{C_{D,\,power\text{-}off}}{C_T}$$

$$\frac{\Delta M}{Td} = \frac{M_{measured}}{Td} - \frac{M'}{Td} - \frac{C_{m,\,power\text{-}off}}{C_T}\frac{\bar{c}}{d}$$

where the prime indicates a direct force or moment due to thrust. These increments do not account for the effects of inlet mass flow on the forces and moments. An estimate of the relative magnitudes of these effects for a similar model may be obtained from reference 5.

Transition with four lift and two cruise nozzles.- The longitudinal aerodynamic characteristics for the configuration with four lift and two cruise nozzles are presented in figures 11, 12, and 13. The effects of thrust coefficient at two nozzle settings are shown in figure 11, the longitudinal aerodynamic characteristics over a range of effective velocity ratios at an angle of attack of 0^o are given in figure 12, and the effects of jet interference are shown in figure 13. The range of effective velocity ratios covered in figure 12 is roughly three times as great as that covered in figure 9 for the six nozzles in the lift mode. The thrust coefficients, effective velocity ratios, and interference increments for this flight mode were obtained in the same manner as those for the six nozzles in the lift mode, even though the thrust of the four lift nozzles was oriented approximately at right angles to the thrust of the two cruise nozzles.

Aerodynamic Characteristics in Sideslip

Cruise.- The power-off lateral-directional and longitudinal aerodynamic characteristics of the cruise configuration at an angle of attack of 0^o are presented in figures 14 and 15 in conventional coefficient form as a function of sideslip angle. The effects of flap deflection with and without the empennage are shown in figure 14, and the rudder effectiveness is shown in figure 15.

Transition with six lift nozzles.- The aerodynamic characteristics in sideslip at an angle of attack of 0^o for the transition with six lift nozzles are given in figures 16 to 19. The lateral-directional data are given in coefficient form, and the longitudinal data are presented as force-to-thrust ratios. The effects of the empennage for a fixed nozzle setting are shown in figure 16, and the effects of thrust coefficient for a fixed nozzle setting are shown in figure 17. The effects of nozzle setting for three values of thrust coefficient are illustrated in figure 18. Data for various model heights above the

ground (in ground effect) are given in figure 19 for three values of thrust coefficient over a range of sideslip angles.

Transition with four lift and two cruise nozzles.- The aerodynamic characteristics in sideslip at an angle of attack of 0^{o} for the configuration with four lift and two cruise nozzles are given in figures 20 and 21. The effects of nozzle setting at three values of thrust coefficient are shown in figure 20, and the effects of height above the ground (in ground effect) for two nozzle settings are illustrated in figure 21.

Langley Research Center,
National Aeronautics and Space Administration,
Langley Station, Hampton, Va., January 10, 1969,
721-01-00-39-23.

REFERENCES

1. Goodson, Kenneth W.: Longitudinal Aerodynamic Characteristics of a Flapped Tilt-Wing Four-Propeller V/STOL Transport Model. NASA TN D-3217, 1966.

2. Goodson, Kenneth W.: Ground Effects on a Four-Propeller Tilt-Wing Configuration Over a Fixed and a Moving Ground Plane. NASA TN D-3938, 1967.

3. Goodson, Kenneth W.: Effect of Ground Proximity on the Longitudinal, Lateral, and Control Aerodynamic Characteristics of a Tilt-Wing Four-Propeller V/STOL Model. NASA TN D-4237, 1967.

4. Vogler, Raymond D.: Investigation Over Moving Ground Plane of a Transport Airplane Model Using Blowing Over Flaps for Boundary-Layer Control. NASA TN D-4083, 1967.

5. Margason, Richard J.; and Gentry, Garl L., Jr.: Aerodynamic Characteristics of a Five-Jet VTOL Configuration in the Transition Speed Range. NASA TN D-4812, 1968.

6. Mechtly, E. A.: The International System of Units – Physical Constants and Conversion Factors. NASA SP-7012, 1964.

7. Margason, Richard J.; and Gentry, Garl L.: Static Calibration of an Ejector Unit for Simulation of Jet Engines in Small-Scale Wind-Tunnel Models. NASA TN D-3867, 1967.

8. Turner, Thomas R.: A Moving-Belt Ground Plane for Wind-Tunnel Ground Simulation and Results for Two Jet-Flap Configurations. NASA TN D-4228, 1967.

9. Heyson, Harry H.: Linearized Theory of Wind-Tunnel Jet-Boundary Corrections and Ground Effect for VTOL-STOL Aircraft. NASA TR R-124, 1962.

GEOMETRIC CHARACTERISTICS

	Wing	Horizontal tail	Vertical tail
Area	2.67 ft^2 (.25 m^2)	.68 ft^2 (.06 m^2)	.70 ft^2 (.07 m^2)
Span	48.00 (121.92)	20.48 (52.02)	11.68 (29.67)
Root chord	11.52 (29.26)	6.80 (17.27)	11.44 (29.06)
Tip chord	4.48 (11.38)	2.72 (6.91)	5.90 (14.99)
Mean aerodynamic chord	8.52 (21.64)	5.05 (12.83)	8.96 (22.76)
Aspect ratio	5.90	4.30	1.35
Taper ratio	.39	.40	.52
Sweep (.25 chord line)	4.18°	12.37°	32.13°
Airfoil section		NACA 0010 (modified)	NACA 64A012
Root	NACA 64A012		
Tip	NACA 64A212		
Tail length		30.82 (78.28)	25.10 (63.75)

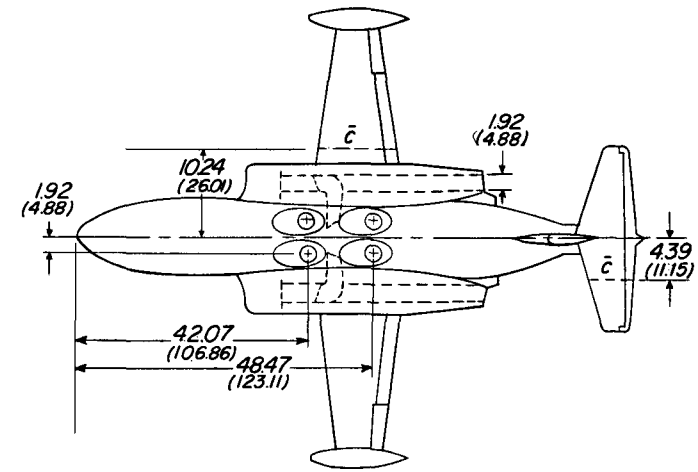

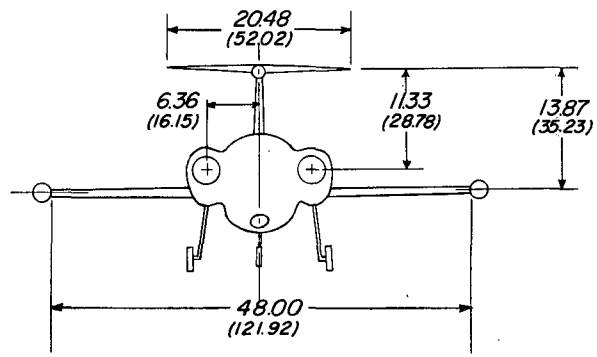

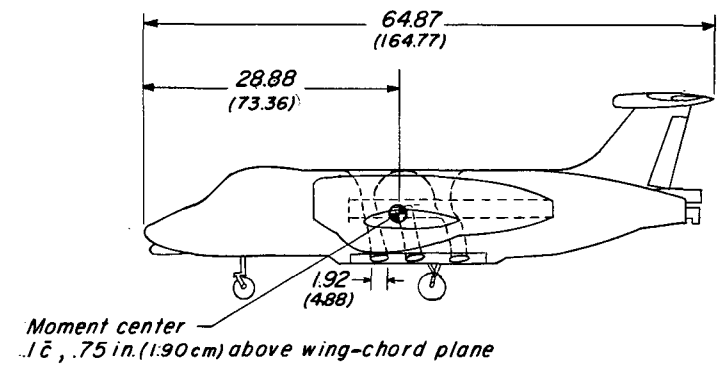

Figure 1.- Model principal dimensions and geometric characteristics. All dimensions are in inches (centimeters) unless otherwise specified.

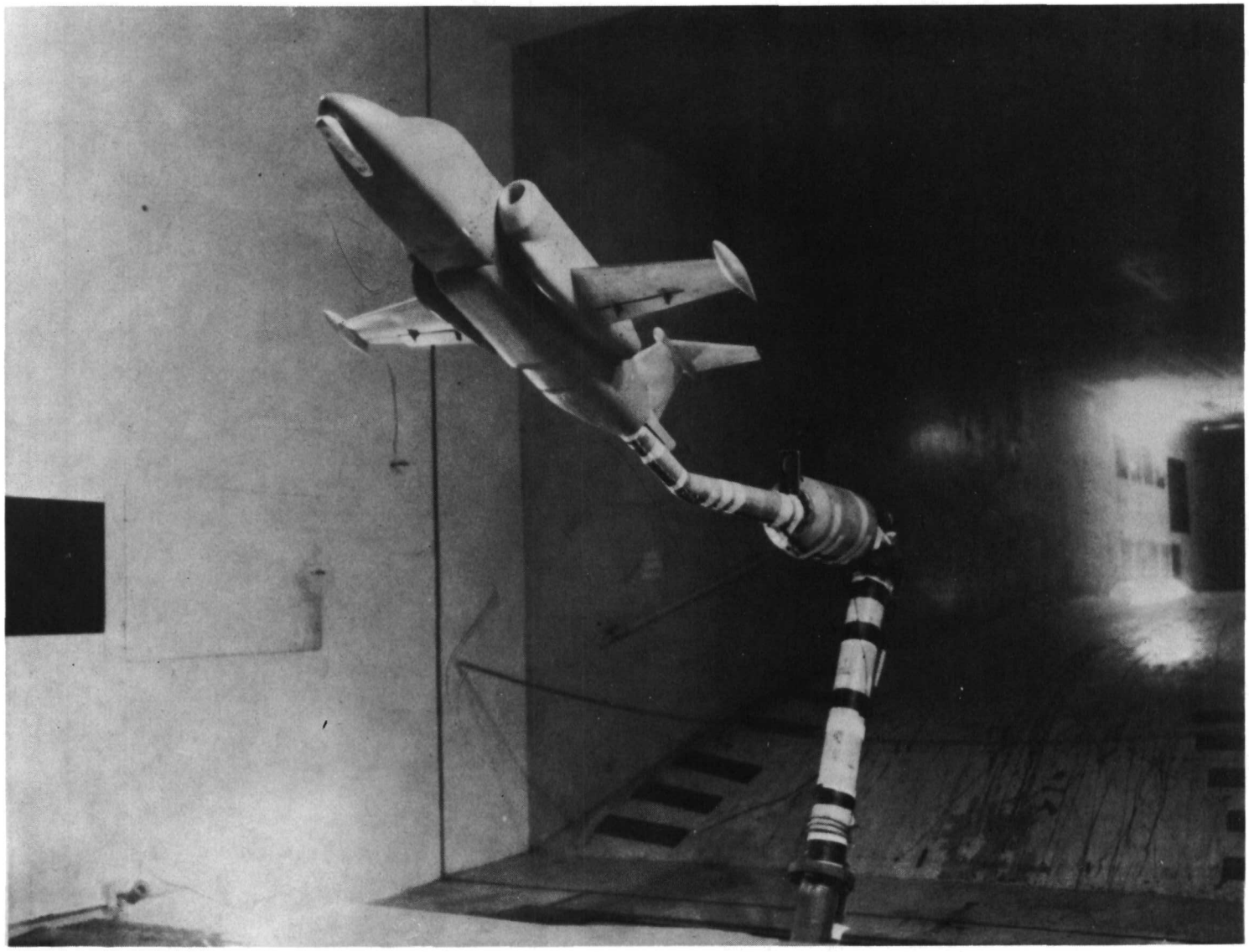

(a) Cruise configuration. L-69-1201

Figure 2. Photographs of the model in the 17-foot (5.18-meter) test section of the Langley 300-mph 7- by 10-foot tunnel.

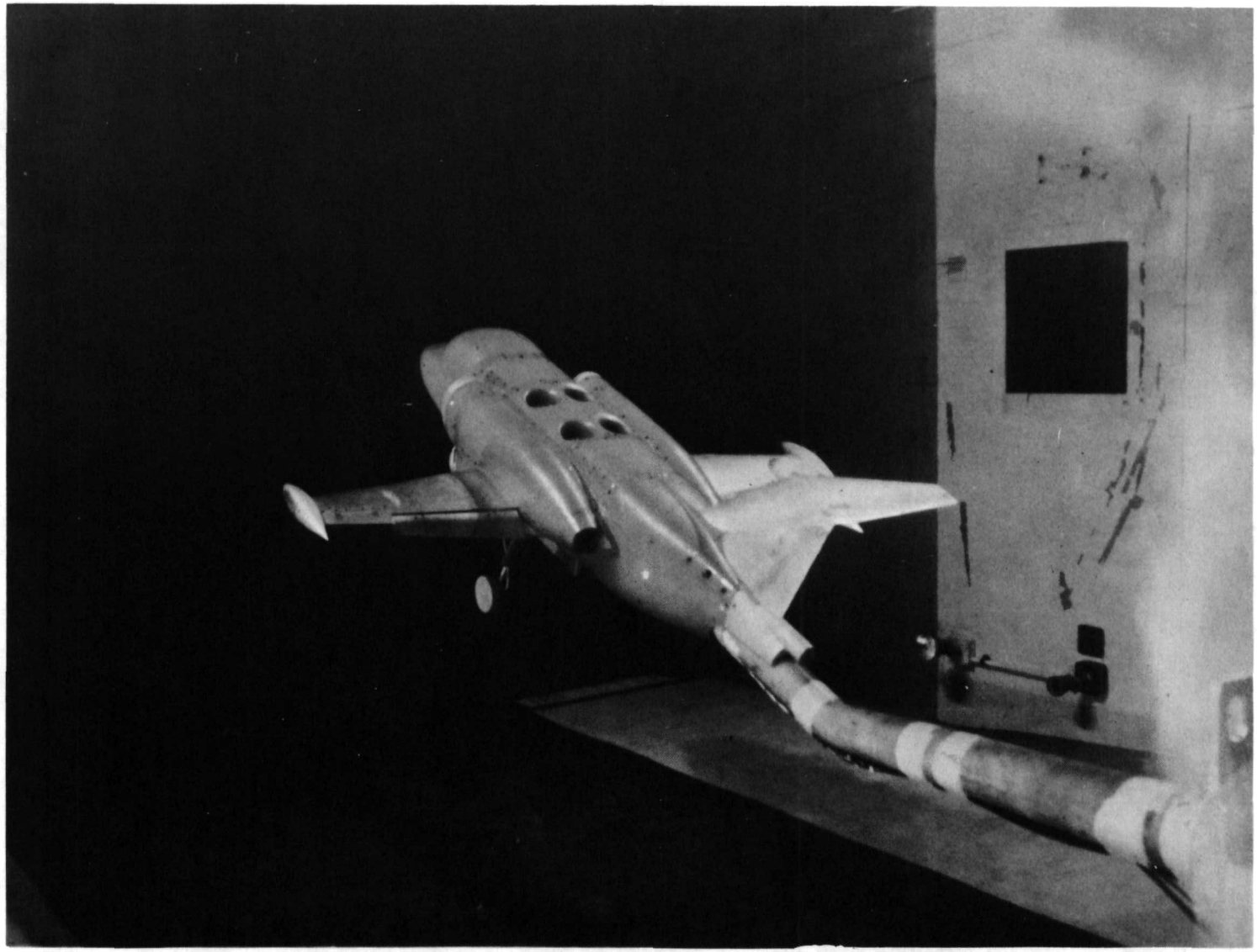

(b) View showing upper inlets. L-69-1202

Figure 2.- Continued.

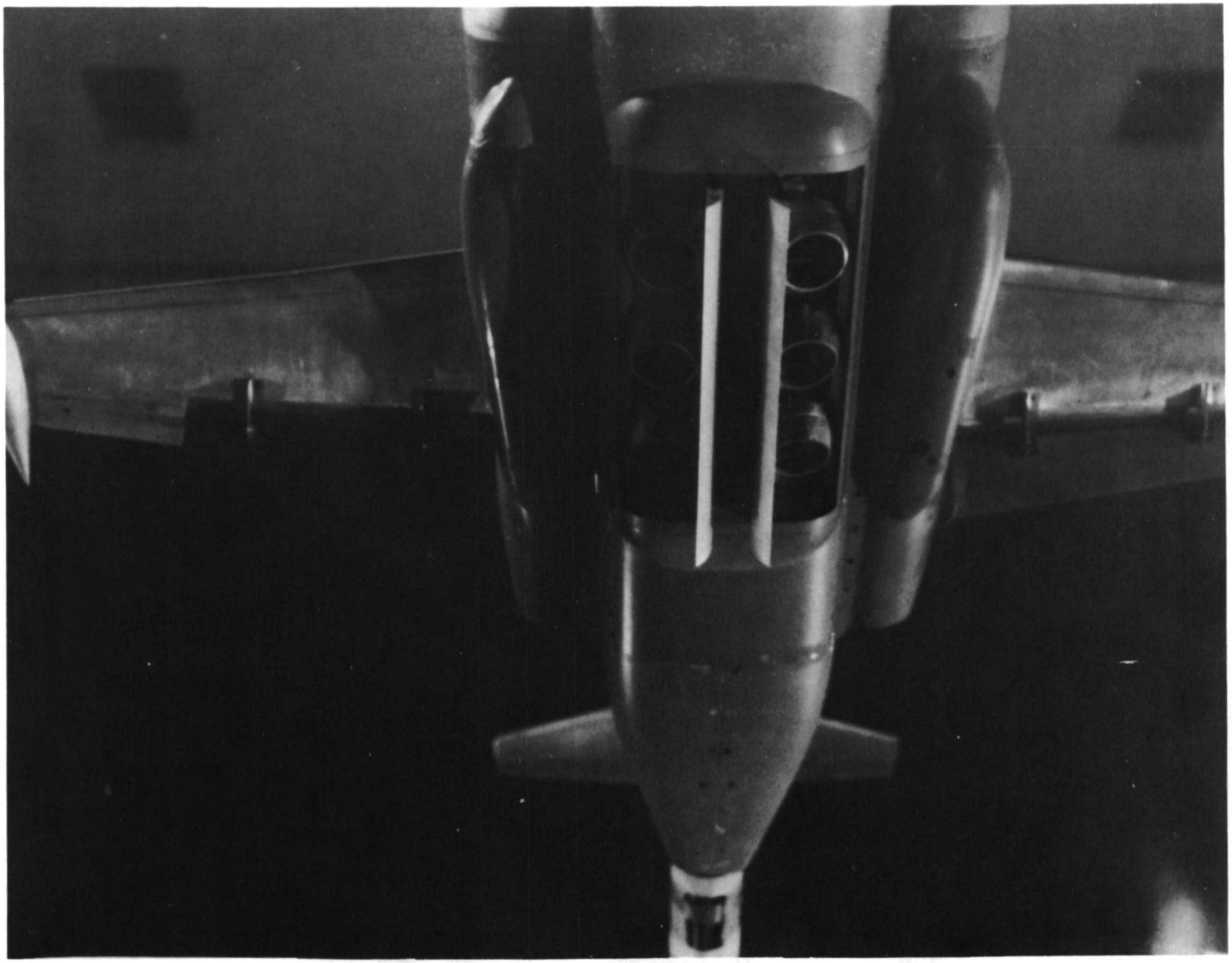

(c) View showing exit nozzles. L-69-1203

Figure 2.- Concluded.

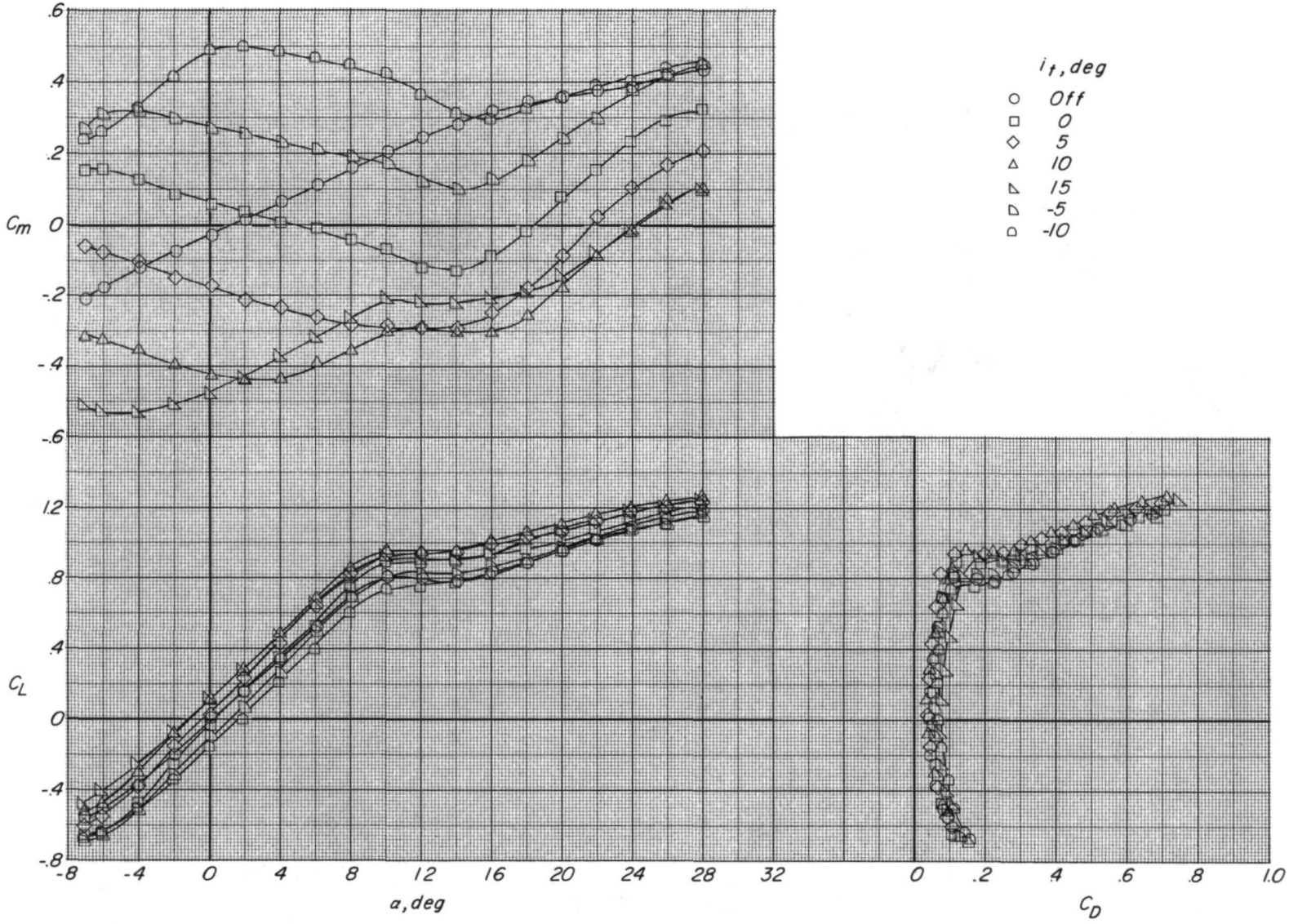

(a) $\delta_f = 0^0$.

Figure 3.- Effect of horizontal-tail incidence on longitudinal aerodynamic characteristics. Cruise configuration; $C_T = 0$.

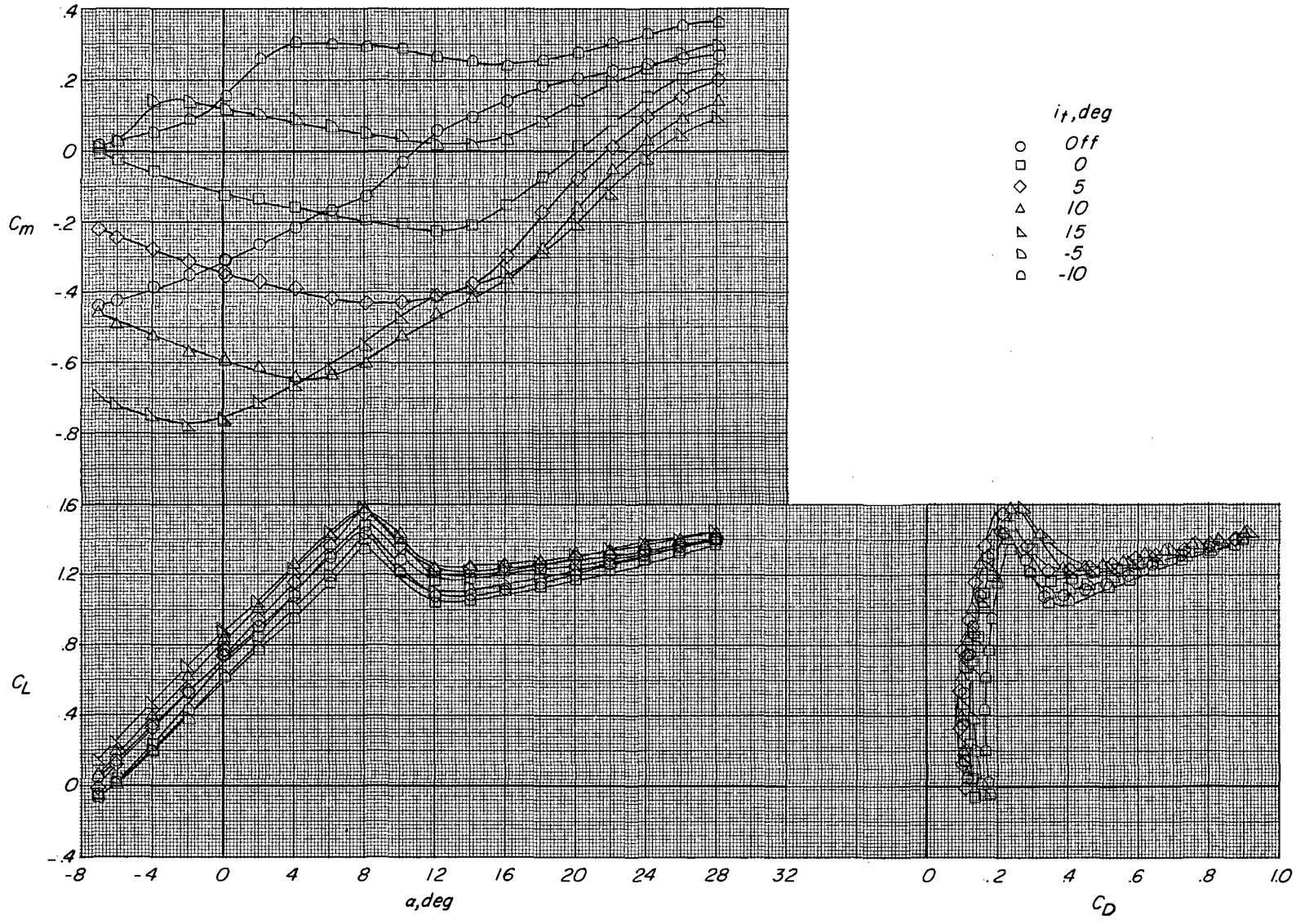

(b) $\delta_f = 40^o$.

Figure 3.- Concluded.

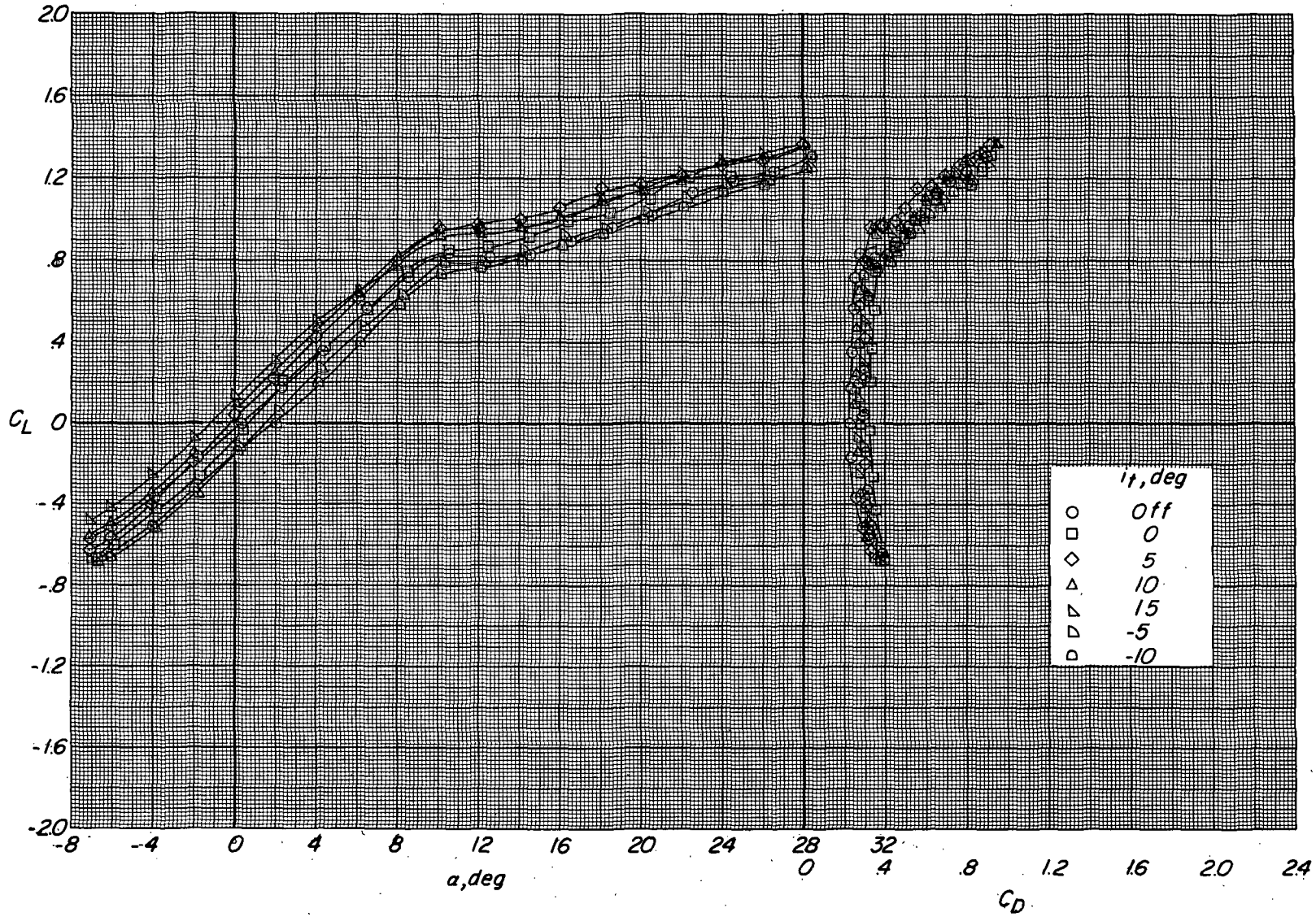

(a) Variation of lift and drag coefficients. $\delta_f = 0^0$.

Figure 4.- Effect of horizontal-tail incidence on longitudinal aerodynamic characteristics. Cruise configuration at cruise power.

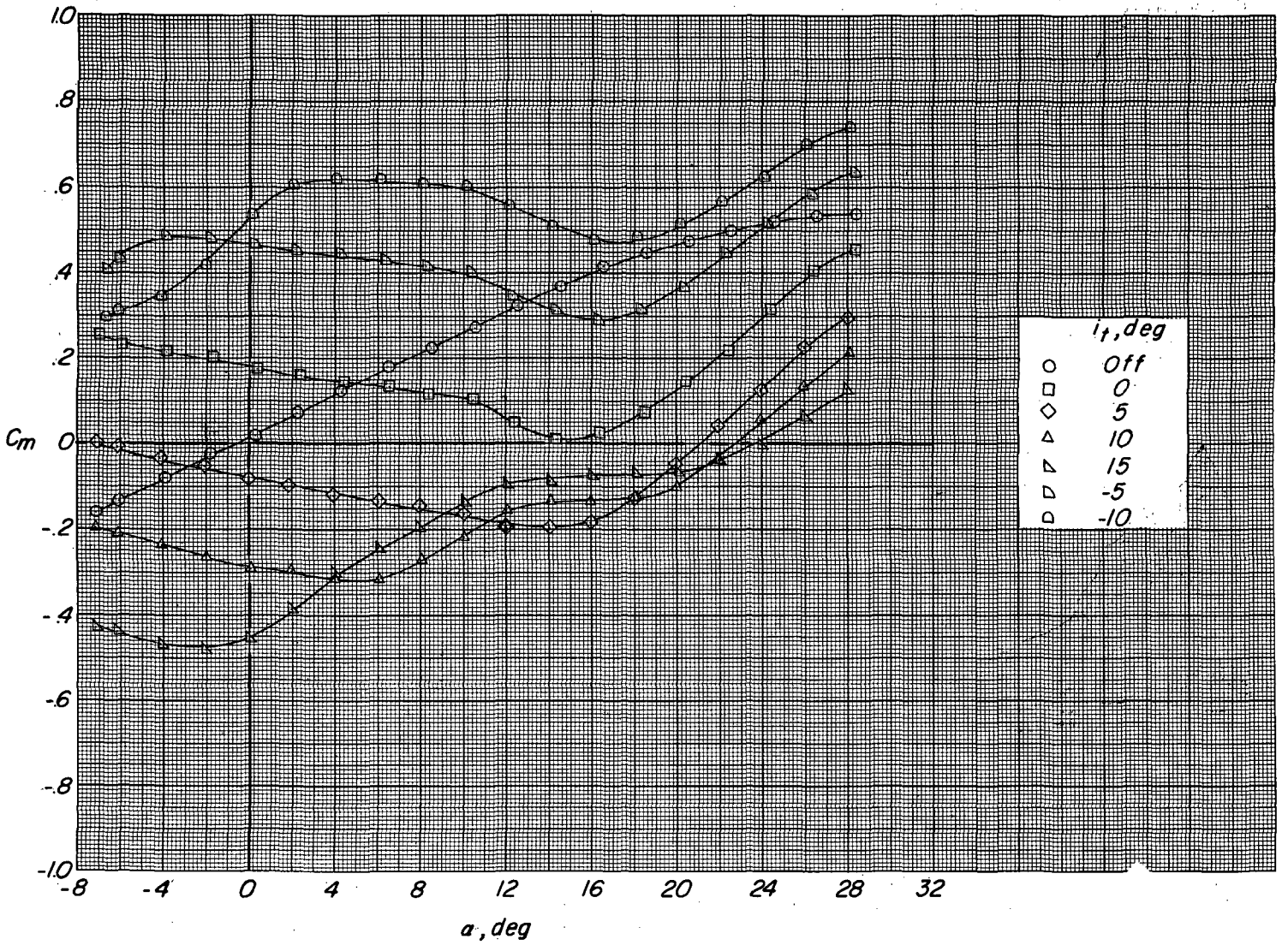

(b) Variation of pitching-moment coefficient with angle of attack. $\delta_f = 0^0$.

Figure 4.- Continued.

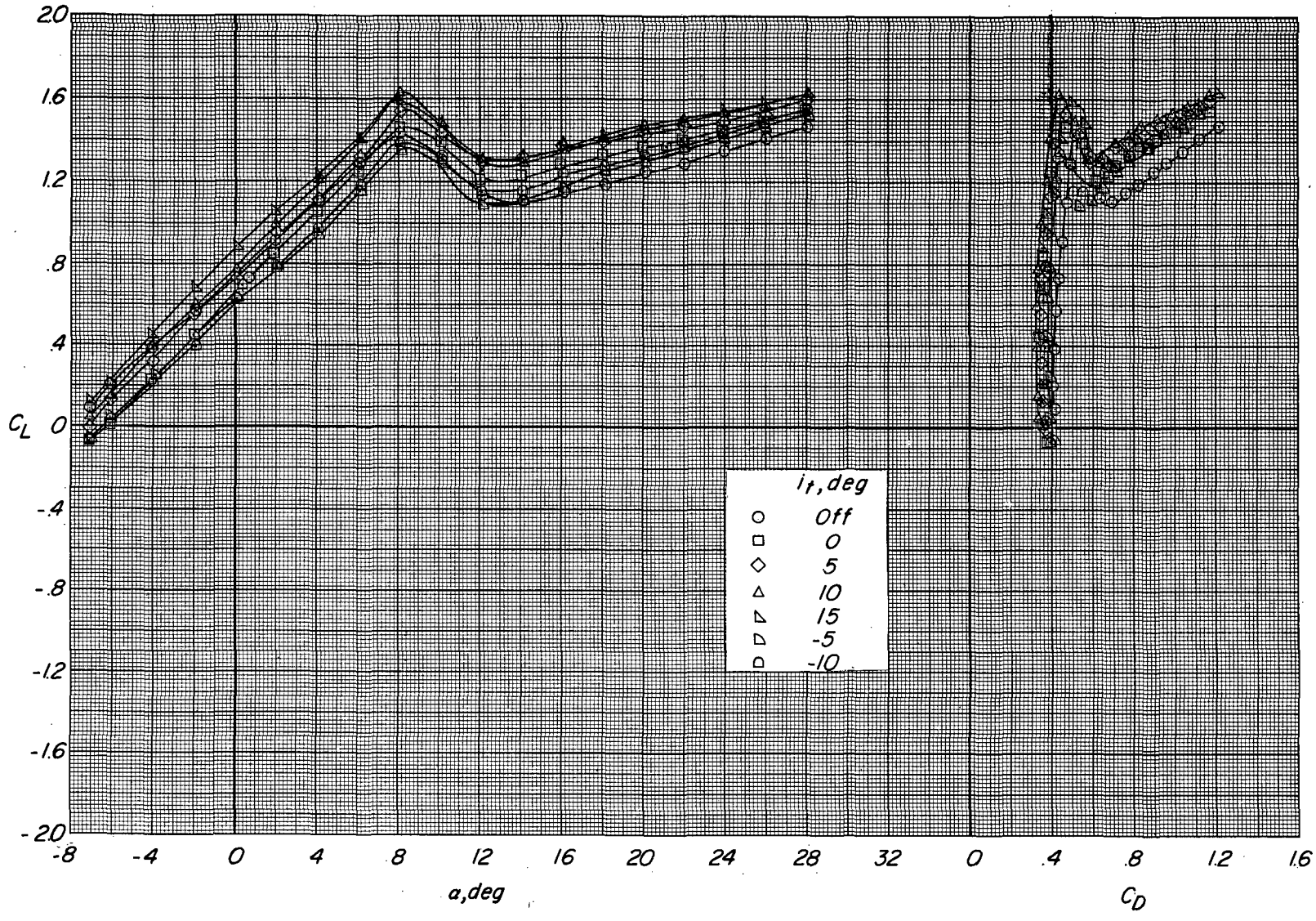

(c) Variation of lift and drag coefficients. $\delta_f = 40^0$.

Figure 4.- Continued.

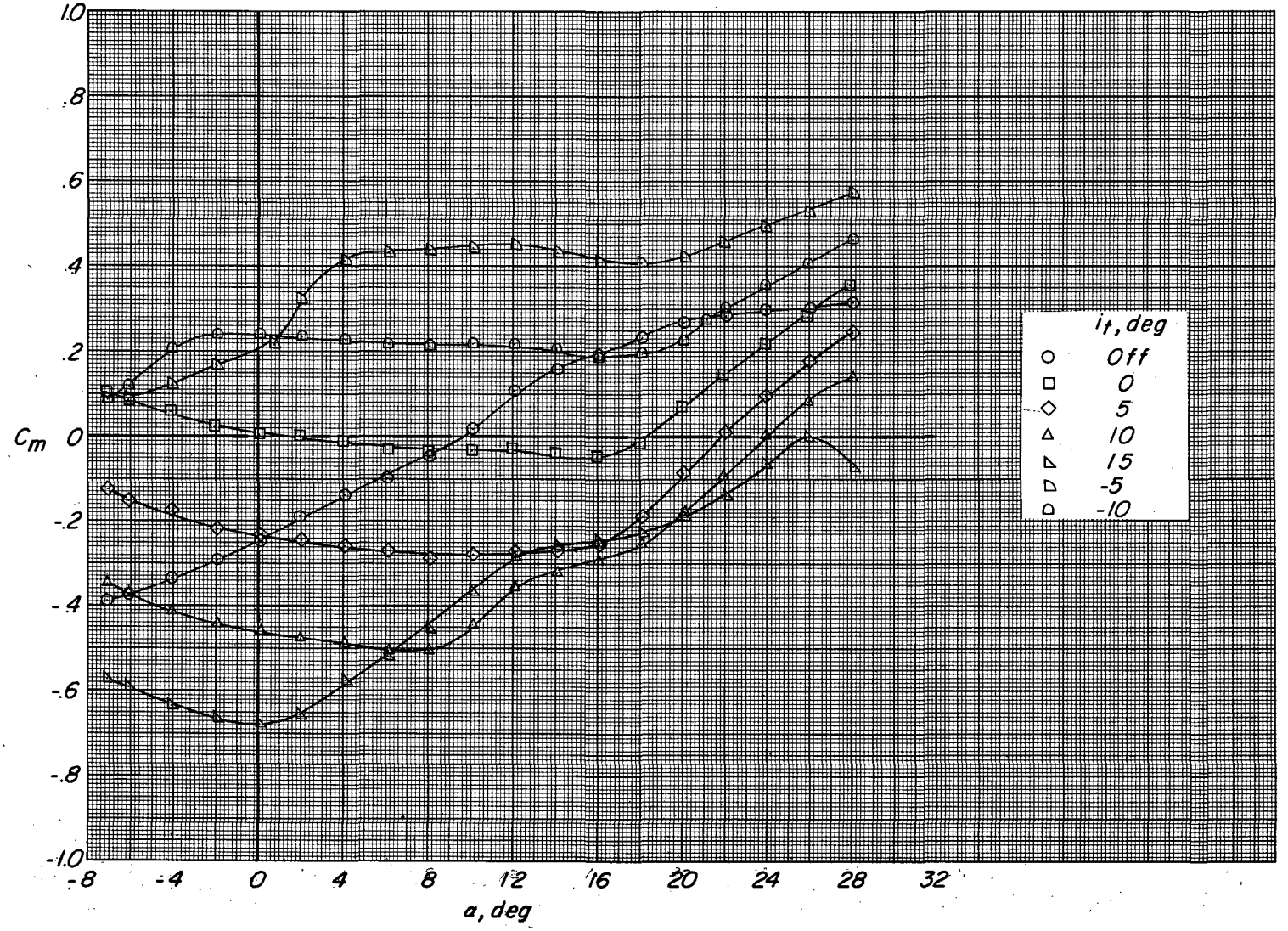

(d) Variation of pitching-moment coefficient with angle of attack. $\delta_f = 40^0$.

Figure 4.- Concluded.

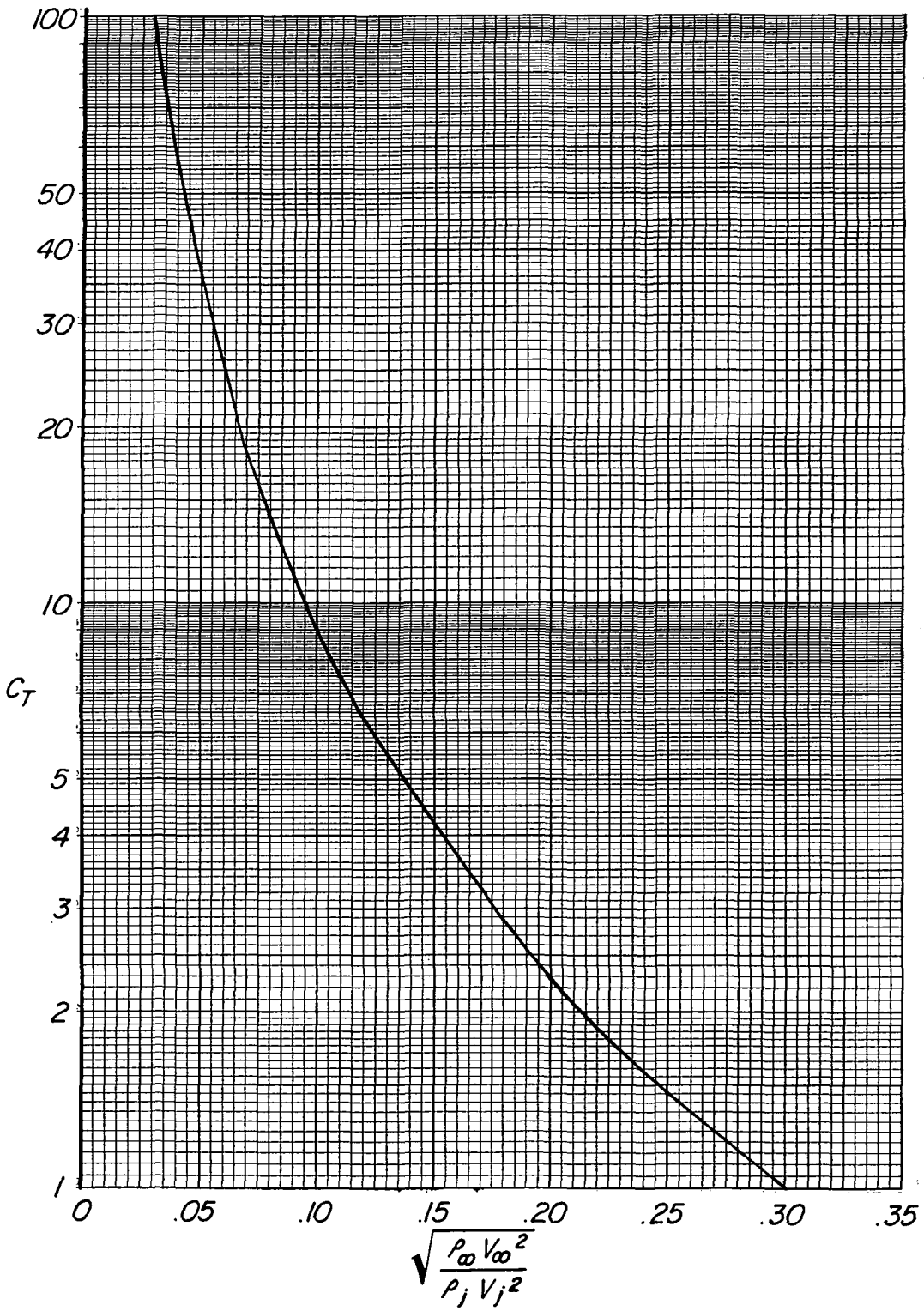

Figure 5.- Variation of thrust coefficient with effective velocity ratio. Six nozzles in lift mode.

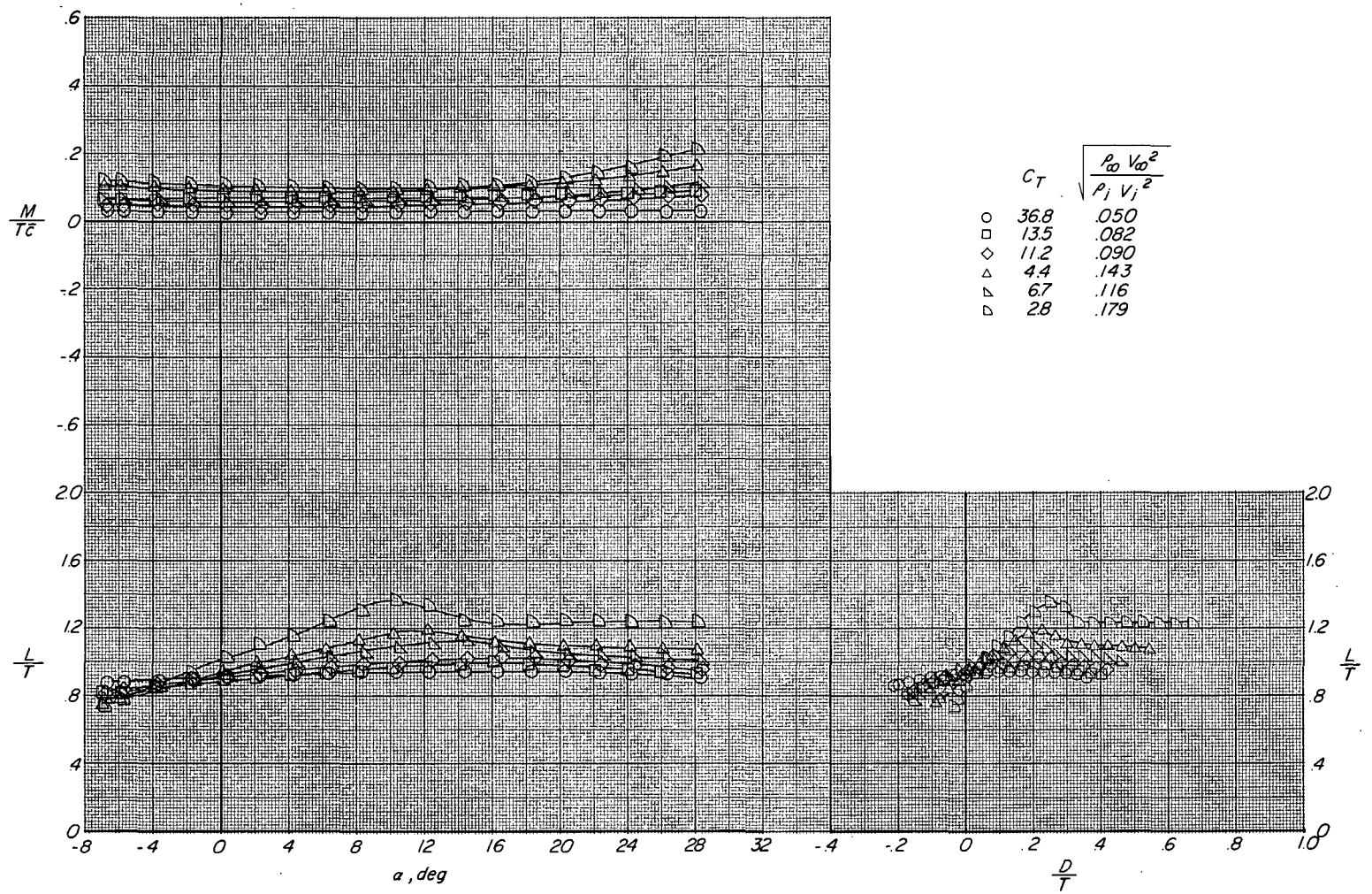

(a) $\delta_n = 0^0$.

Figure 6.- Effect of thrust coefficient on longitudinal aerodynamic characteristics. Six nozzles in lift mode; $i_t = 0^0$.

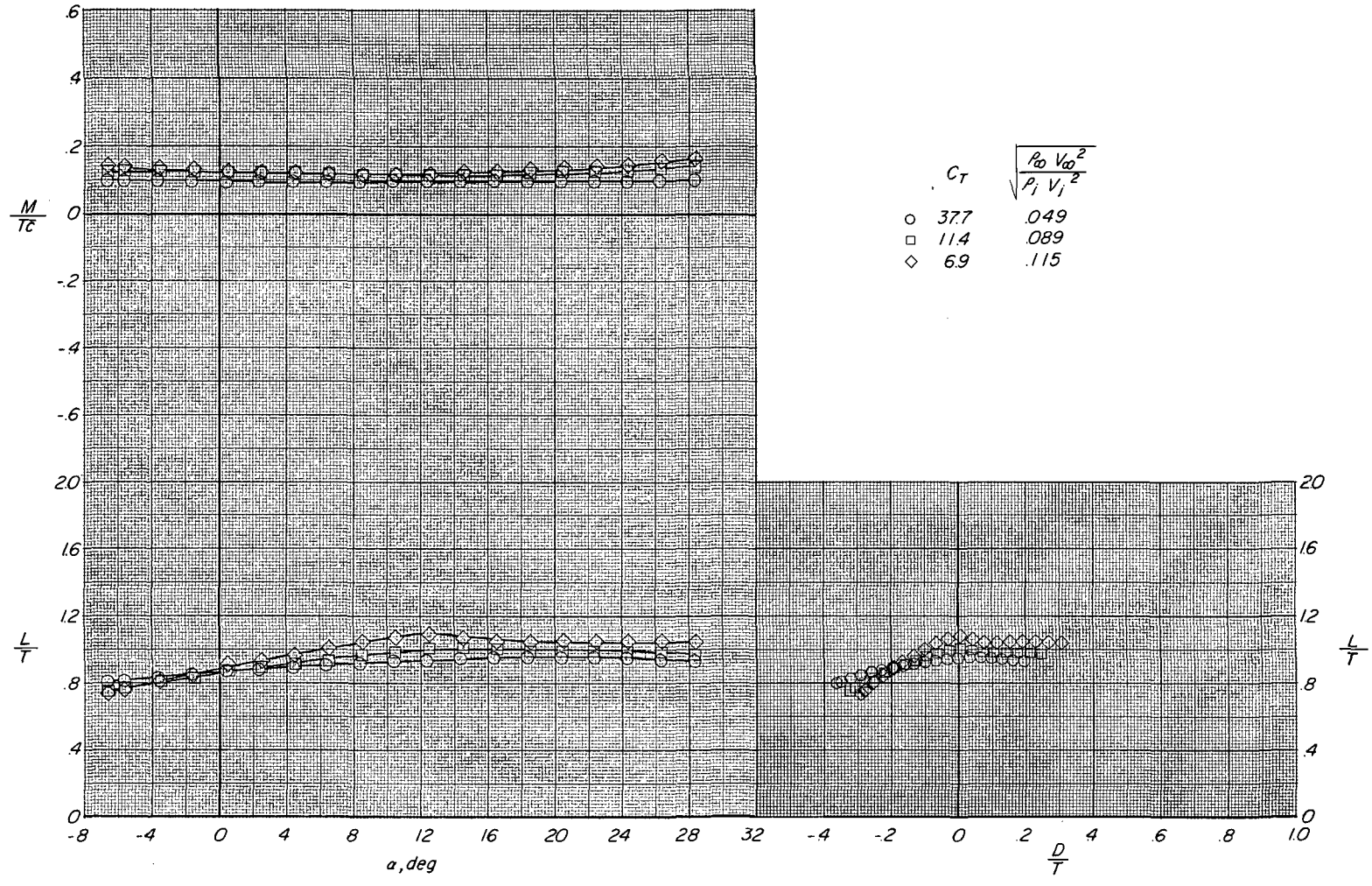

(b) $\delta_n = 10^0$.

Figure 6.- Continued.

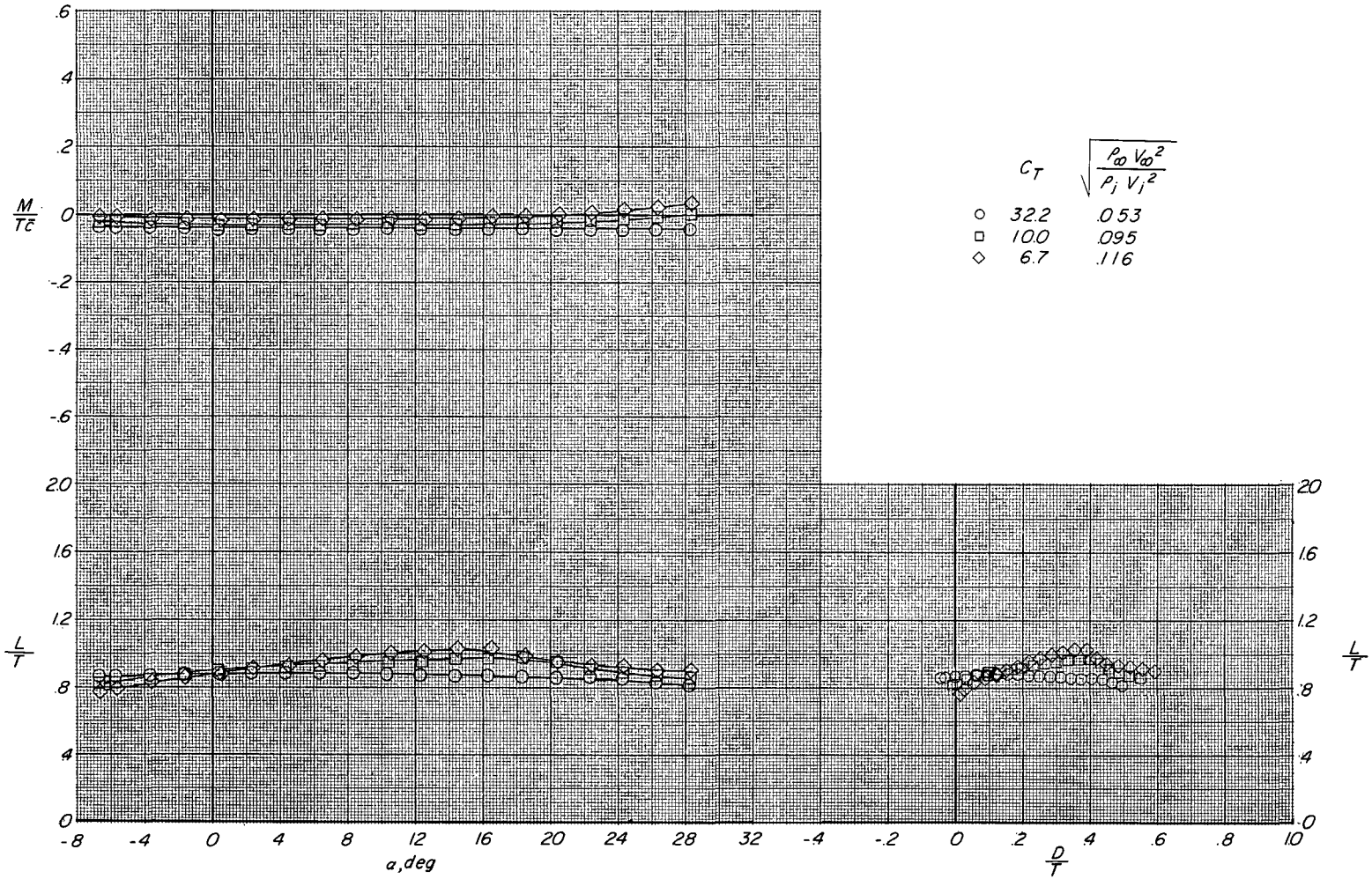

(c) $\delta_n = -10^0$.

Figure 6.- Concluded.

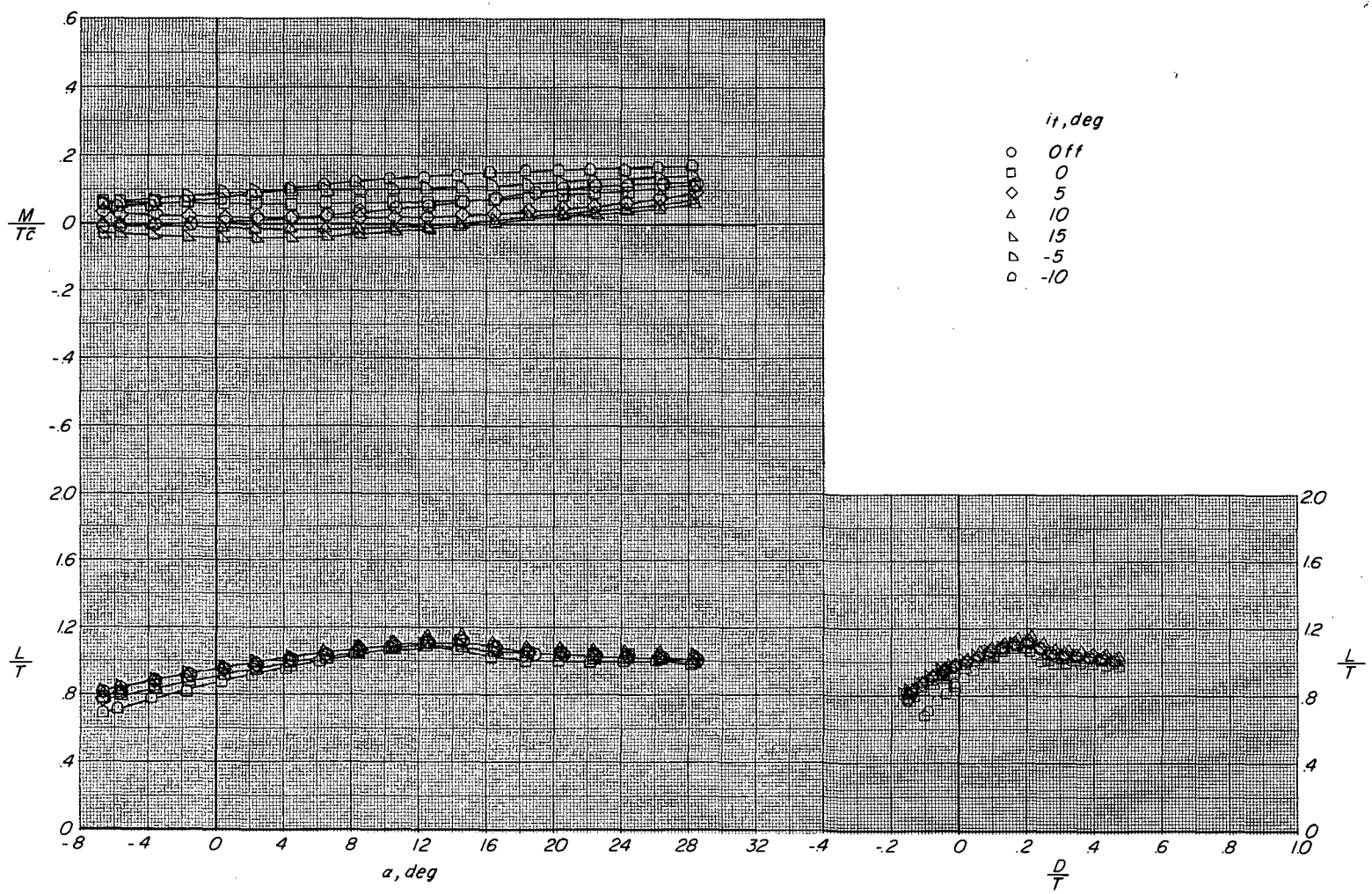

(a) $\delta_n = 0^0$; $C_T = 6.7$.

Figure 7.- Effect of horizontal-tail incidence on longitudinal aerodynamic characteristics. Six nozzles in lift mode.

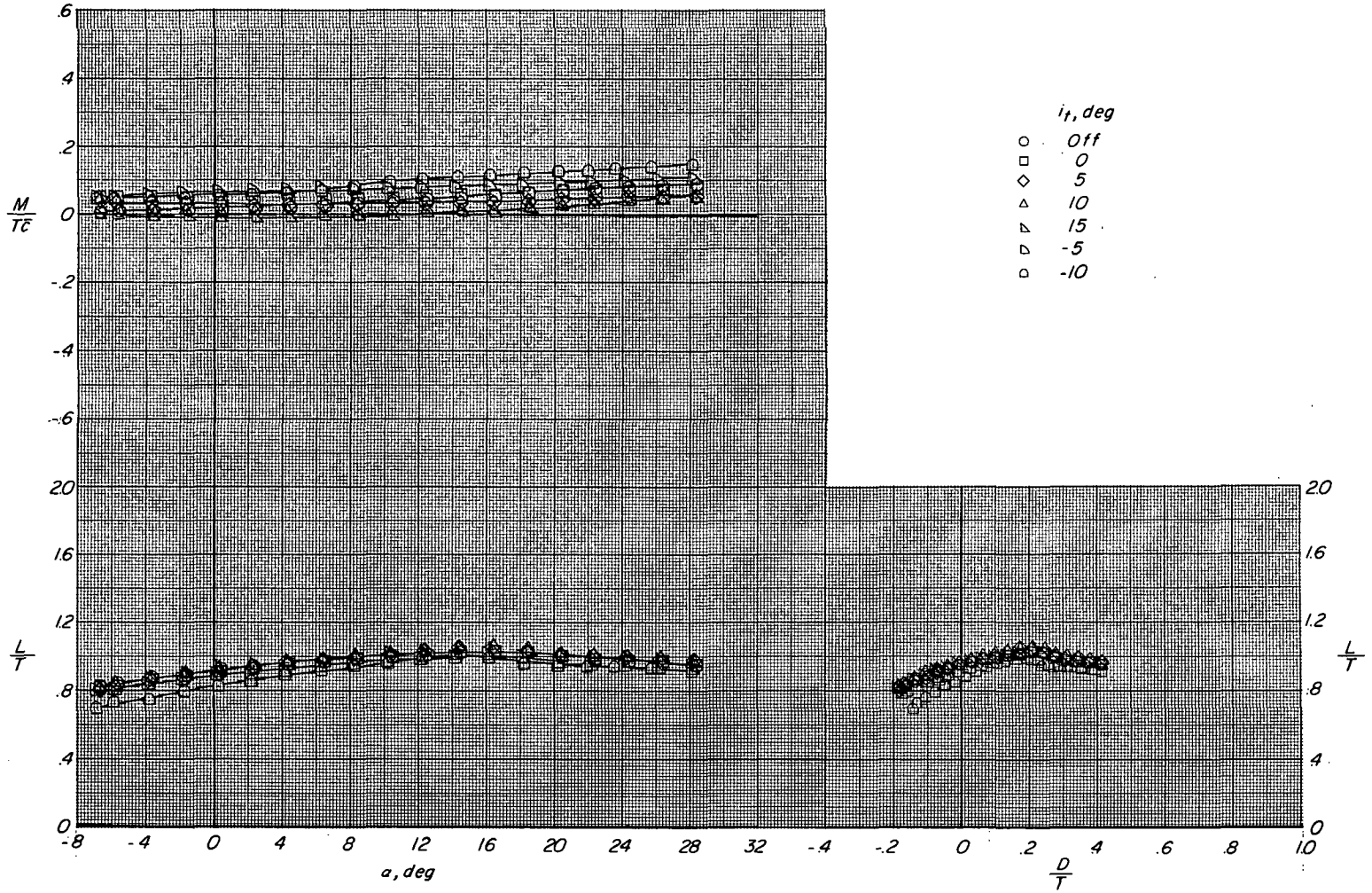

(b) $\delta_n = 0^0$; $C_T = 11.0$.

Figure 7.- Continued.

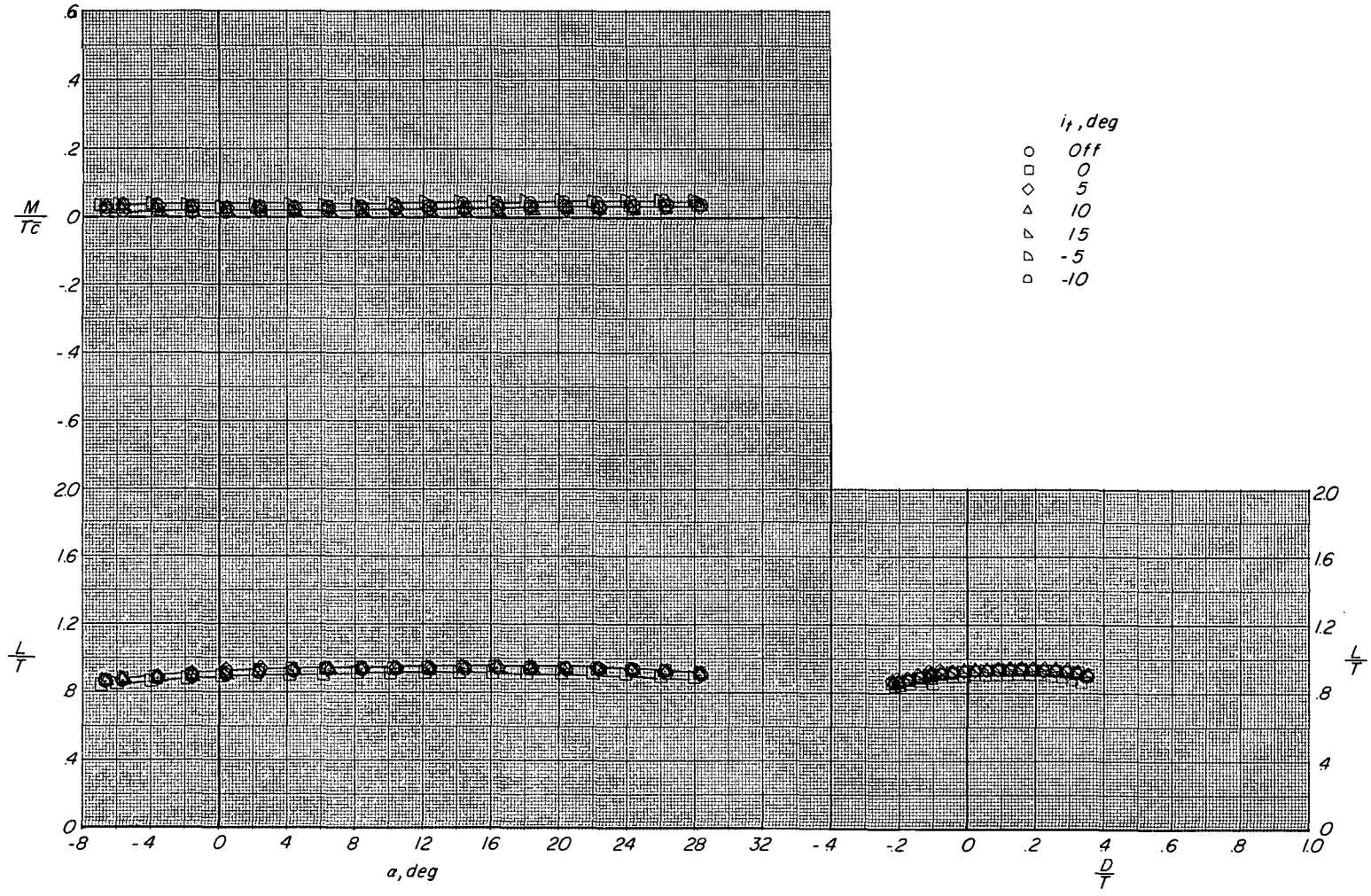

(c) $\delta_n = 0^o$; $C_T = 35.0$.

Figure 7.- Continued.

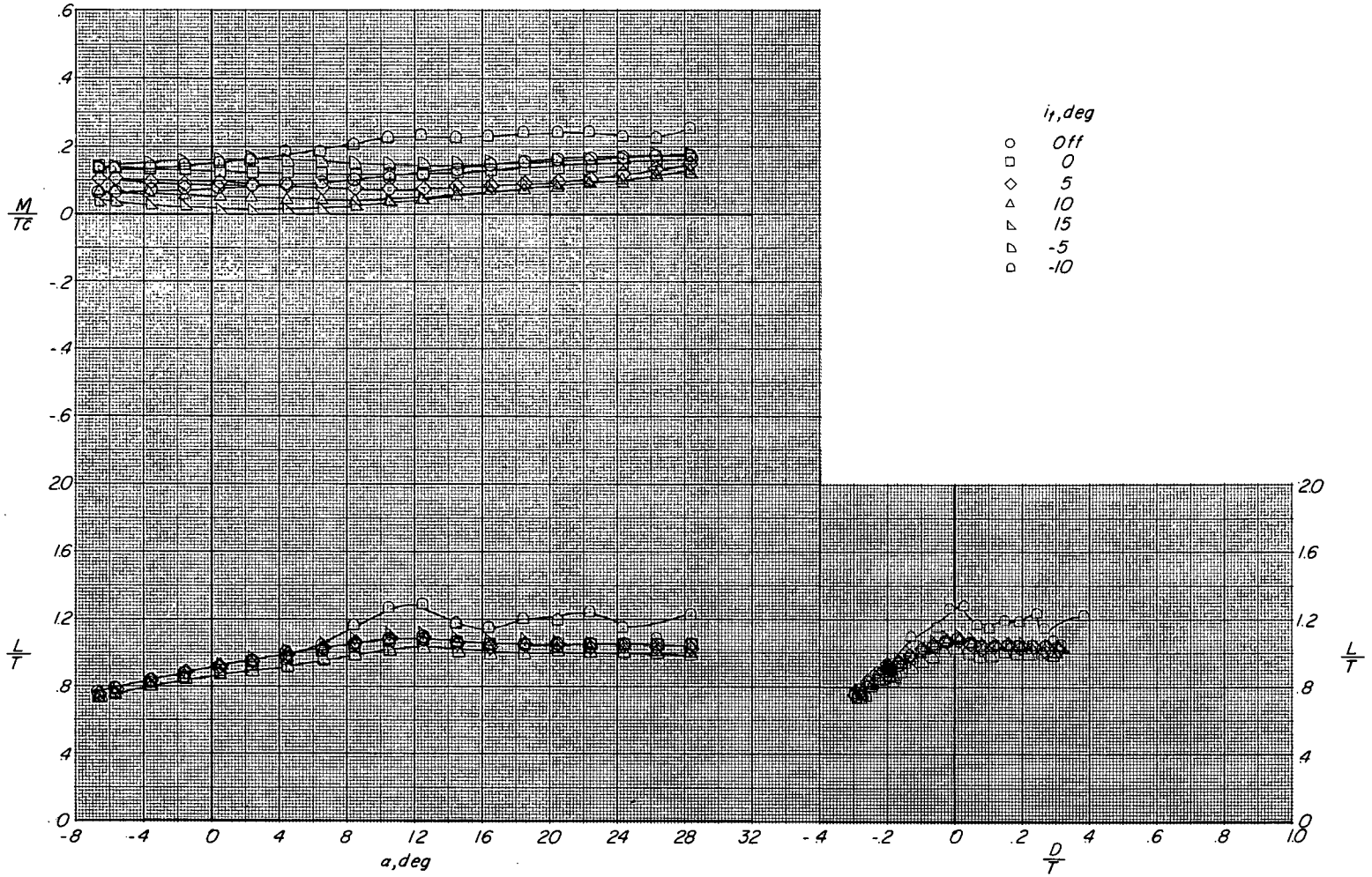

(d) $\delta_n = 10^0$; $C_T = 6.7$.

Figure 7.- Continued.

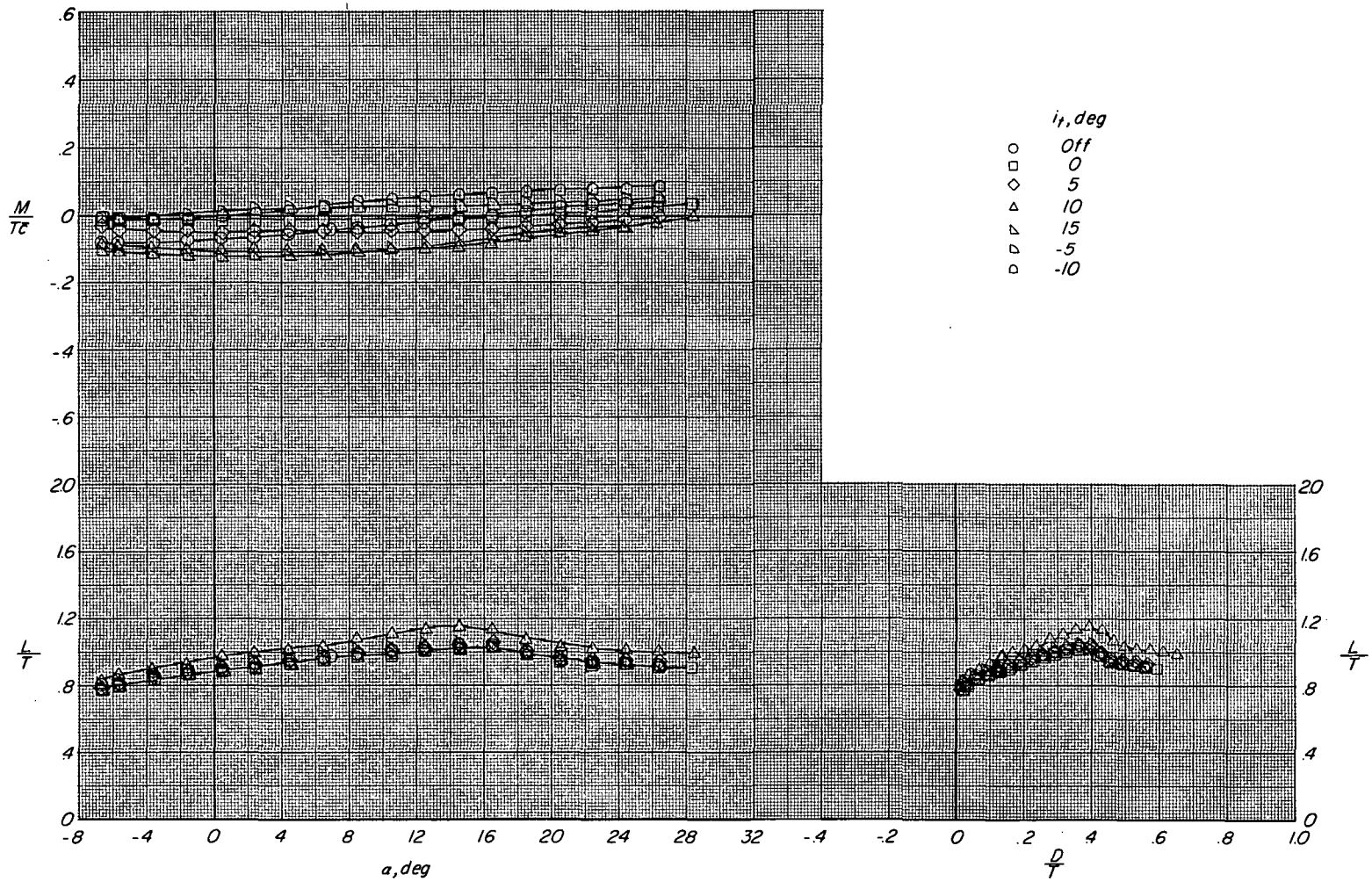

(e) $\delta_n = -10^0$; $C_T = 6.7$.

Figure 7.- Concluded.

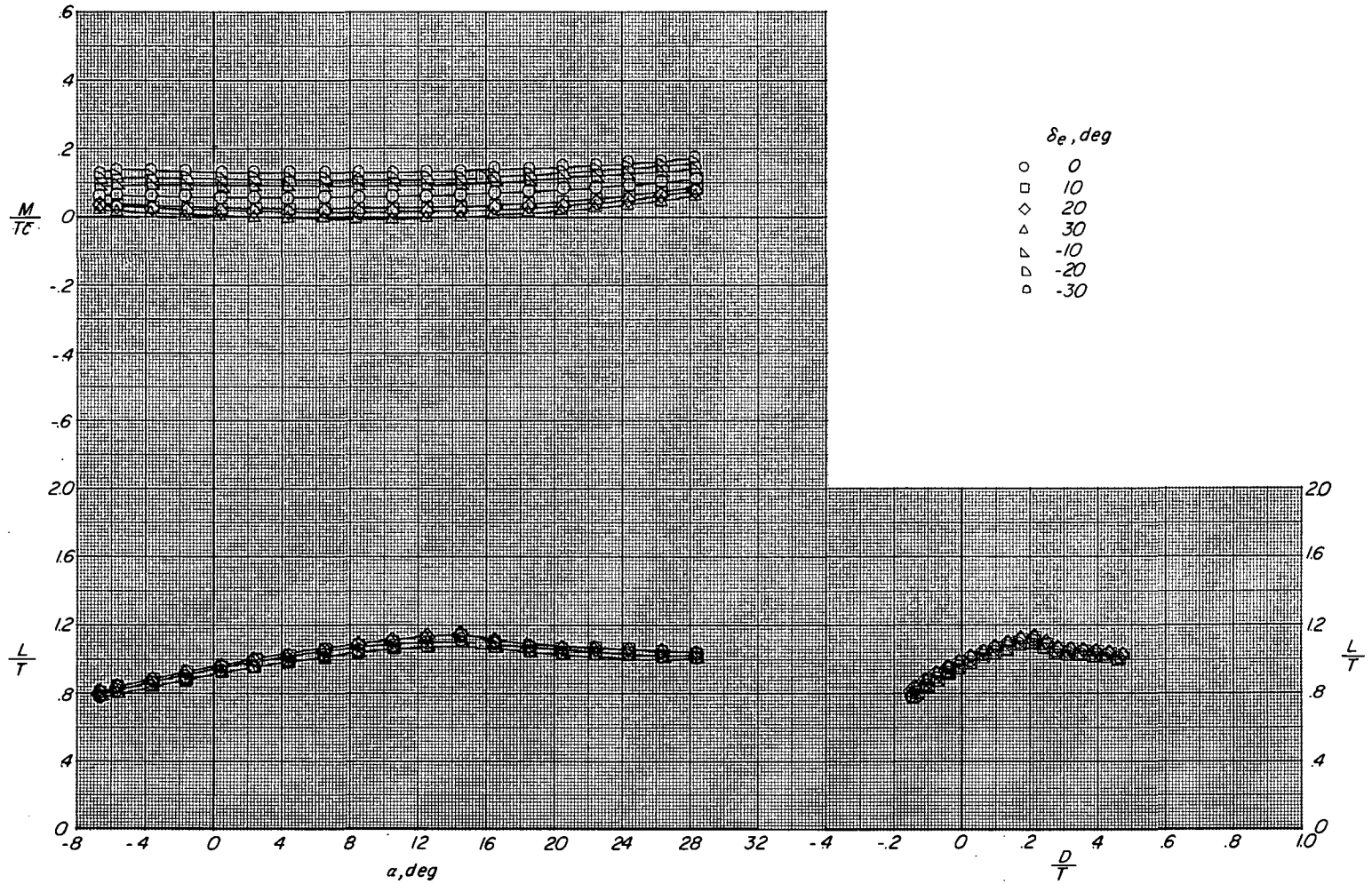

(a) $C_T = 6.7$.

Figure 8.- Effect of elevator deflection on longitudinal aerodynamic characteristics. Six nozzles in lift mode; $\delta_n = 0^o$; $i_t = 0^o$.

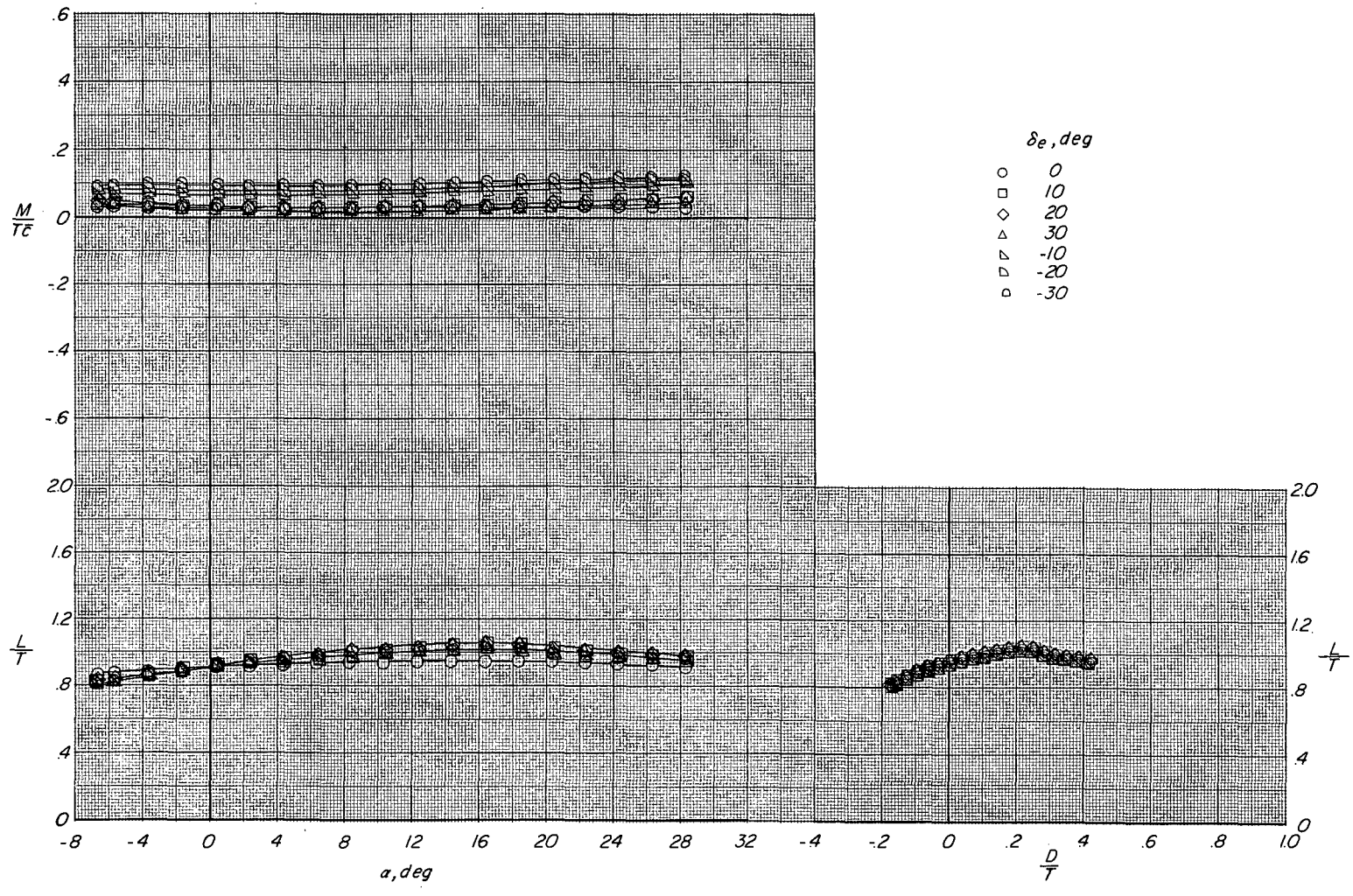

(b) C_T = 11.0.

Figure 8.- Continued.

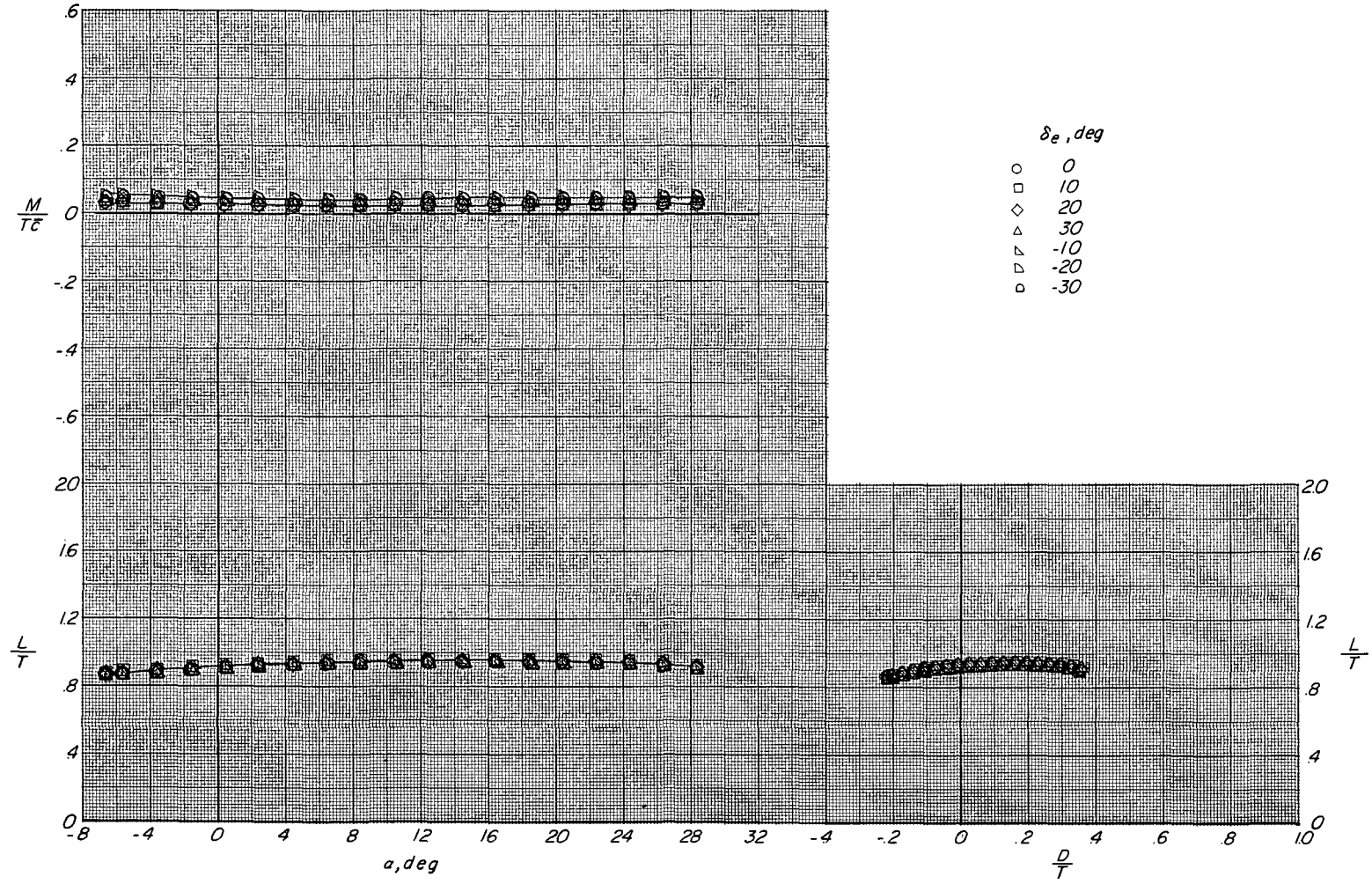

(c) C_T = 35.0.

Figure 8.- Concluded.

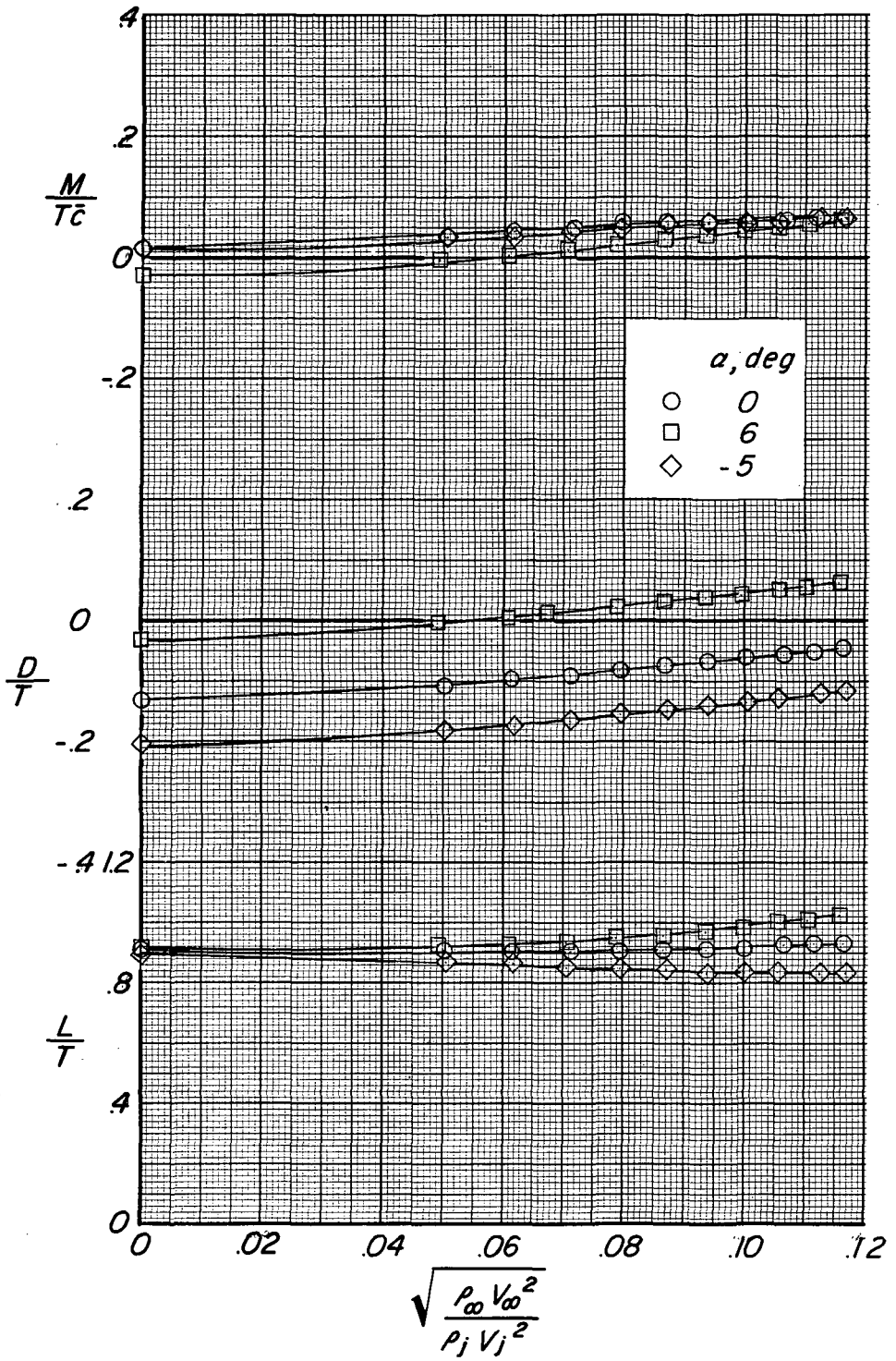

(a) $\delta_n = 0^0$.

Figure 9.- Variation of $M/T\bar{c}$, D/T, and L/T with effective velocity ratio. Six nozzles in lift mode; $i_t = 0^0$.

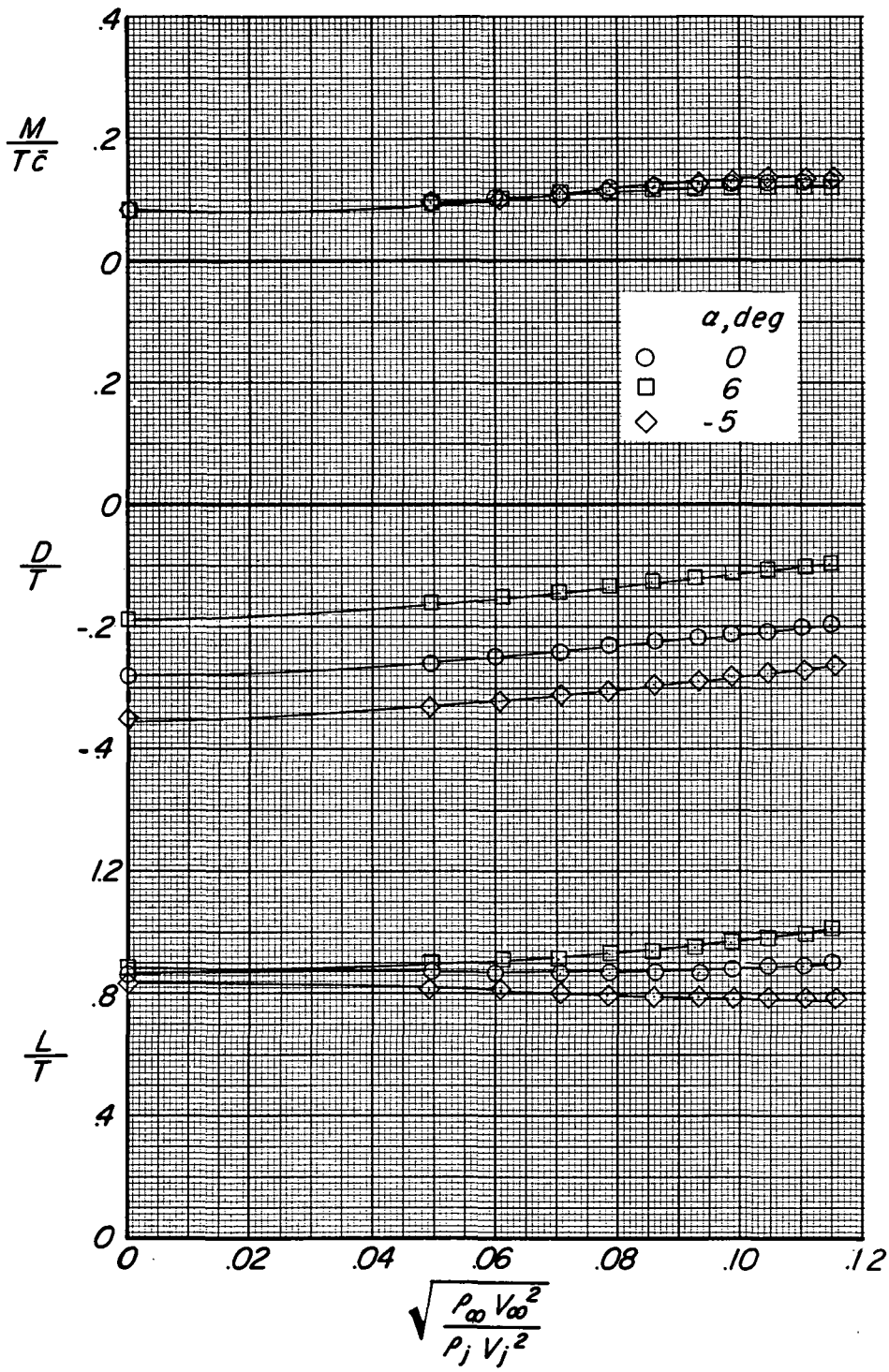

(b) $\delta_n = 10^0$.

Figure 9.- Continued.

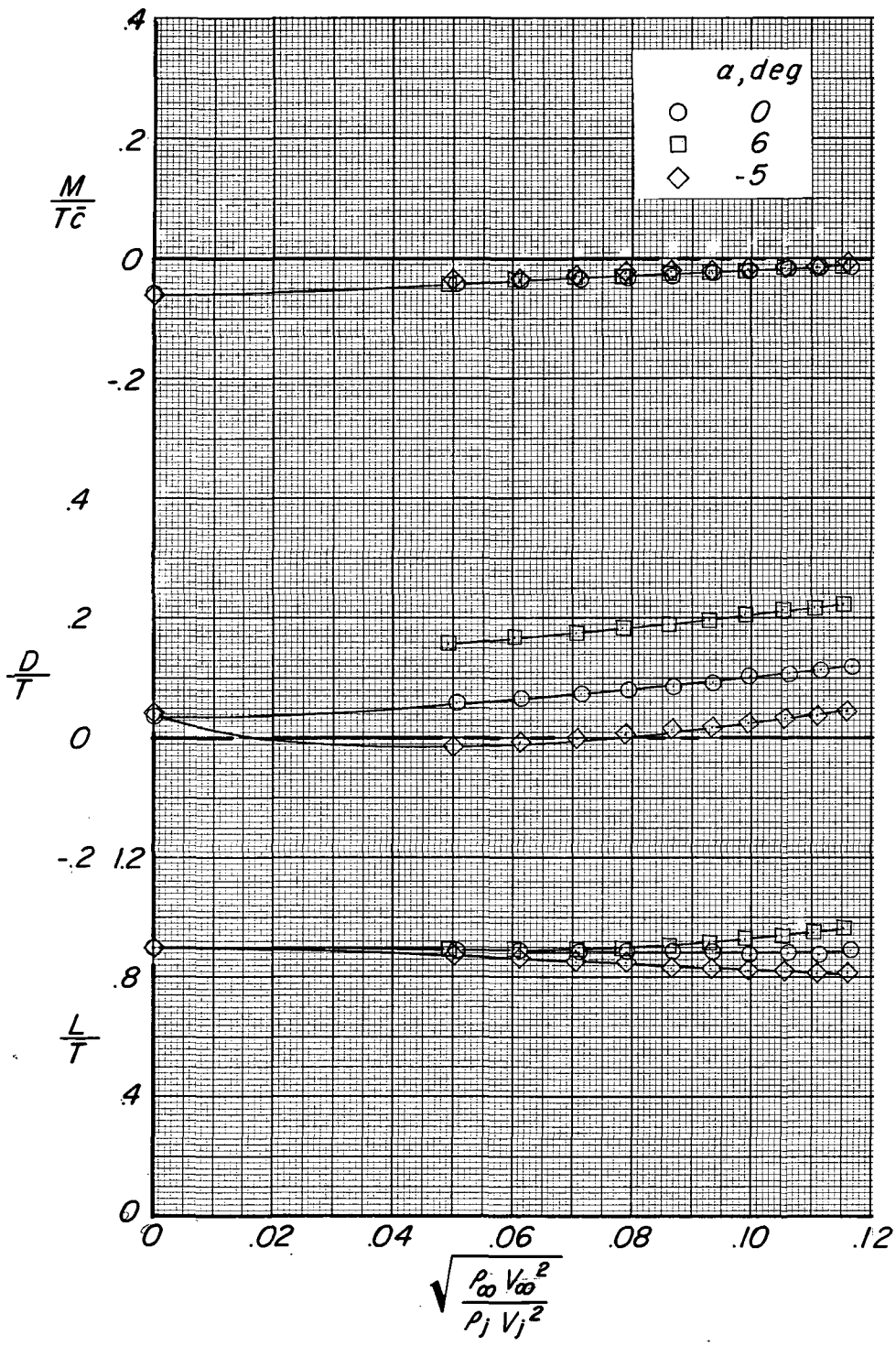

(c) $\delta_n = -10^0$.

Figure 9.- Concluded.

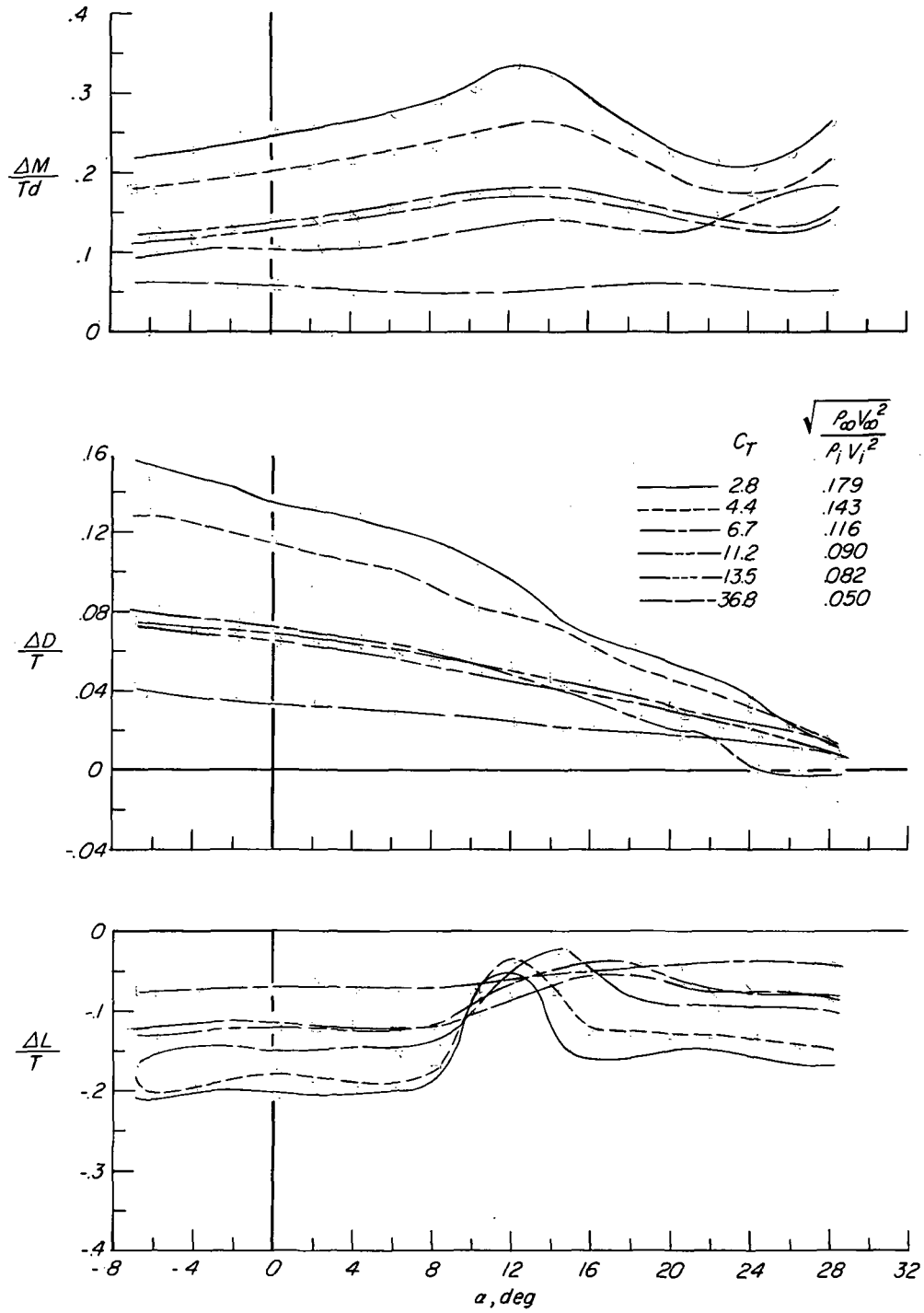

(a) $\delta_n = 0^0$.

Figure 10.- Effect of jet interference on longitudinal aerodynamic characteristics. Six nozzles in lift mode; $i_t = 0^0$.

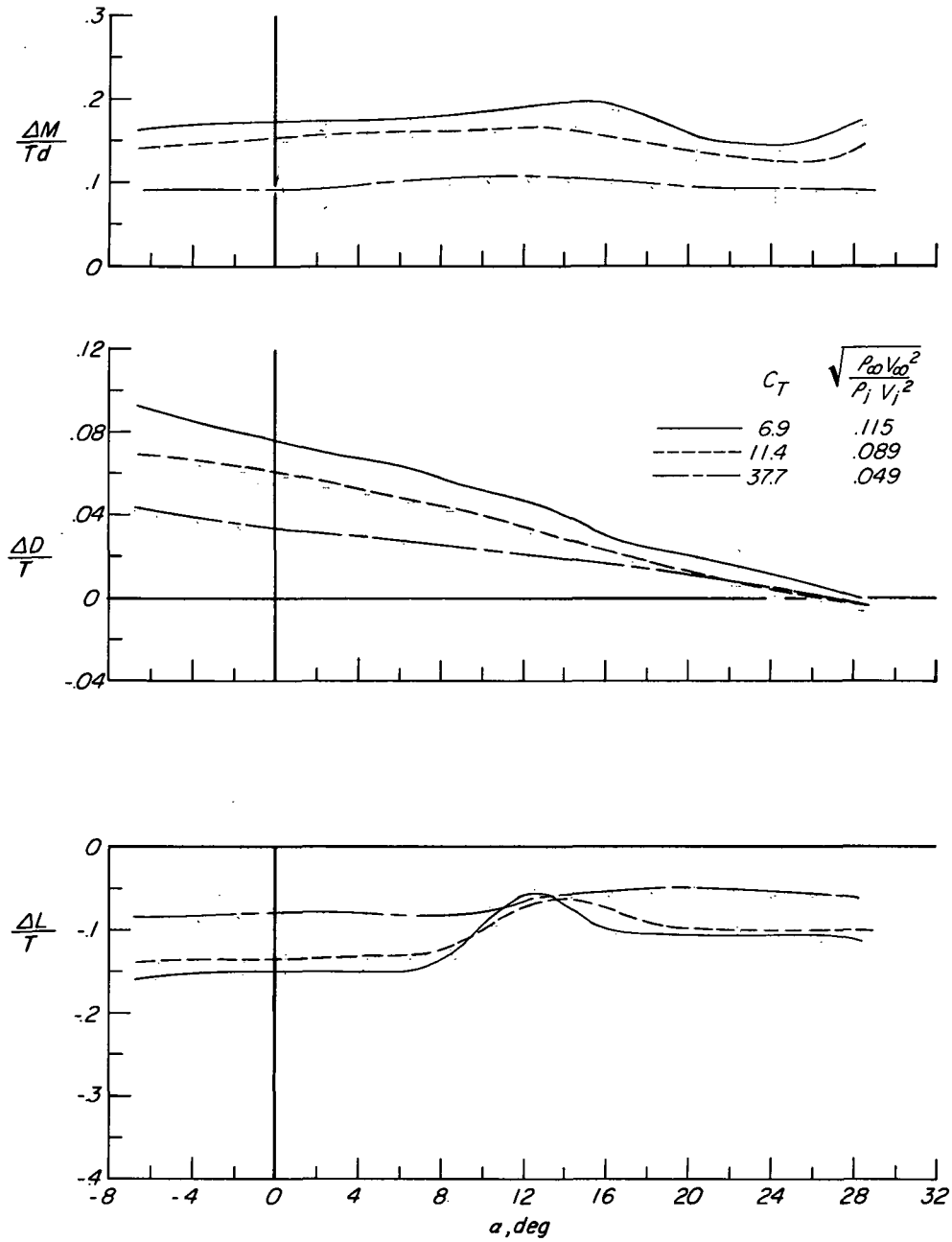

(b) $\delta_n = 10^0$.

Figure 10.- Continued.

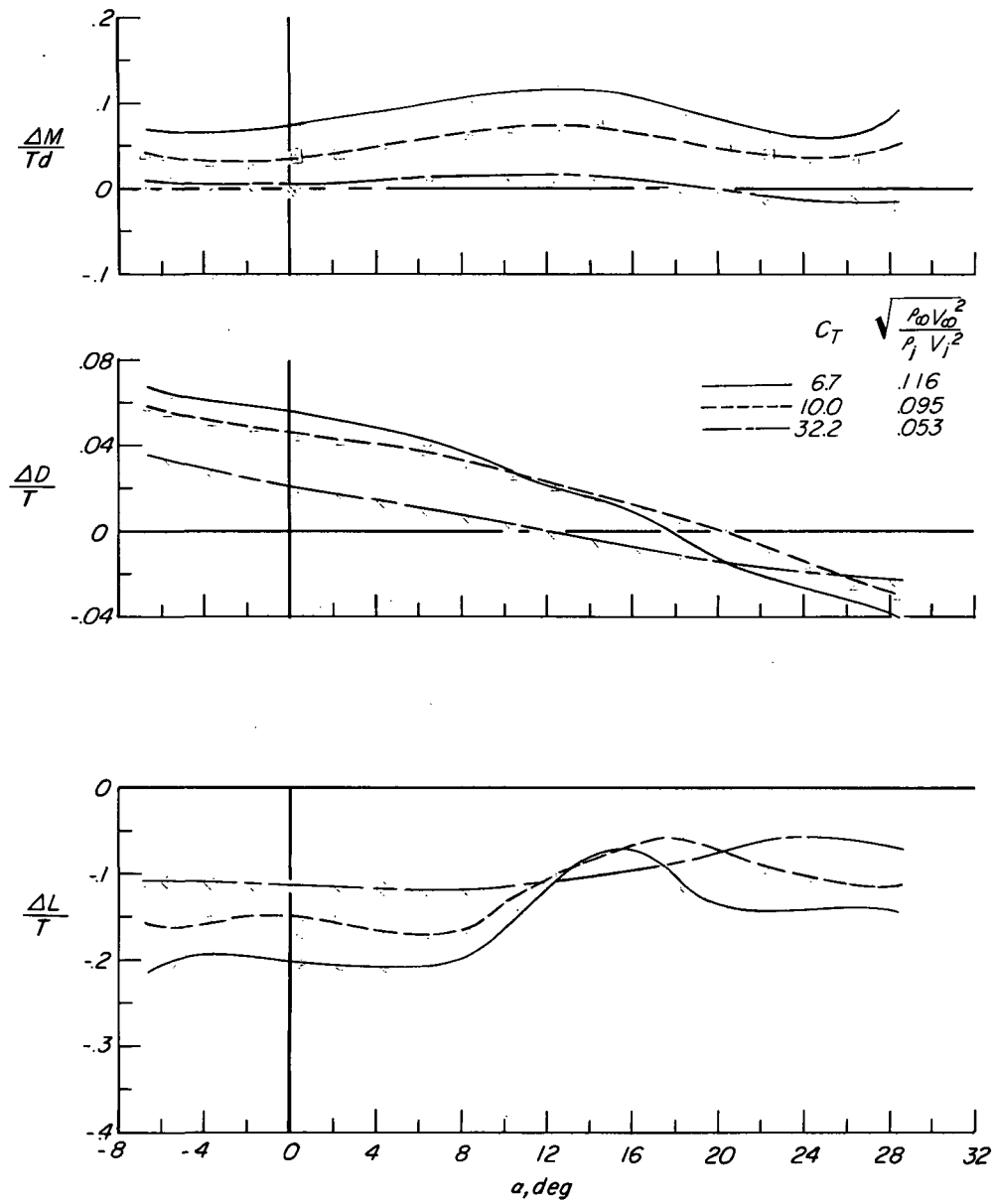

(c) $\delta_n = -10^0$.

Figure 10.- Concluded.

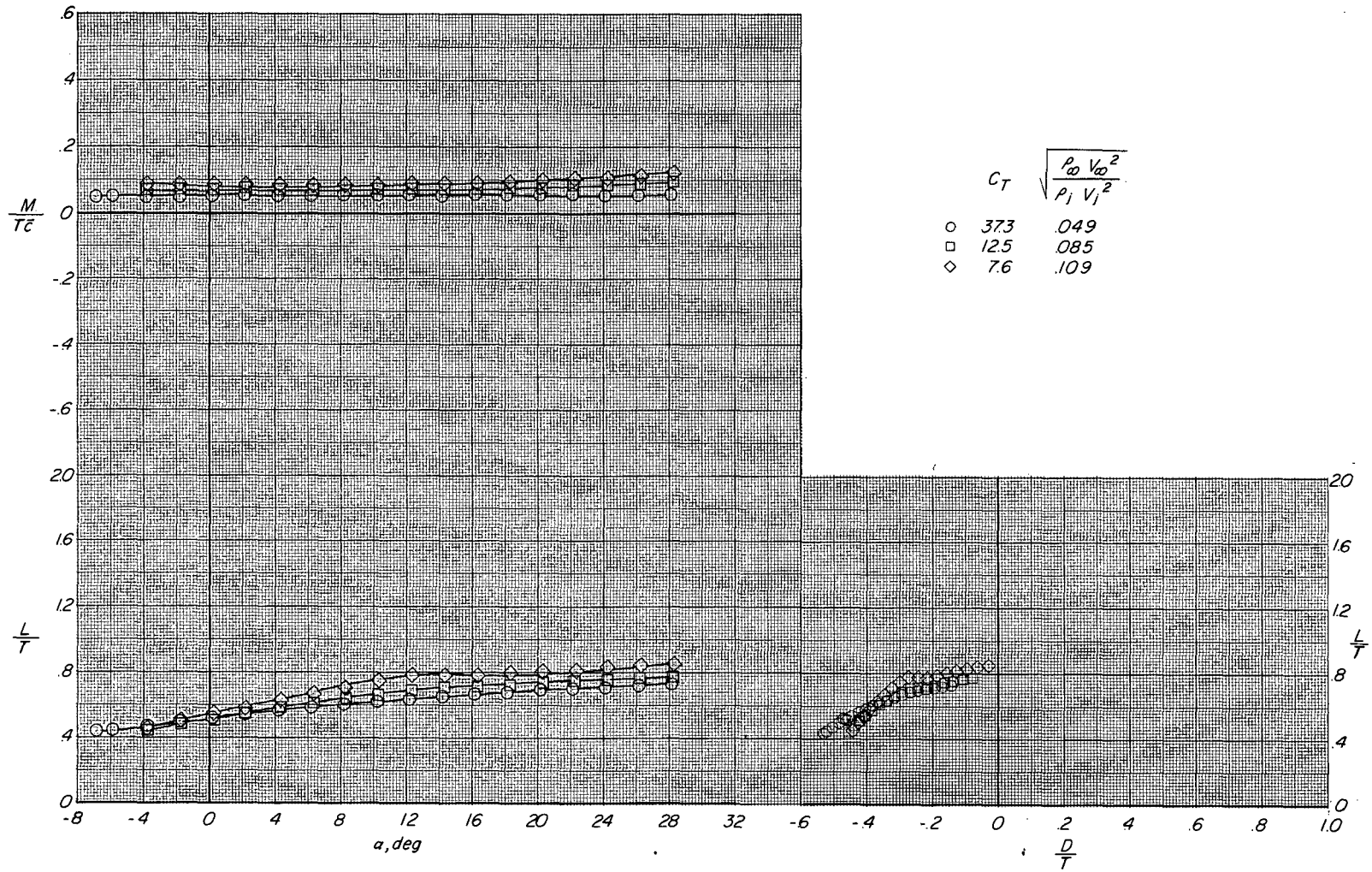

(a) $\delta_n = 10^0$.

Figure 11.- Effect of thrust coefficient on longitudinal aerodynamic characteristics. Four lift nozzles and two cruise nozzles; $i_t = 0^0$.

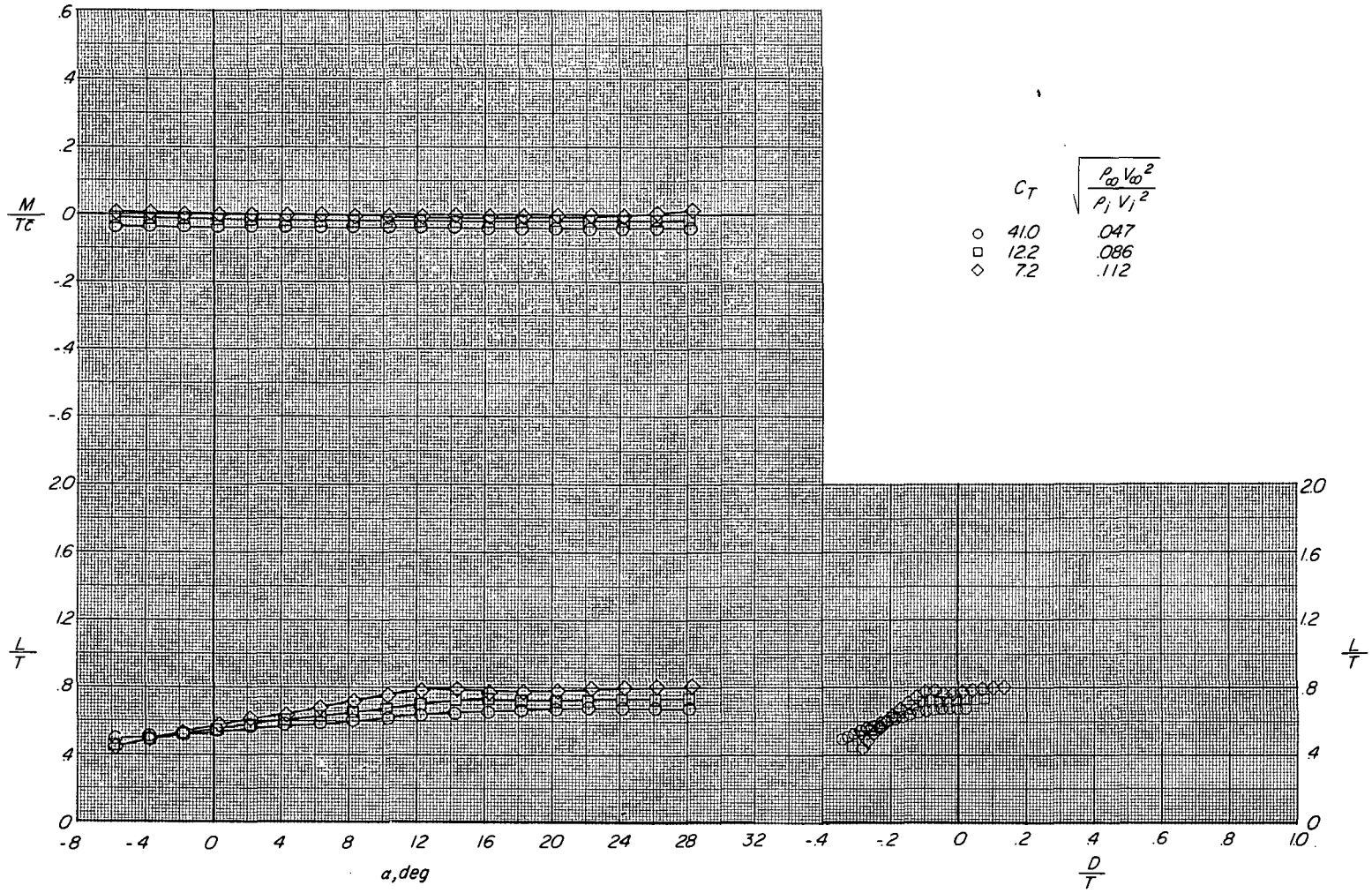

(b) $\delta_n = -10^0$.

Figure 11.- Concluded.

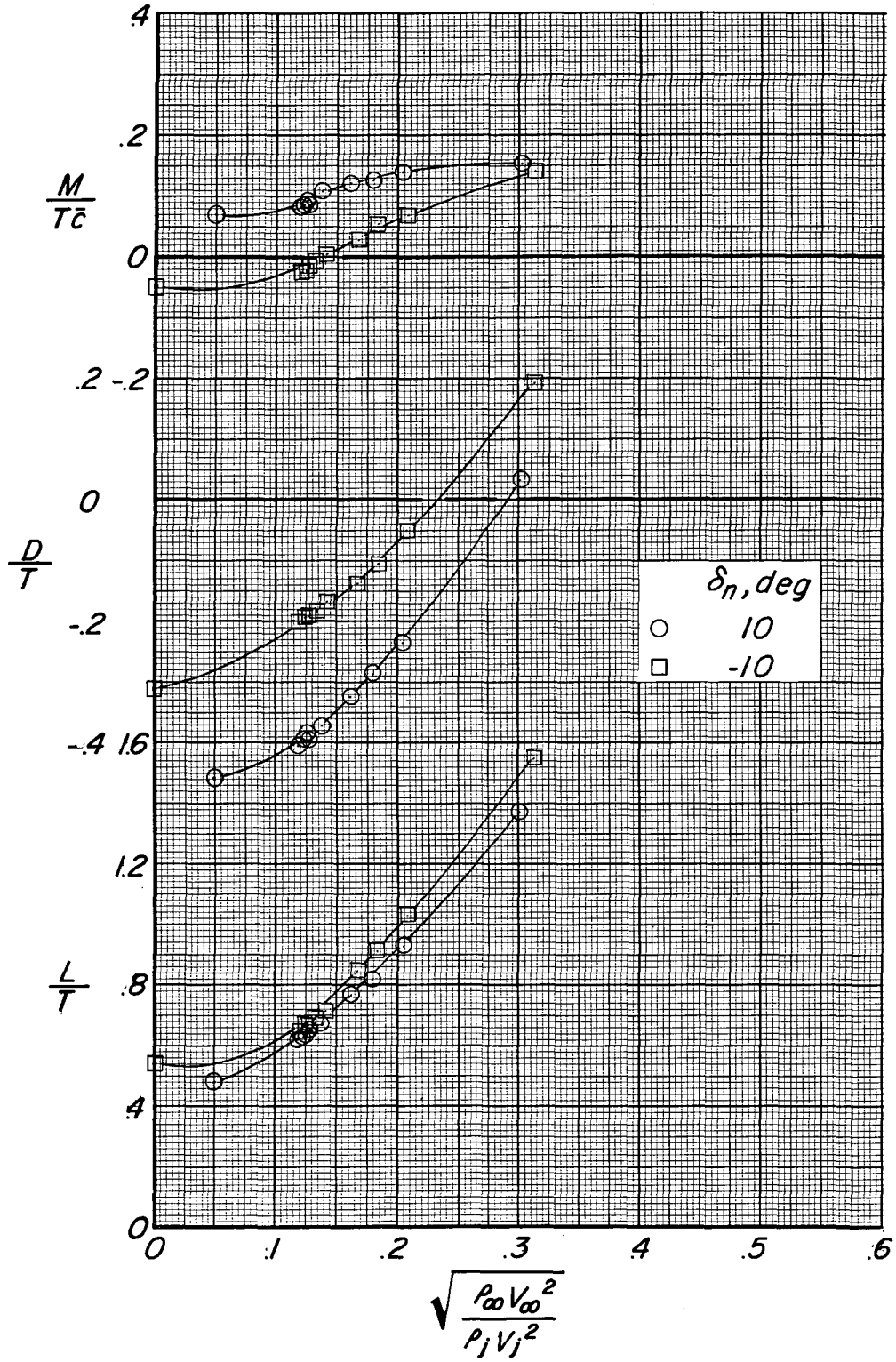

Figure 12.- Variation of $M/T\bar{c}$, D/T, and L/T with effective velocity ratio. Four lift nozzles and two cruise nozzles; $i_t = 0^0$; $\alpha = 0^0$.

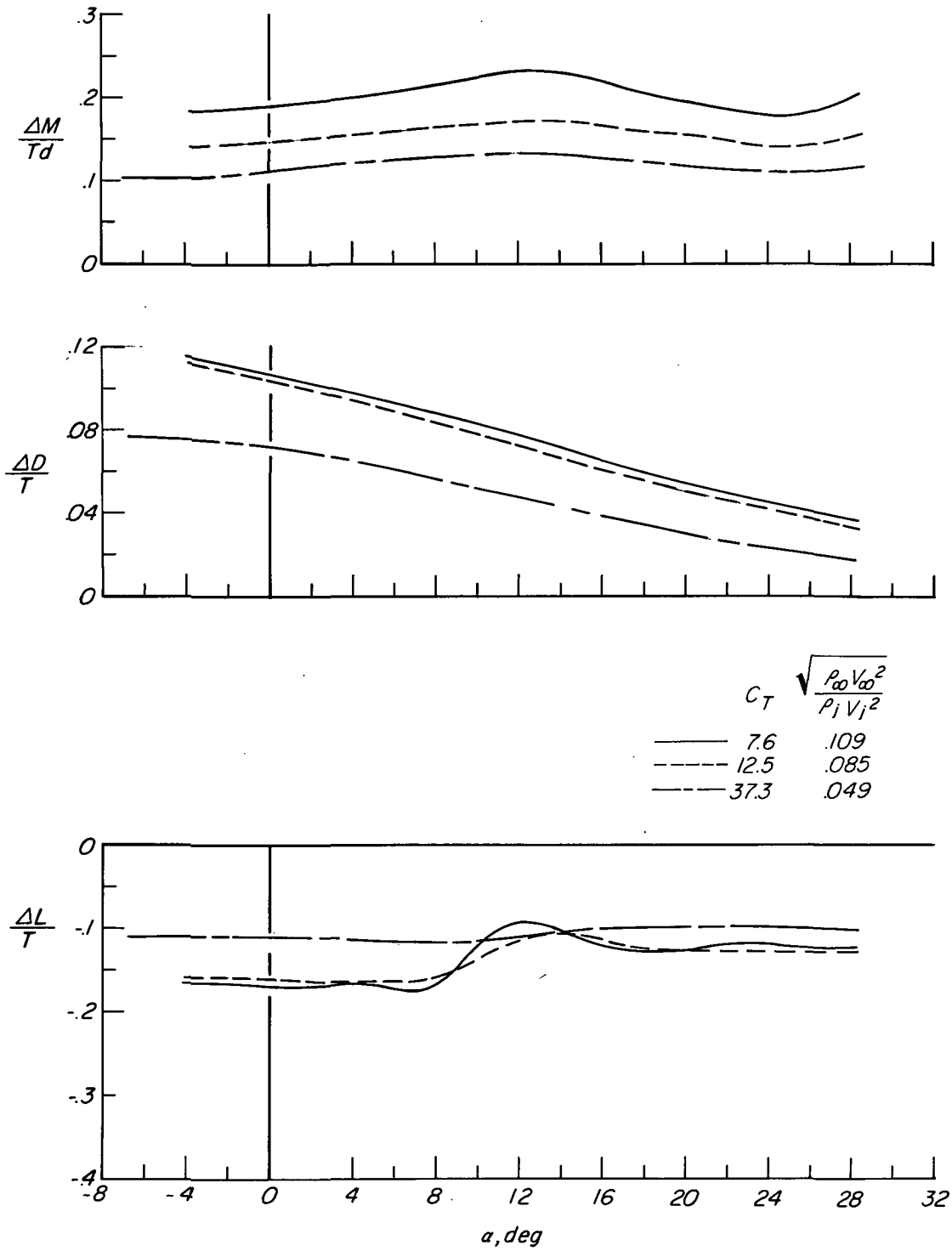

(a) $\delta_n = 10^0$.

Figure 13.- Effect of jet interference on longitudinal aerodynamic characteristics. Four lift nozzles and two cruise nozzles; $i_t = 0^0$.

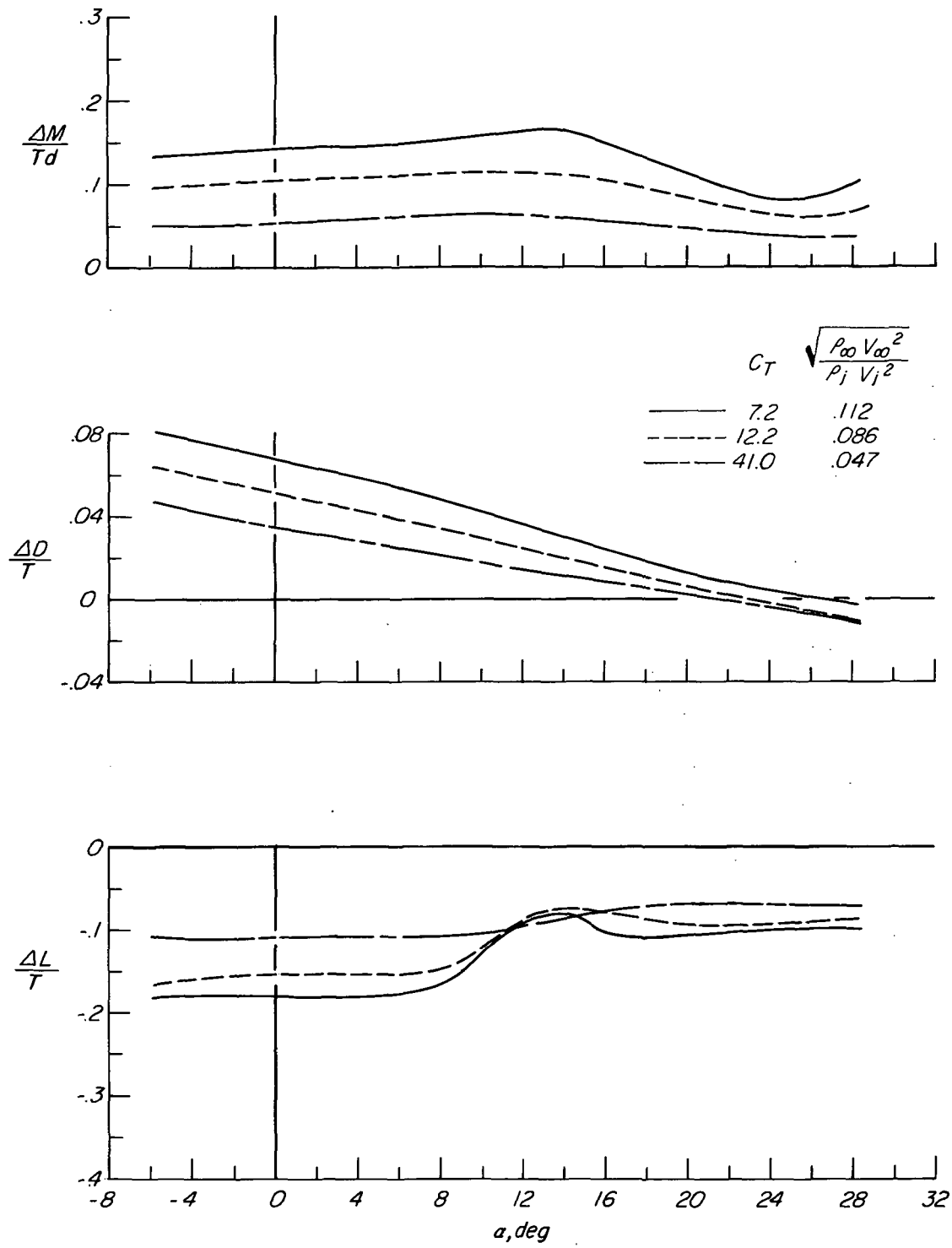

(b) $\delta_n = -10^0$.

Figure 13.- Concluded.

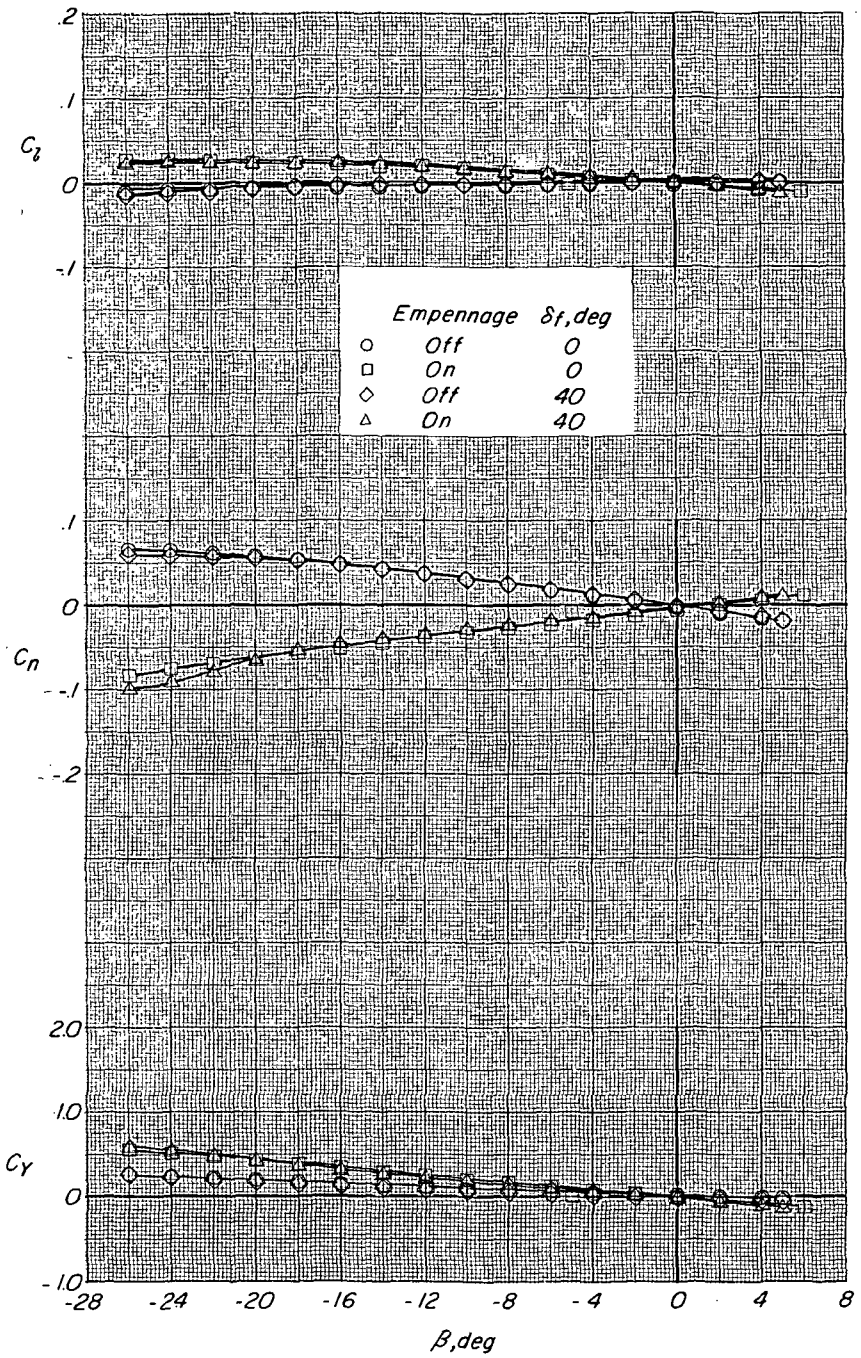

(a) Lateral-directional characteristics.

Figure 14.- Aerodynamic characteristics in sideslip showing effect of flap deflection with and without the empennage. Cruise configuration; $\alpha = 0^0$; $C_T = 0$.

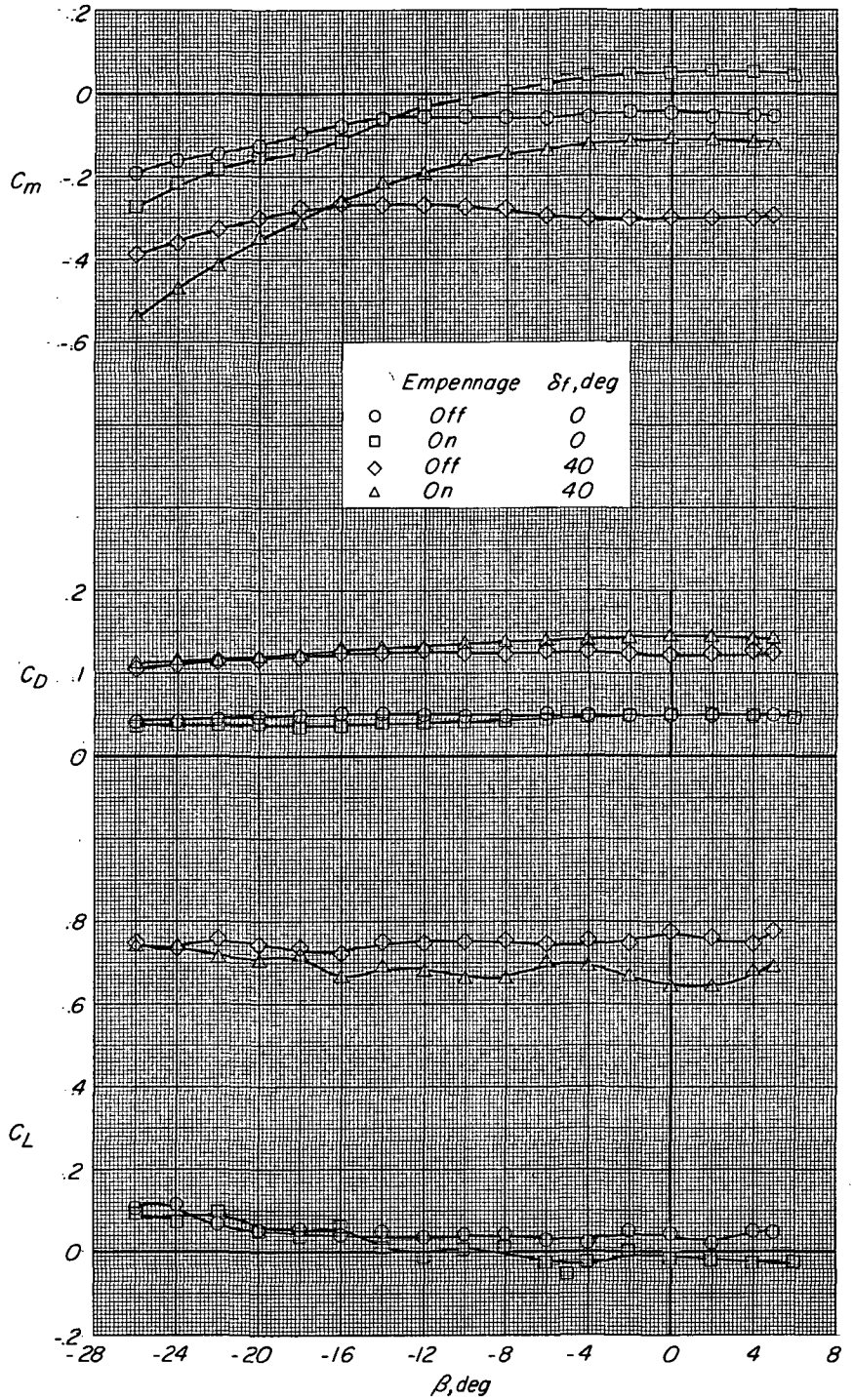

(b) Longitudinal characteristics.

Figure 14.- Concluded.

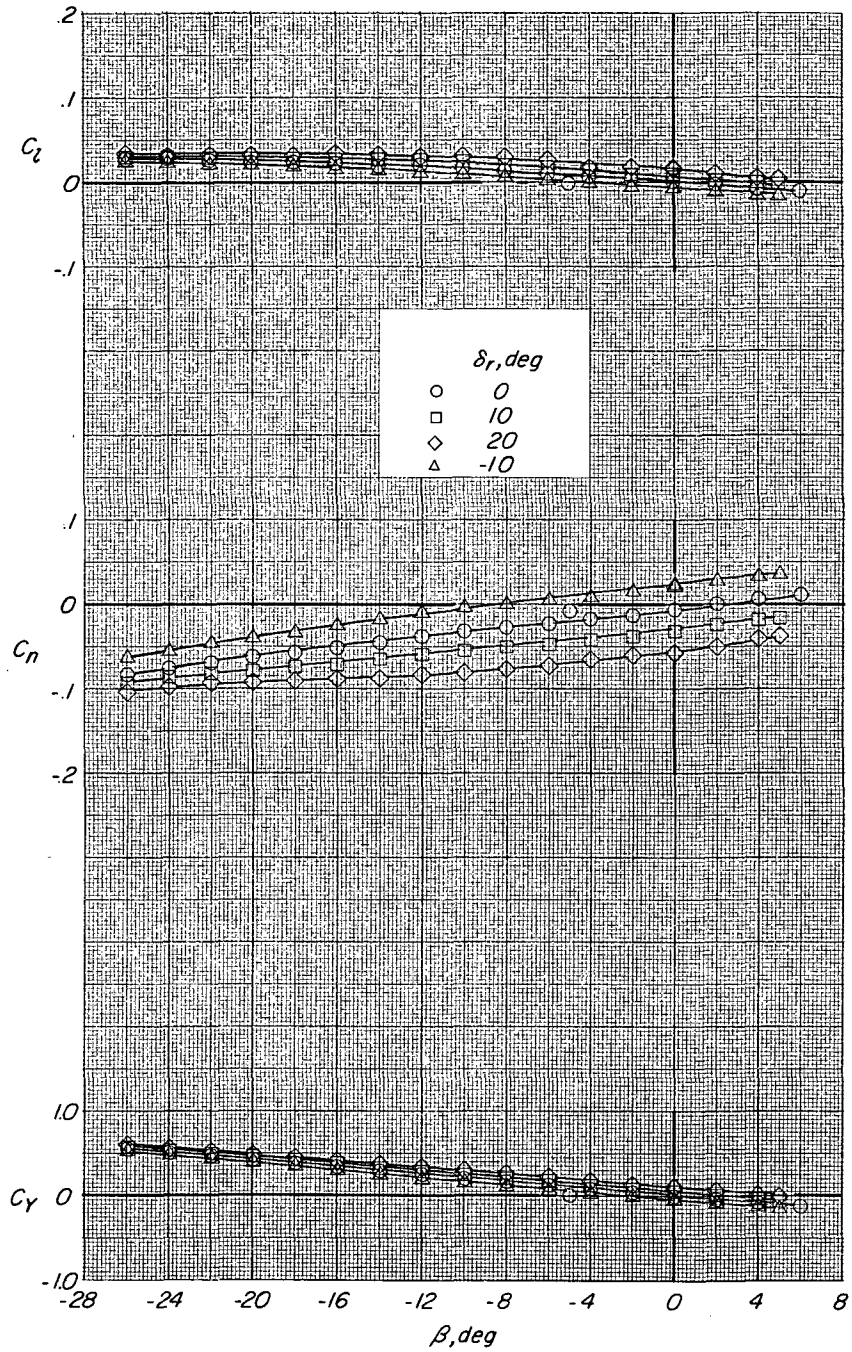

(a) Lateral-directional characteristics.

Figure 15.- Aerodynamic characteristics in sideslip showing effect of rudder deflection. Cruise configuration; $\alpha = 0^0$; $C_T = 0$; $\delta_f = 0^0$.

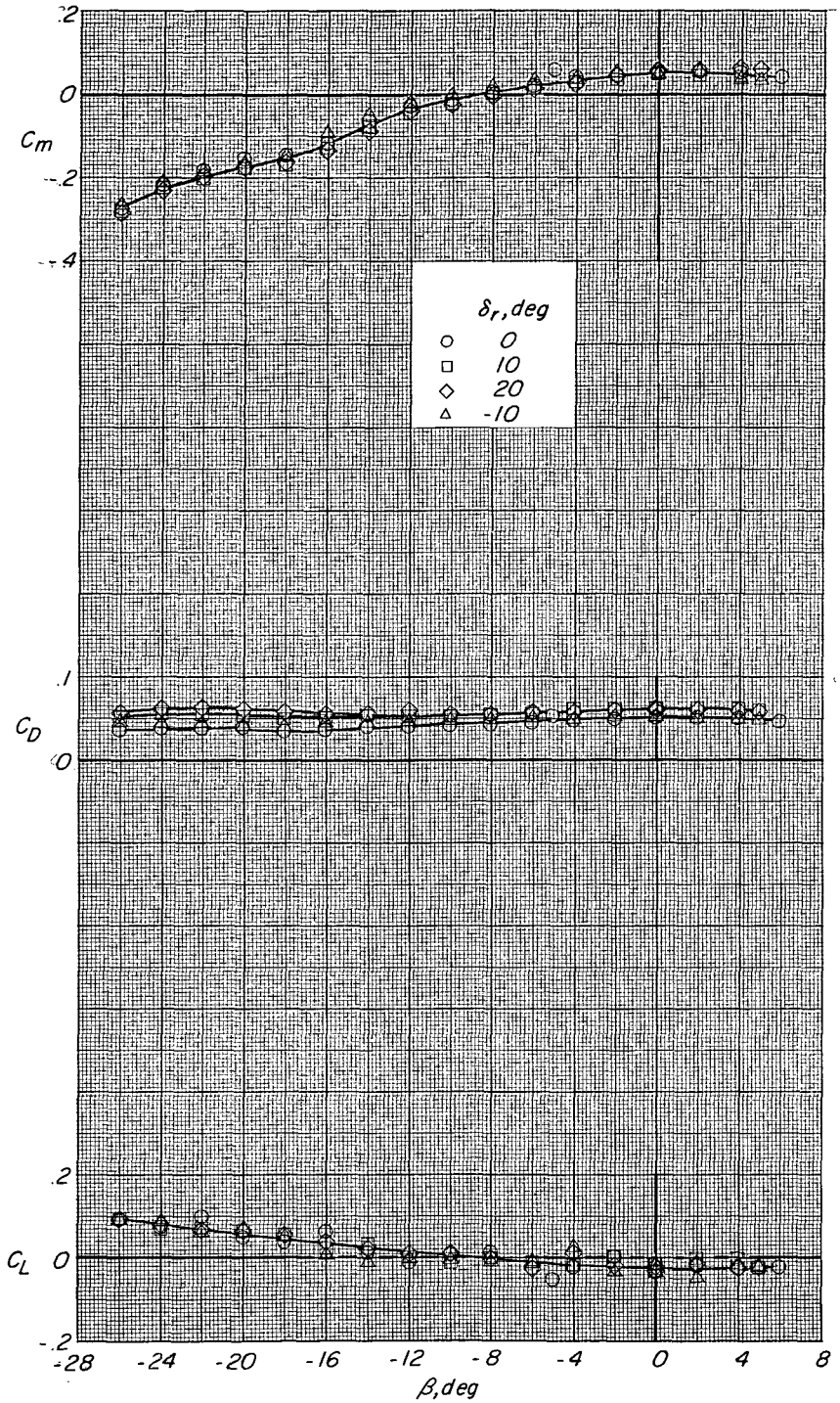

(b) Longitudinal characteristics.

Figure 15.- Concluded.

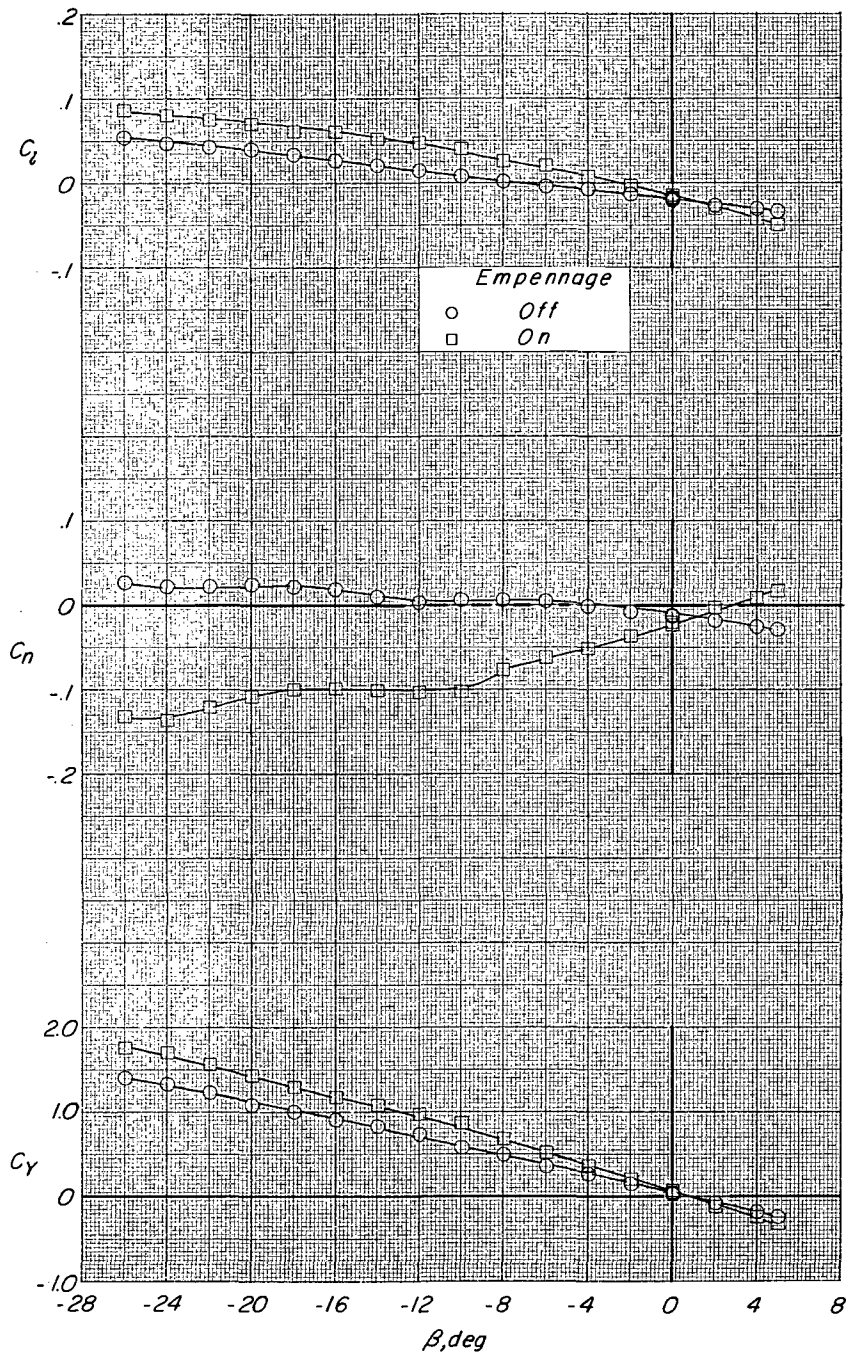

(a) Lateral-directional characteristics.

Figure 16.- Aerodynamic characteristics in sideslip showing effect of empennage. Six nozzles in lift mode; $\alpha = 0^0$; $C_T = 6.7$; $\delta_n = 0^0$.

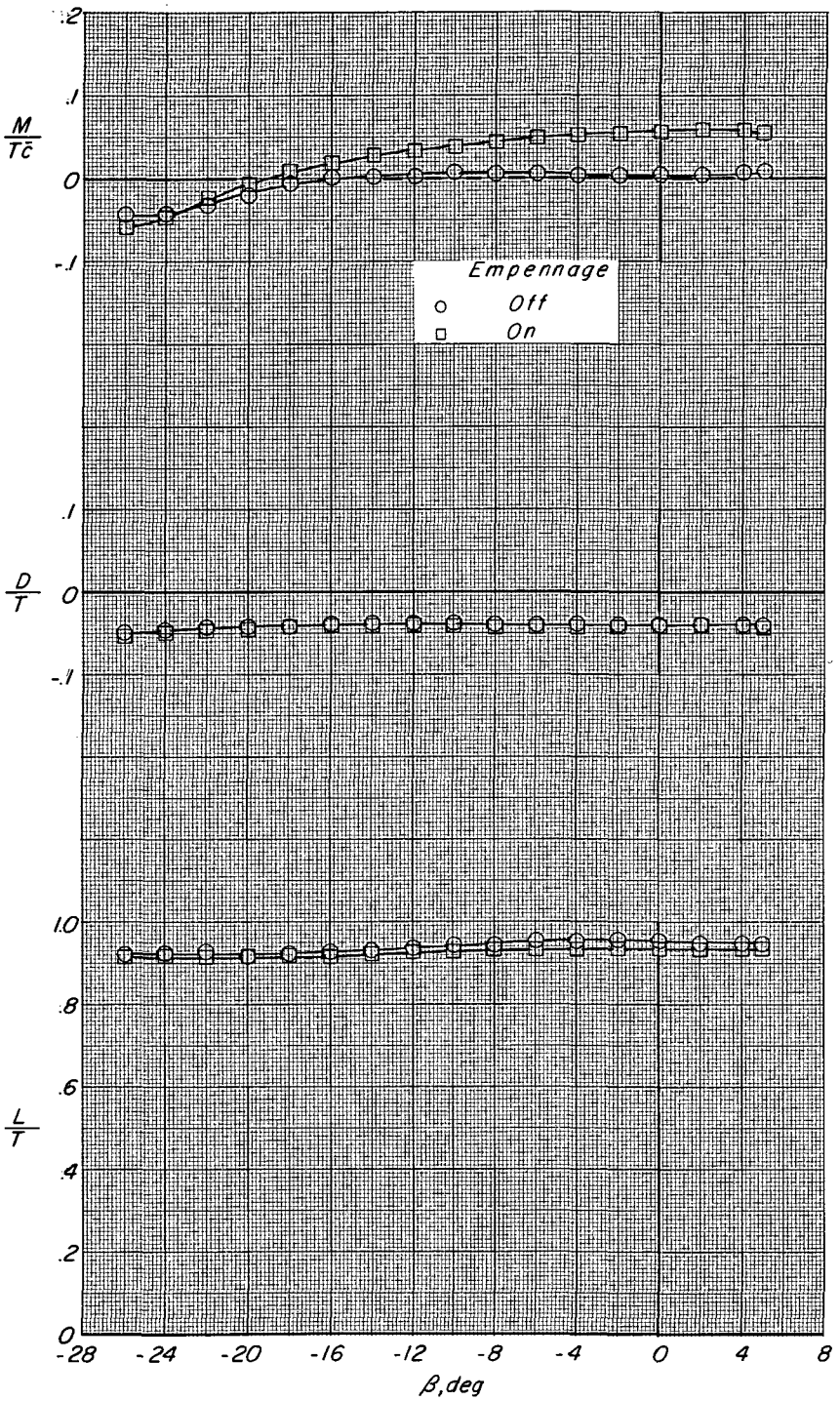

(b) Longitudinal characteristics.

Figure 16.- Concluded.

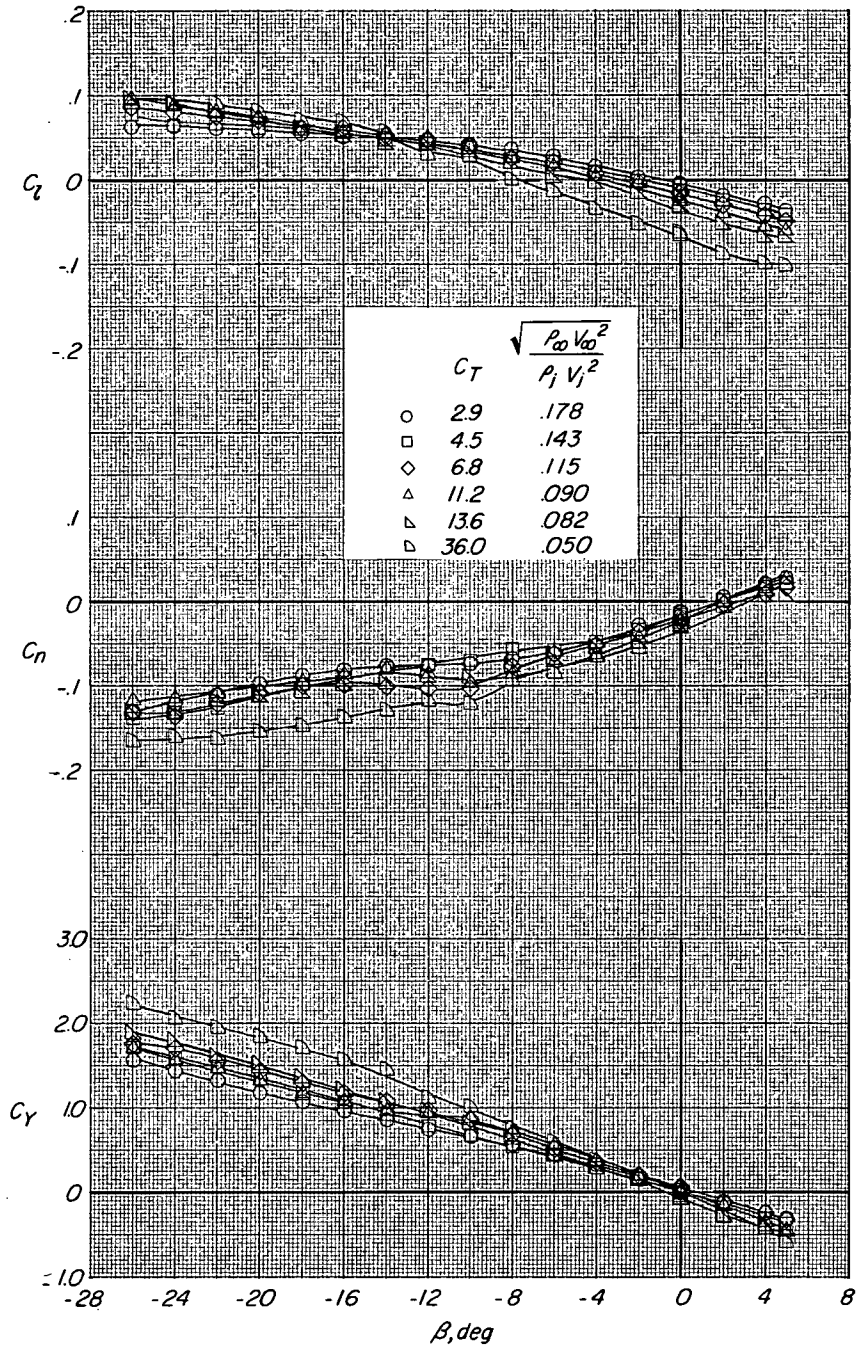

(a) Lateral-directional characteristics.

Figure 17.- Aerodynamic characteristics in sideslip showing effect of thrust coefficient. Six nozzles in lift mode; $\alpha = 0^0$; $\delta_n = 0^0$; $\delta_r = 0^0$.

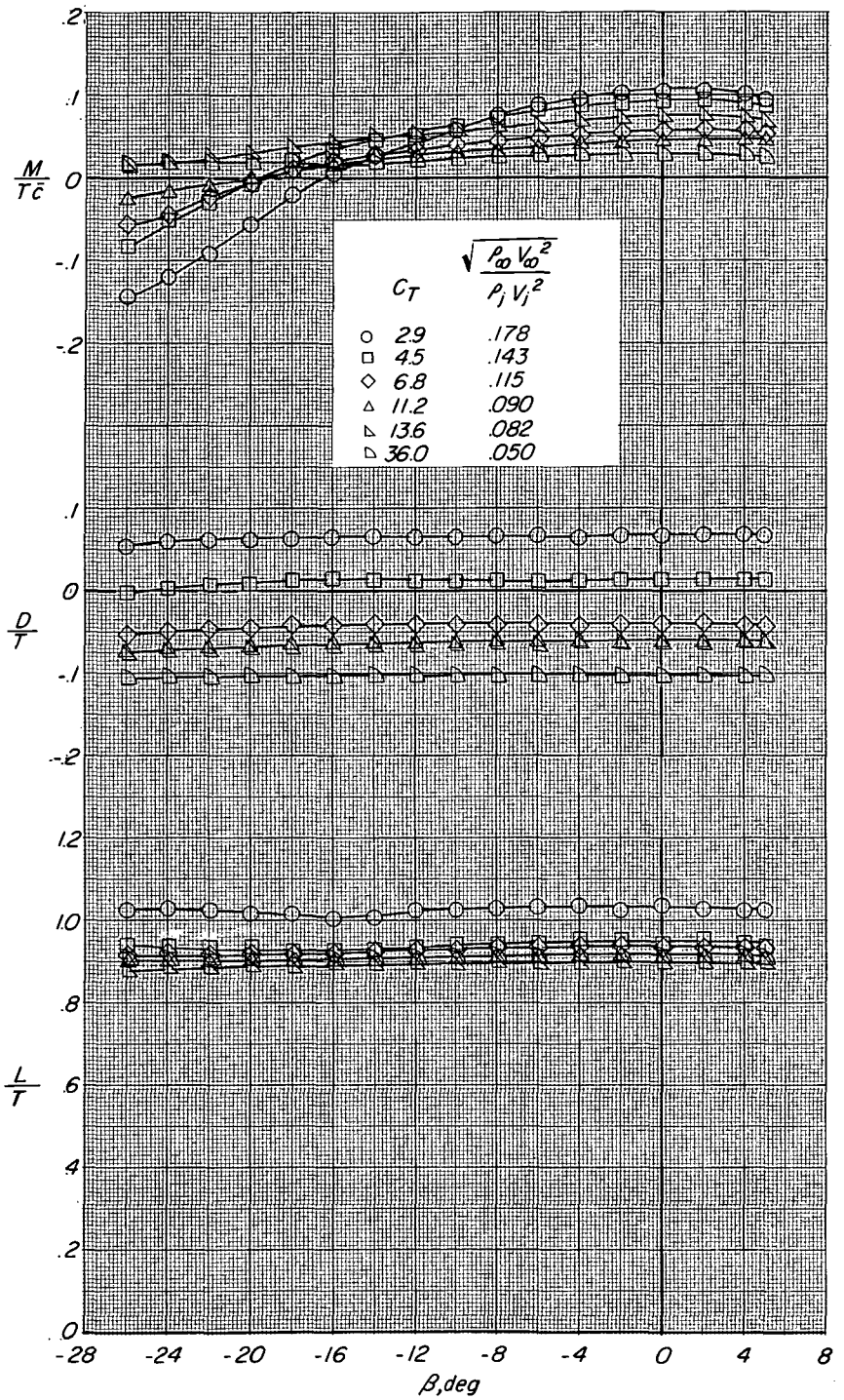

(b) Longitudinal characteristics.

Figure 17.- Concluded.

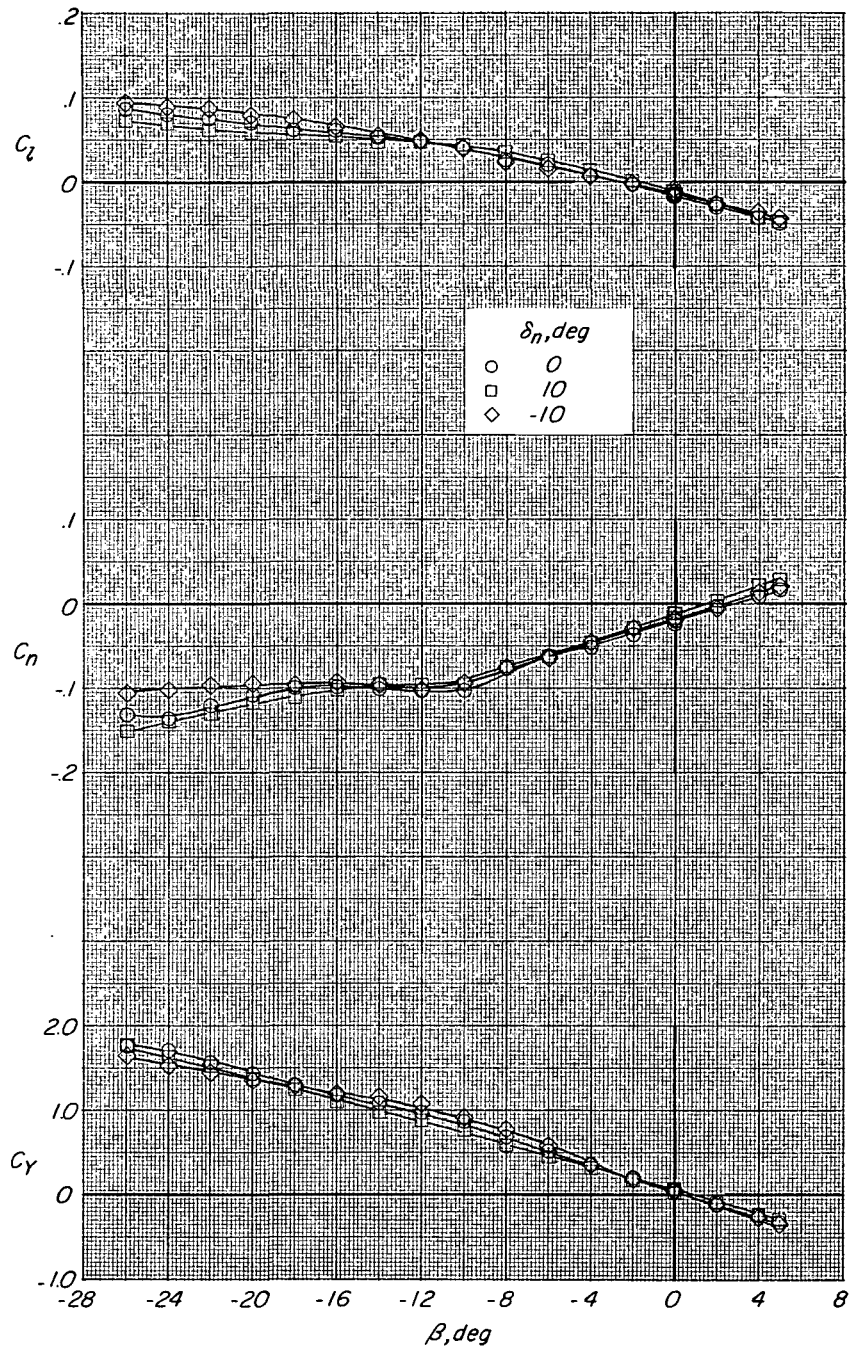

(a) Lateral-directional characteristics. C_T = 6.7.

Figure 18.- Aerodynamic characteristics in sideslip showing effect of jet exit-nozzle setting. Six nozzles in lift mode; $\alpha = 0^o$; $\delta_r = 0^o$.

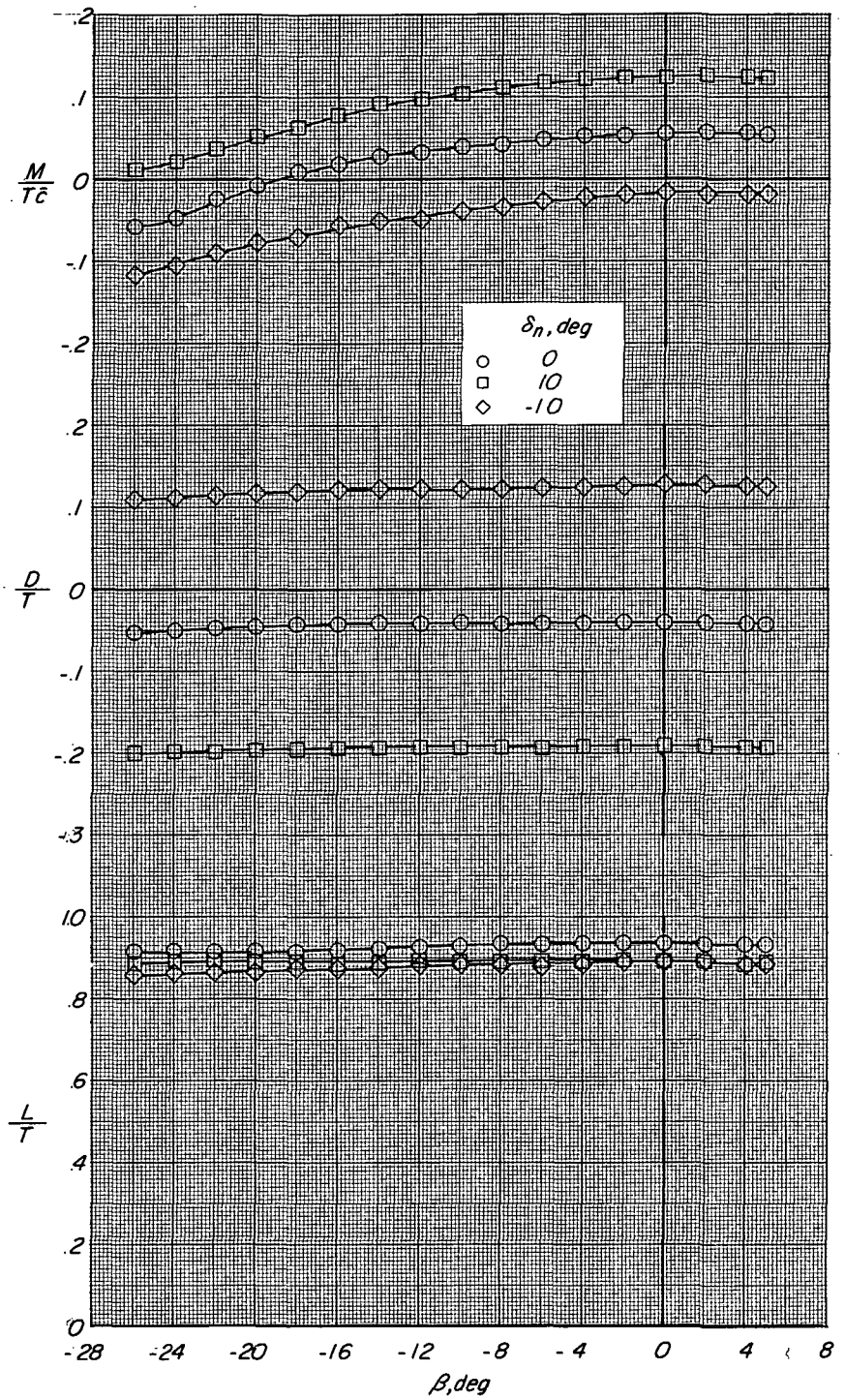

(b) Longitudinal characteristics. C_T = 6.7.

Figure 18.- Continued.

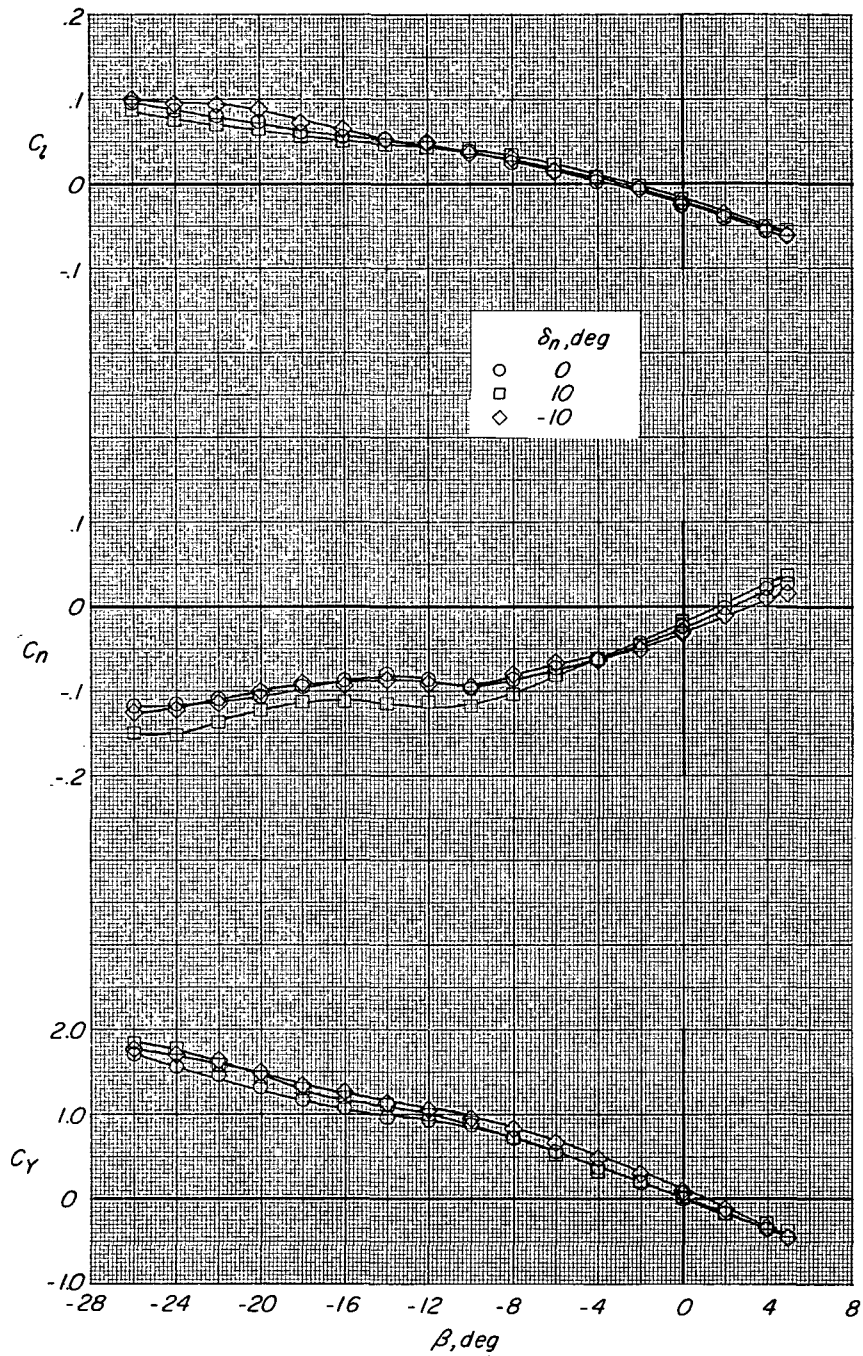

(c) Lateral-directional characteristics. C_T = 11.0.

Figure 18.- Continued.

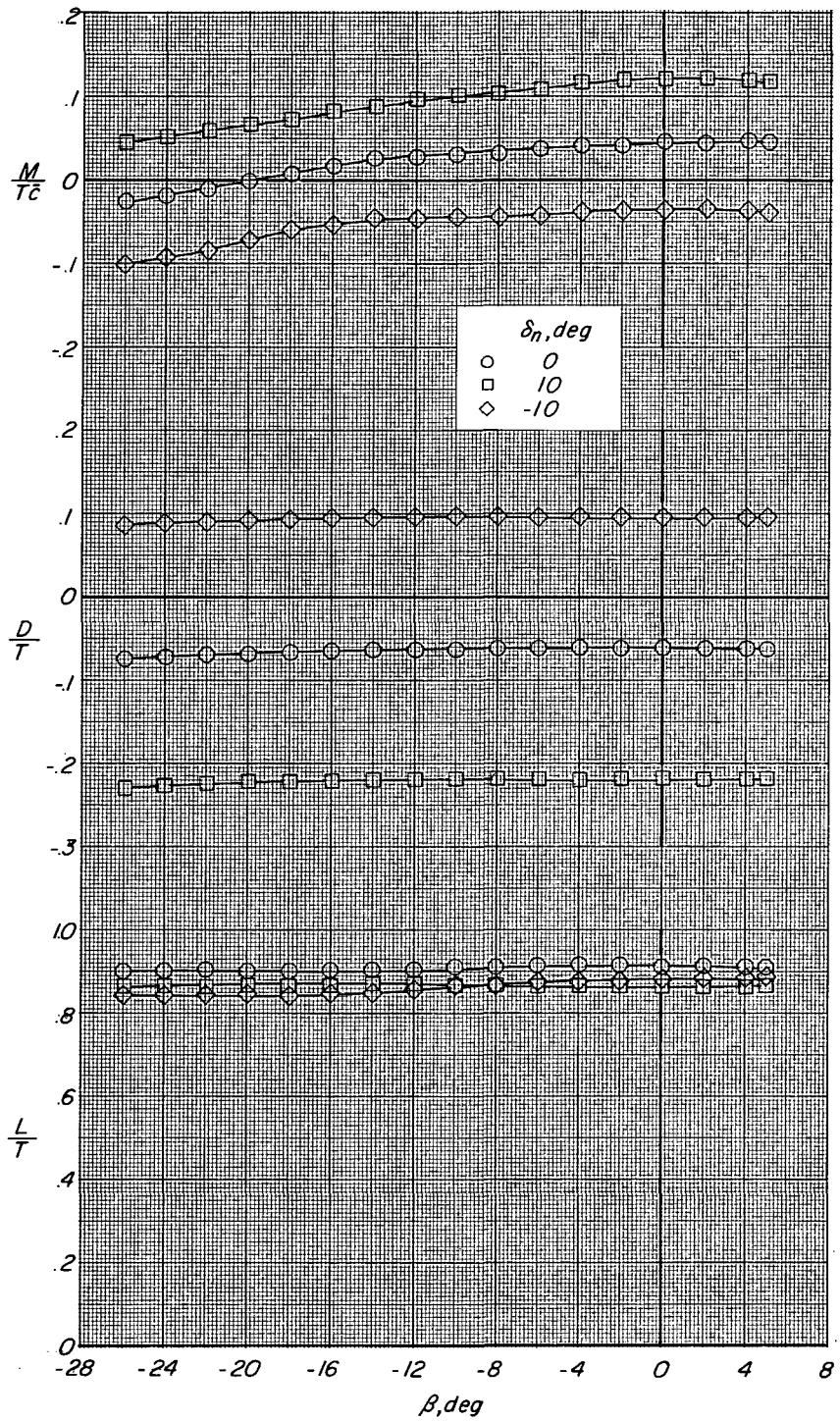

(d) Longitudinal characteristics. C_T = 11.0.

Figure 18.- Continued.

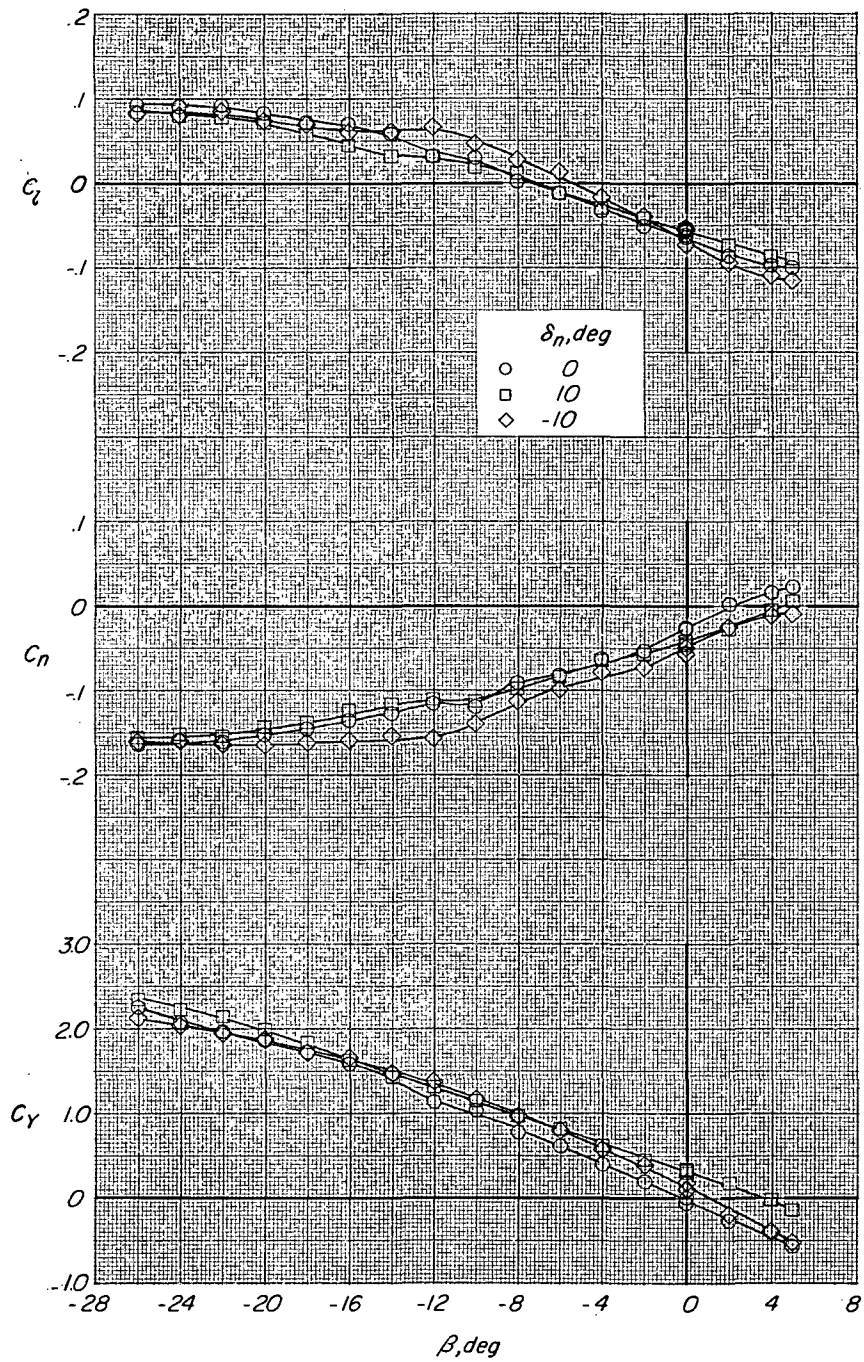

(e) Lateral-directional characteristics. C_T = 35.0.

Figure 18.- Continued.

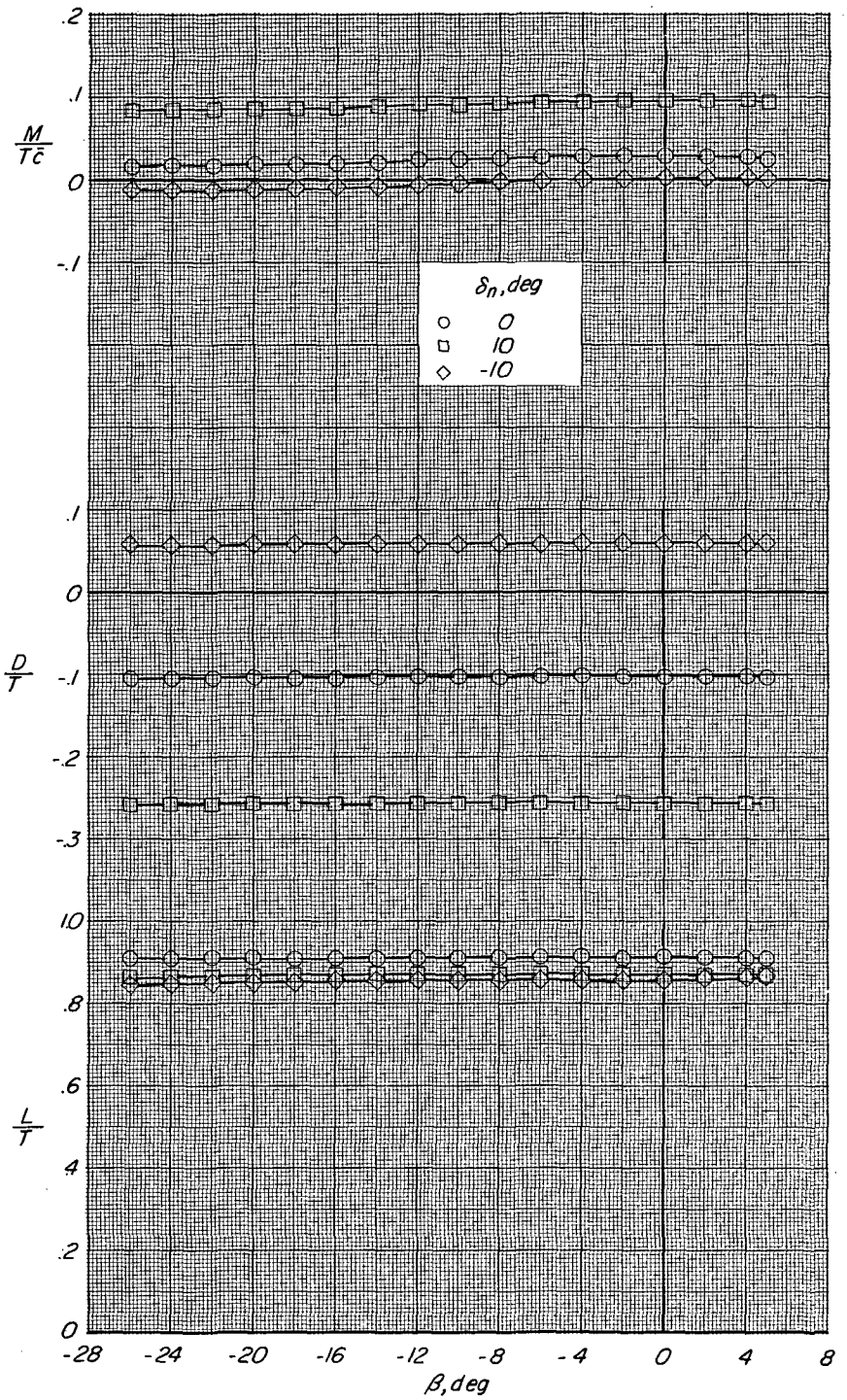

(f) Longitudinal characteristics. C_T = 35.0.

Figure 18.- Concluded.

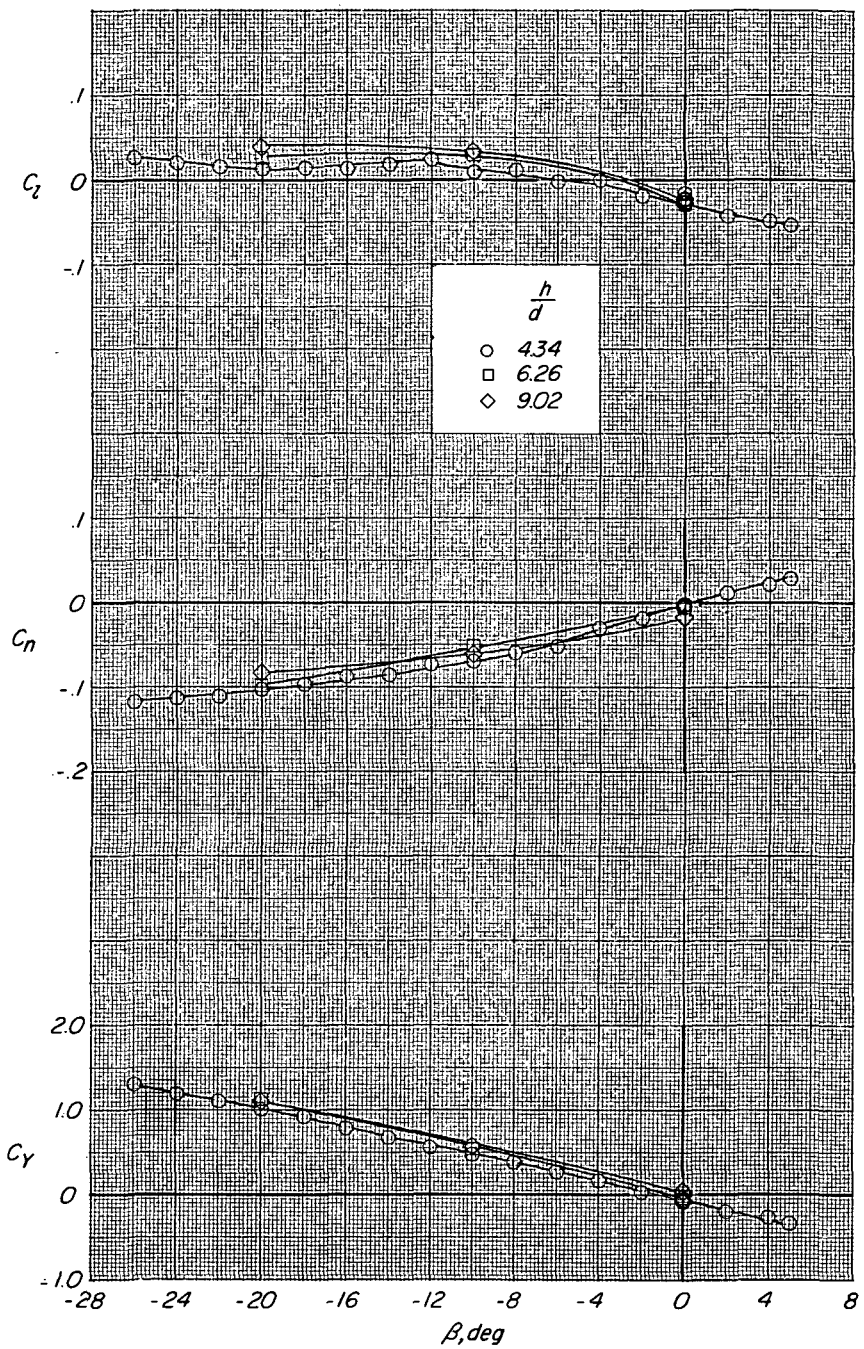

(a) Lateral-directional characteristics. $C_T = 6.7$.

Figure 19.- Aerodynamic characteristics in sideslip over moving ground plane. Six nozzles in lift mode; $\alpha = 0^0$; $\delta_n = 0^0$; $\delta_r = 0^0$.

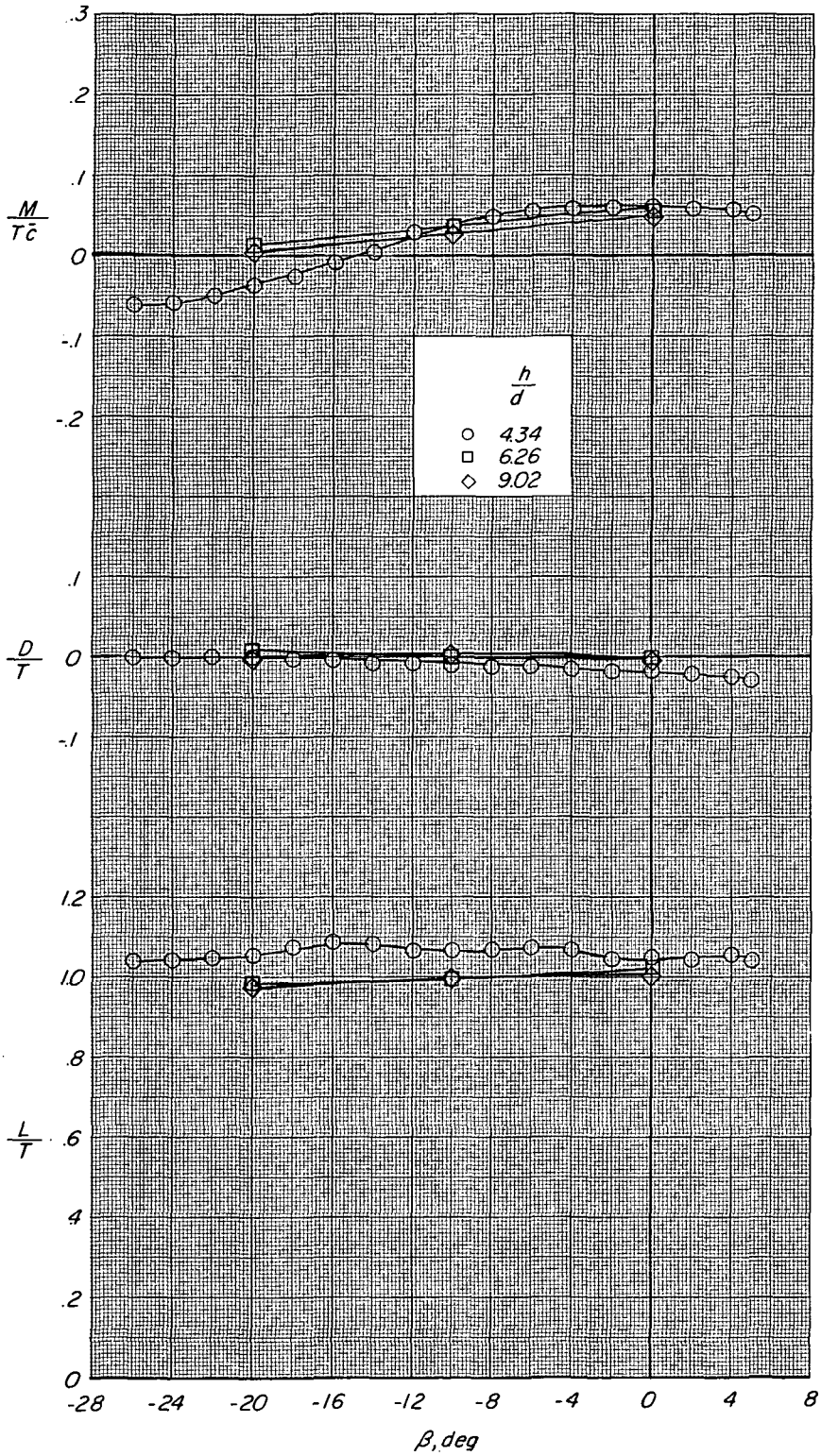

(b) Longitudinal characteristics. $C_T = 6.7$.

Figure 19.- Continued.

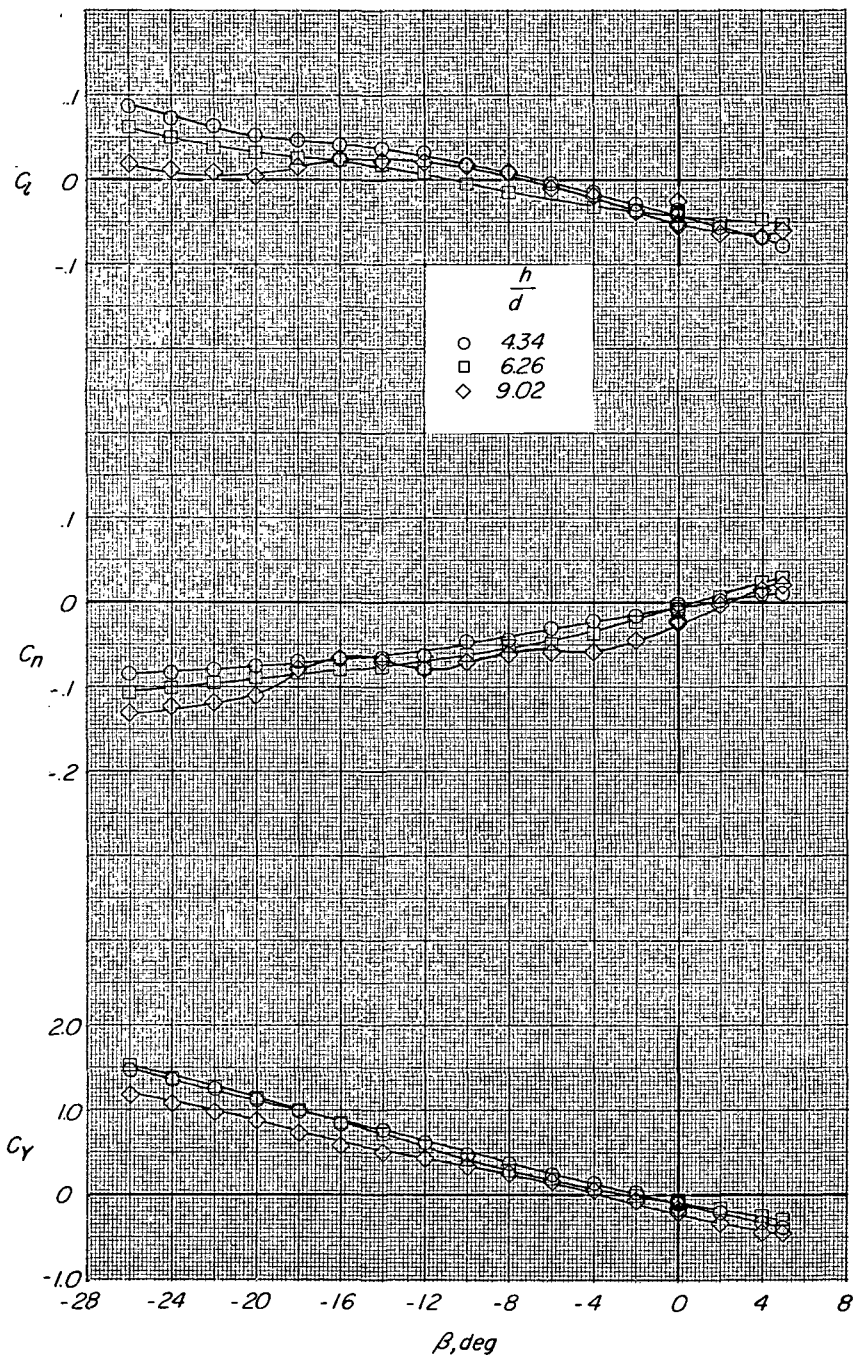

(c) Lateral-directional characteristics. C_T = 11.0.

Figure 19.- Continued.

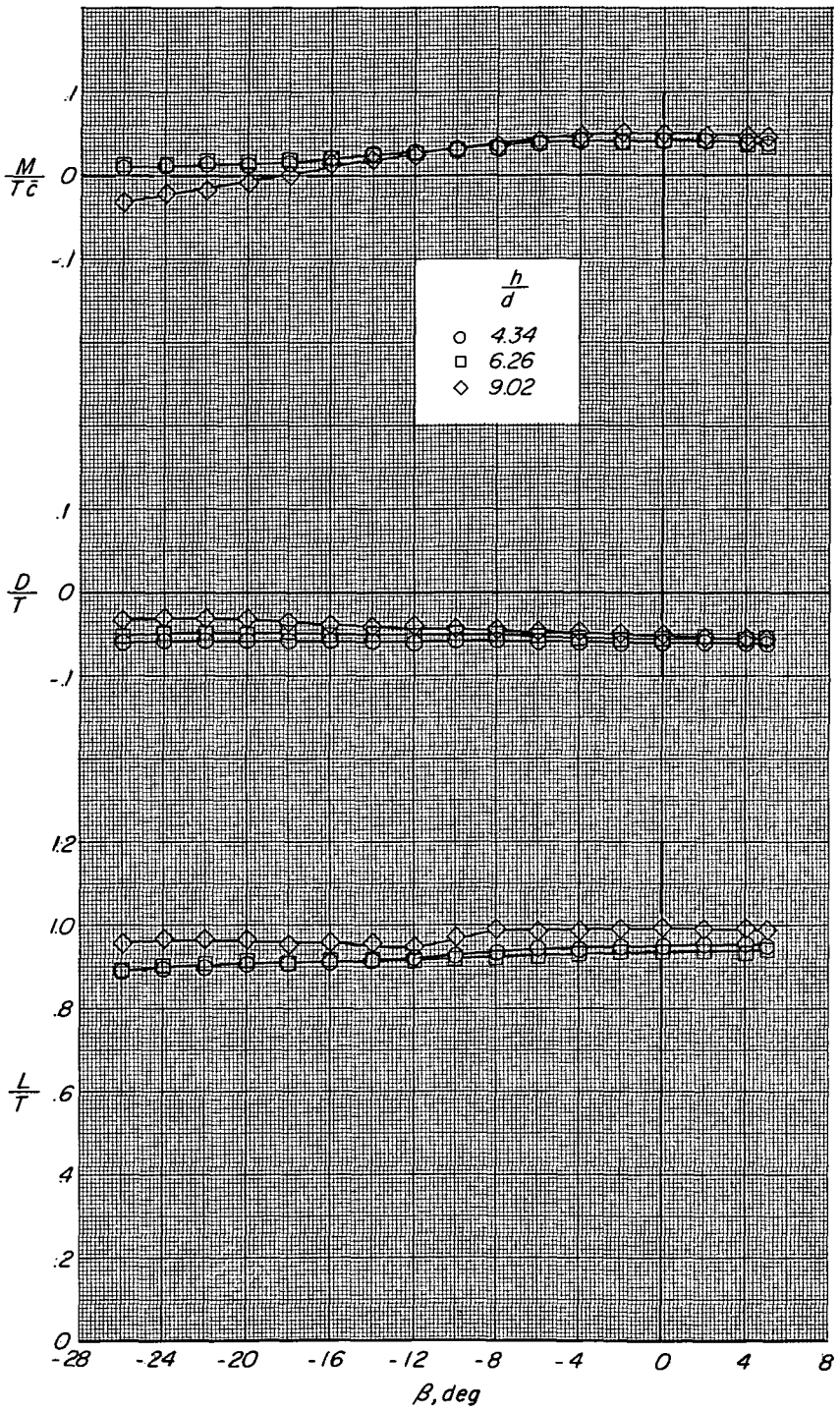

(d) Longitudinal characteristics. C_T = 11.0.

Figure 19.- Continued.

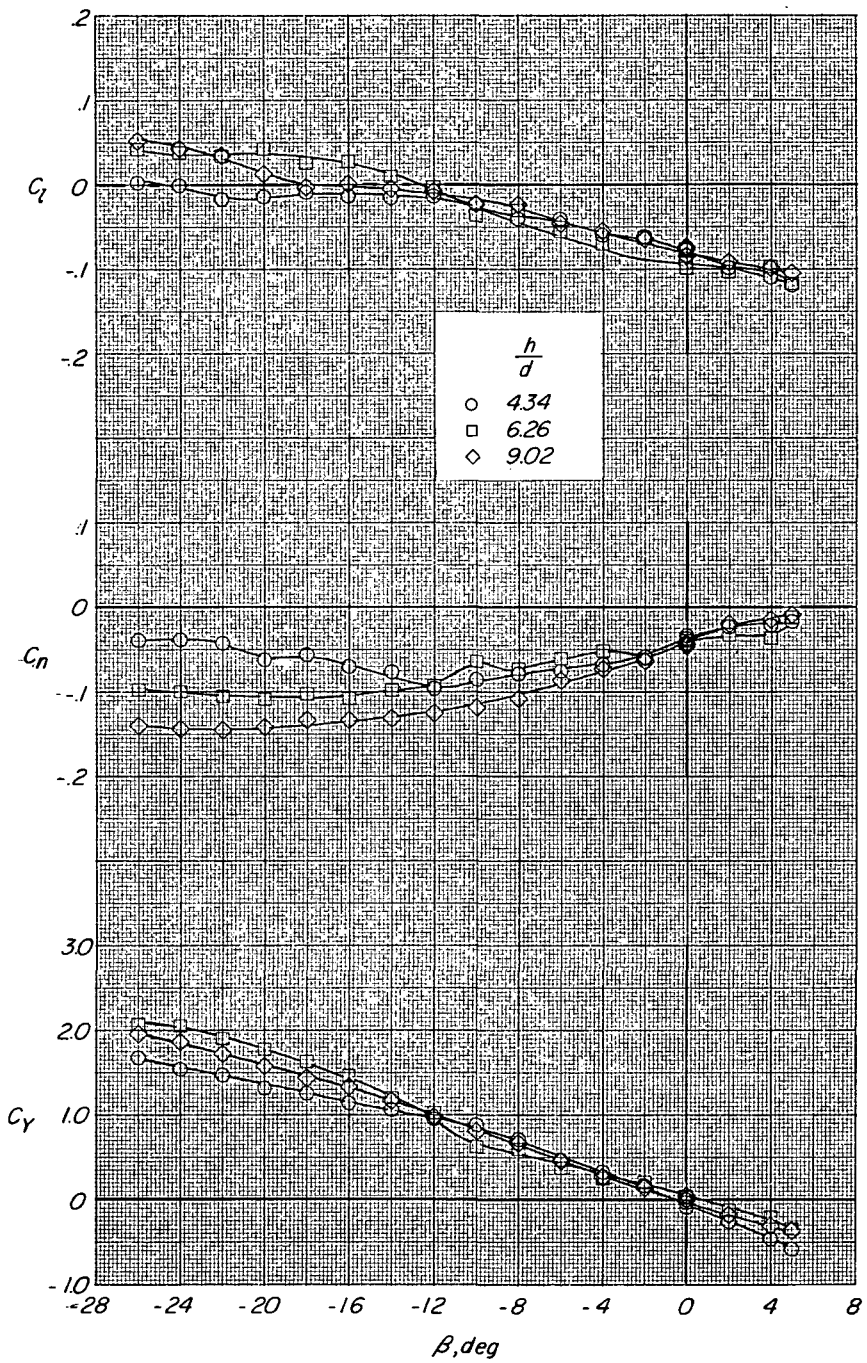

(e) Lateral-directional characteristics. C_T = 35.0.

Figure 19.- Continued.

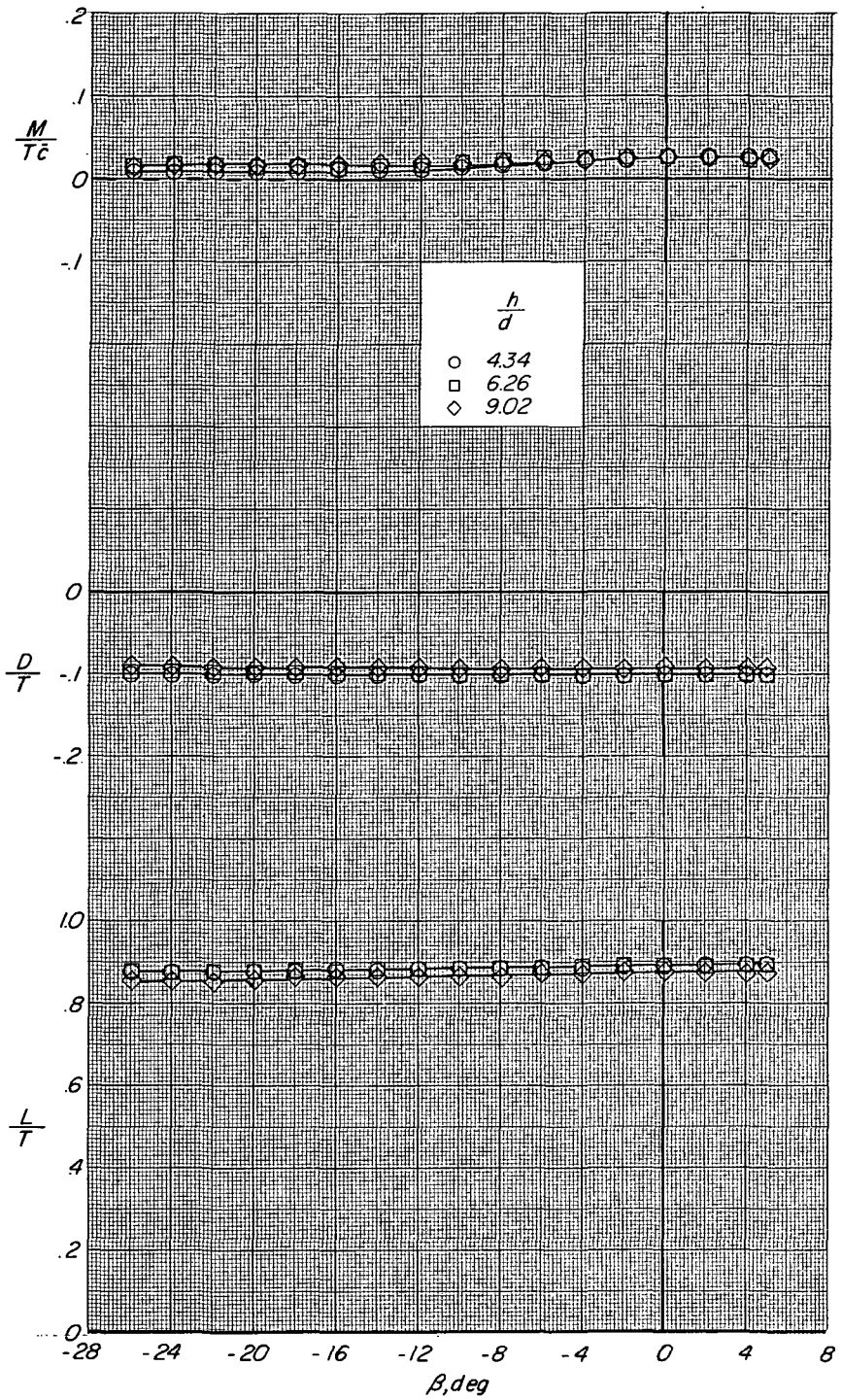

(f) Longitudinal characteristics. $C_T = 35.0$.

Figure 19.- Concluded.

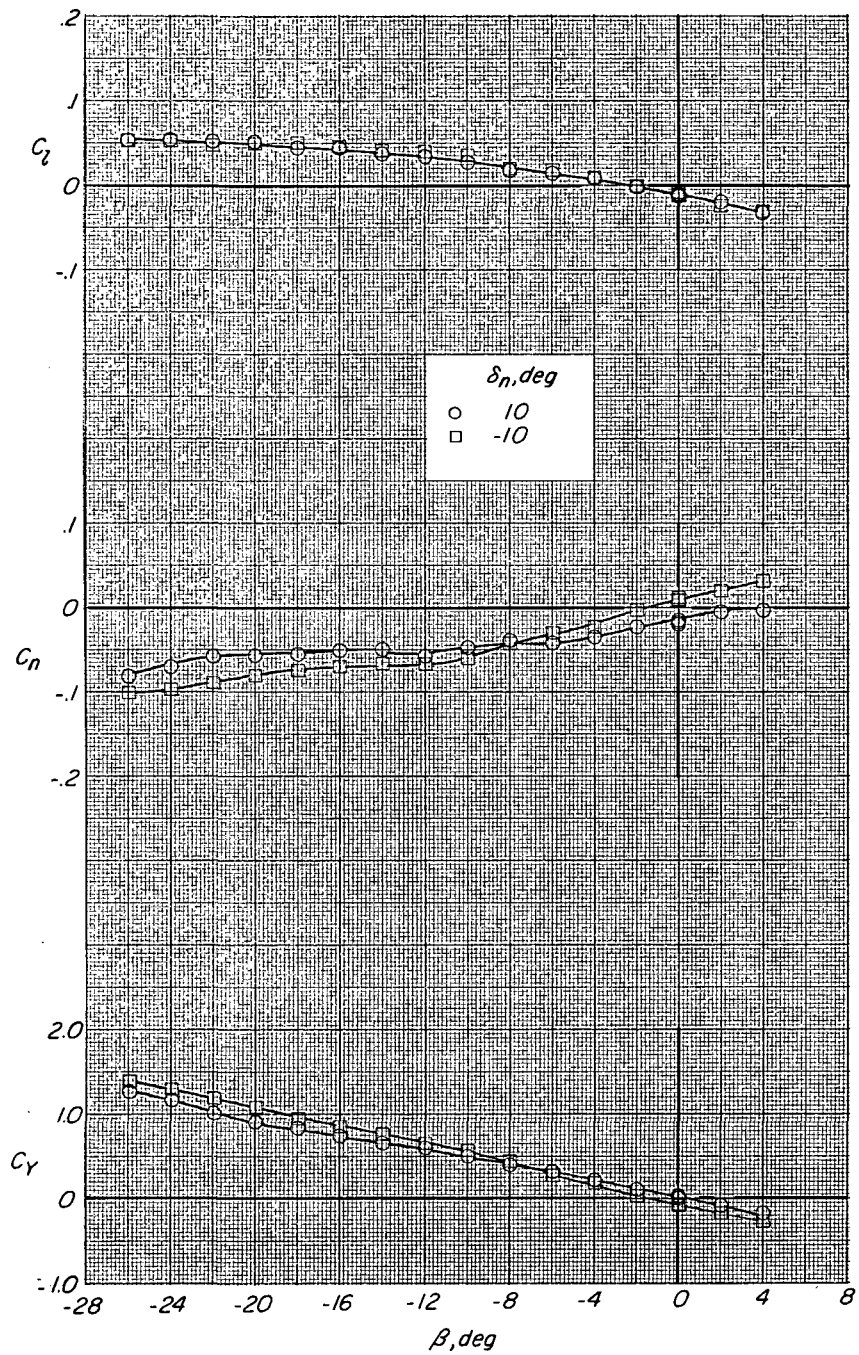

(a) Lateral-directional characteristics. $C_T = 7.5$.

Figure 20.- Aerodynamic characteristics in sideslip showing effect of jet exit-nozzle setting. Four lift nozzles and two cruise nozzles; $\alpha = 0^0$; $\delta_r = 0^0$.

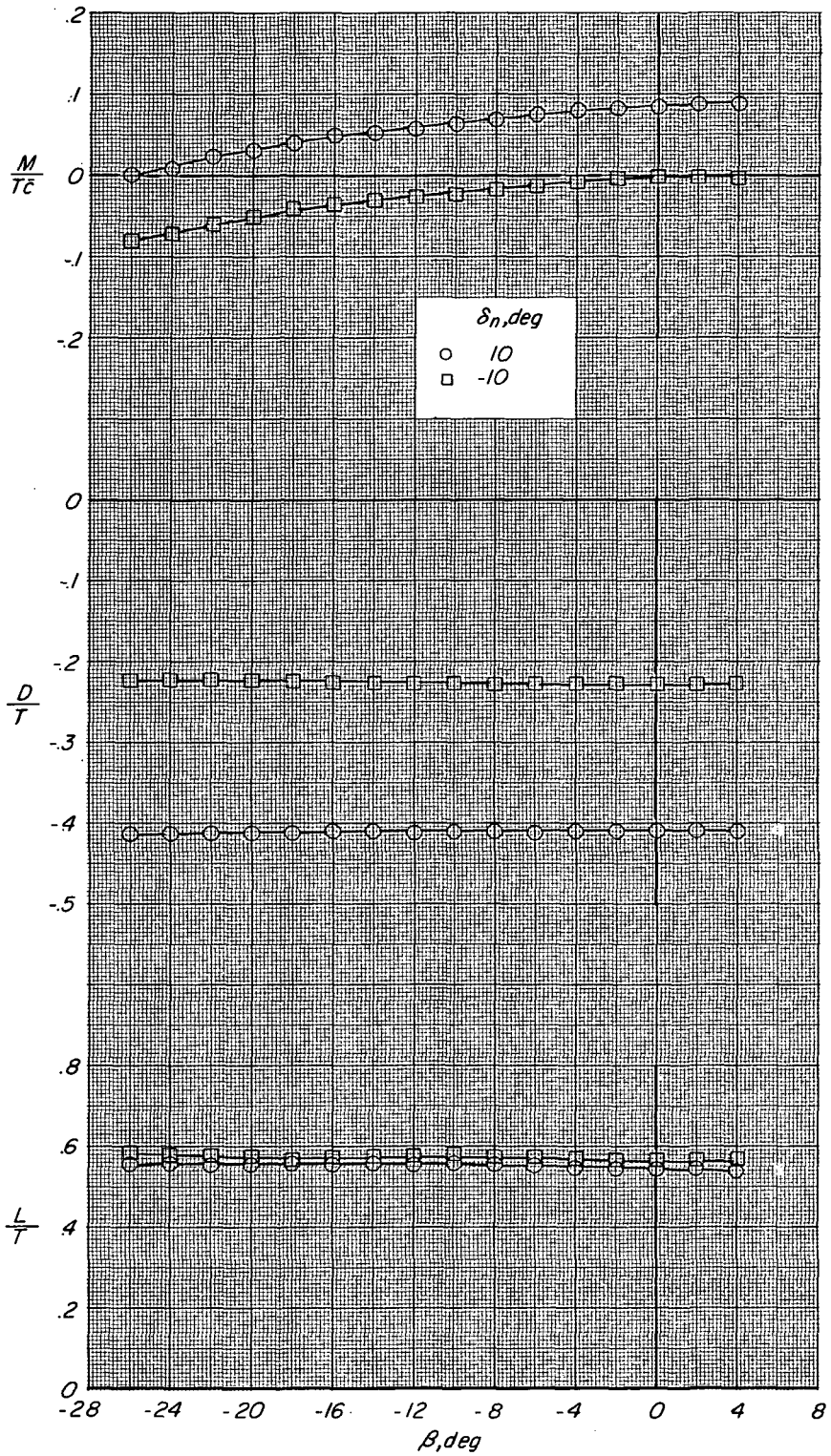

(b) Longitudinal characteristics. C_T = 7.5.

Figure 20.- Continued.

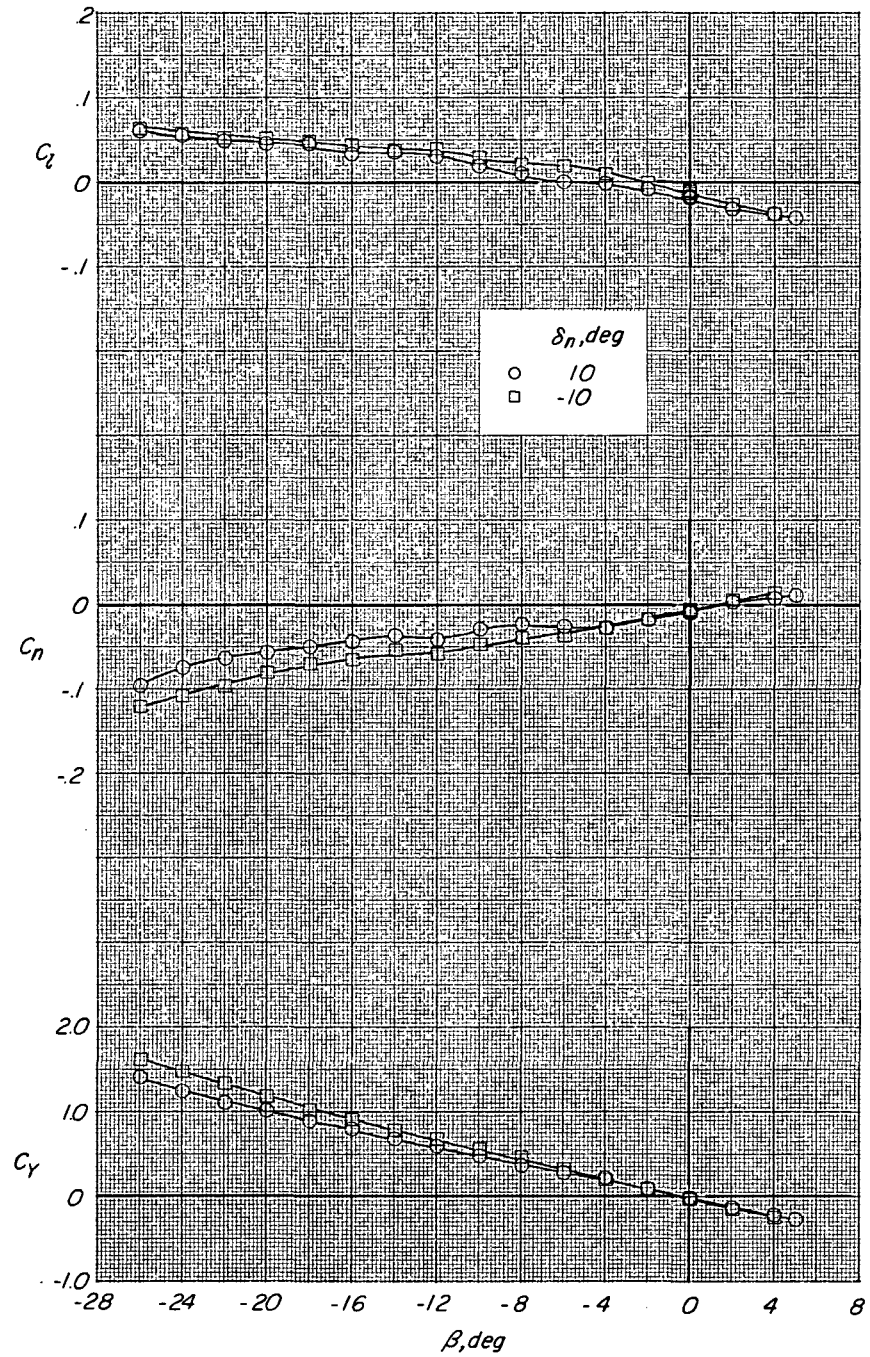

(c) Lateral-directional characteristics. C_T = 12.5.

Figure 20.- Continued.

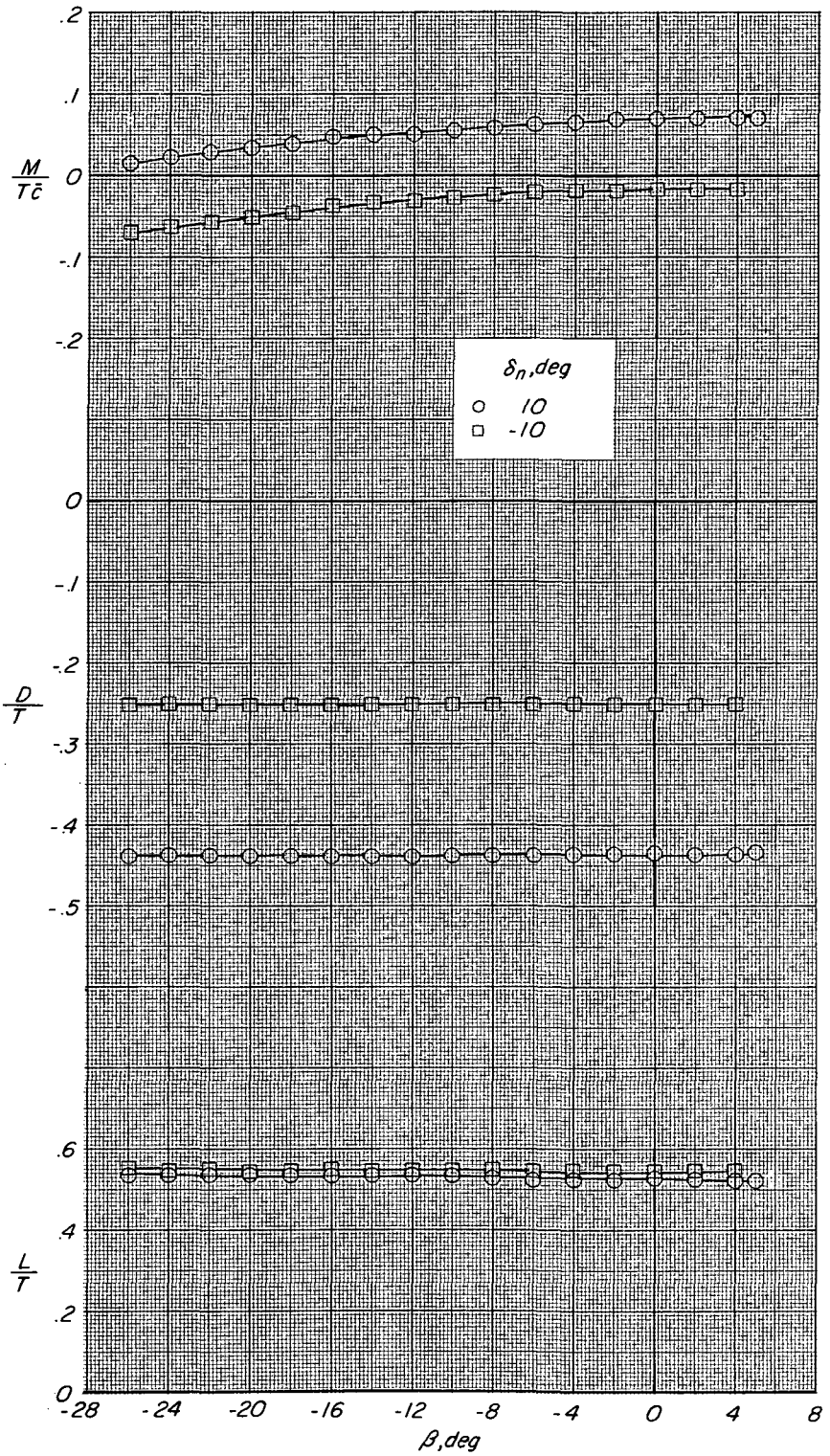

(d) Longitudinal characteristics. C_T = 12.5.

Figure 20.- Continued.

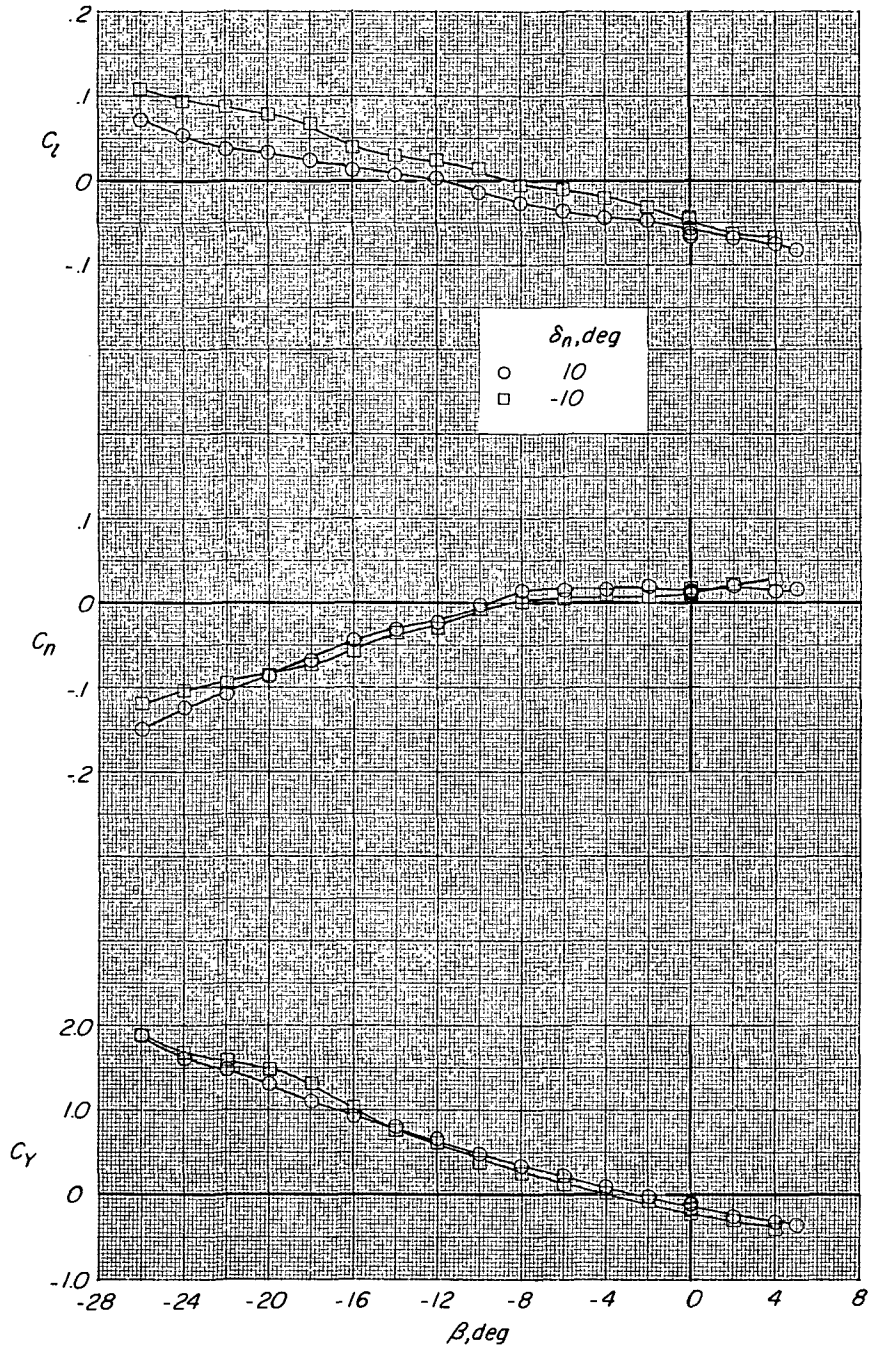

(e) Lateral-directional characteristics. C_T = 40.0.

Figure 20.- Continued.

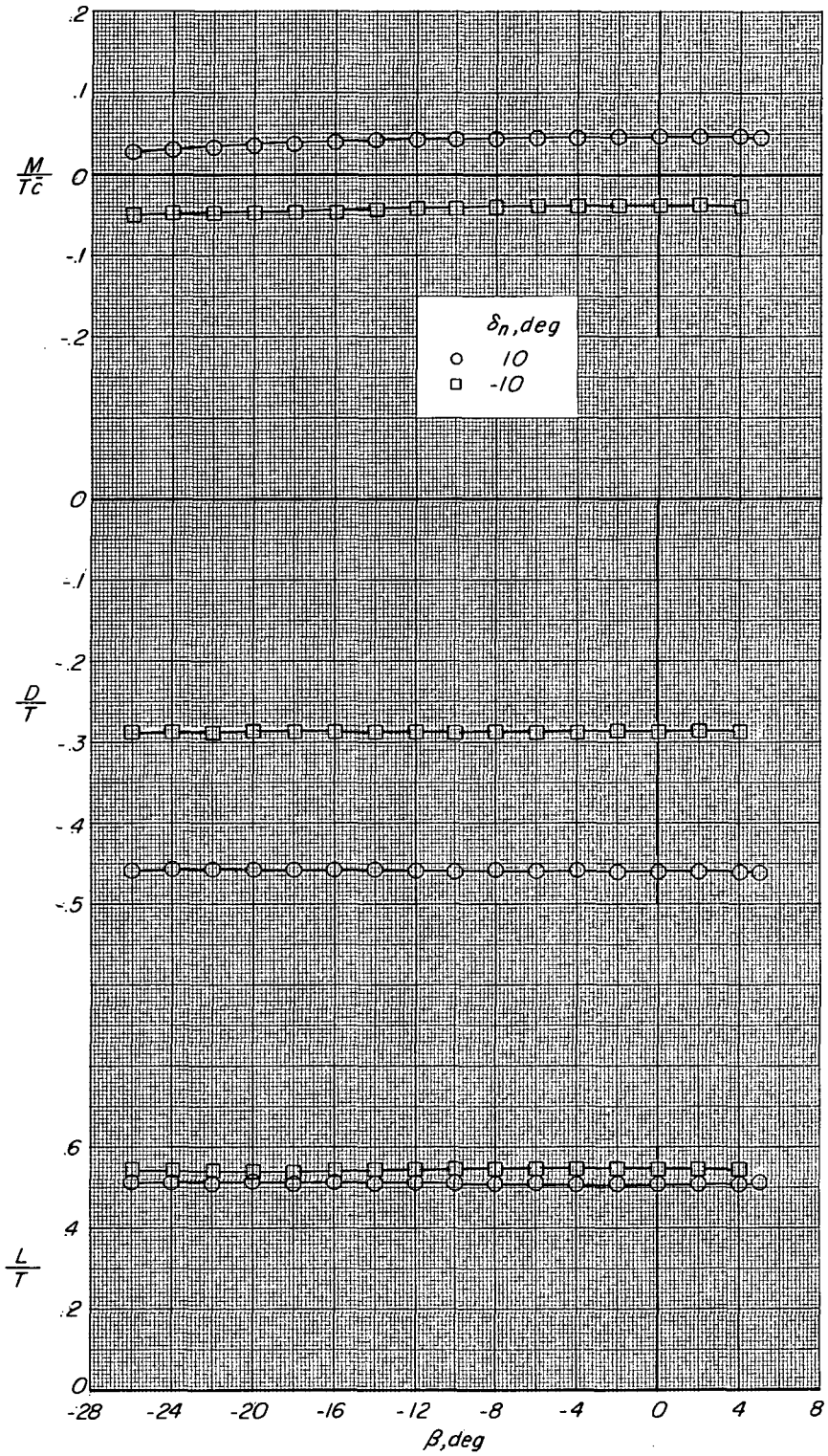

(f) Longitudinal characteristics. C_T = 40.0.

Figure 20.- Concluded.

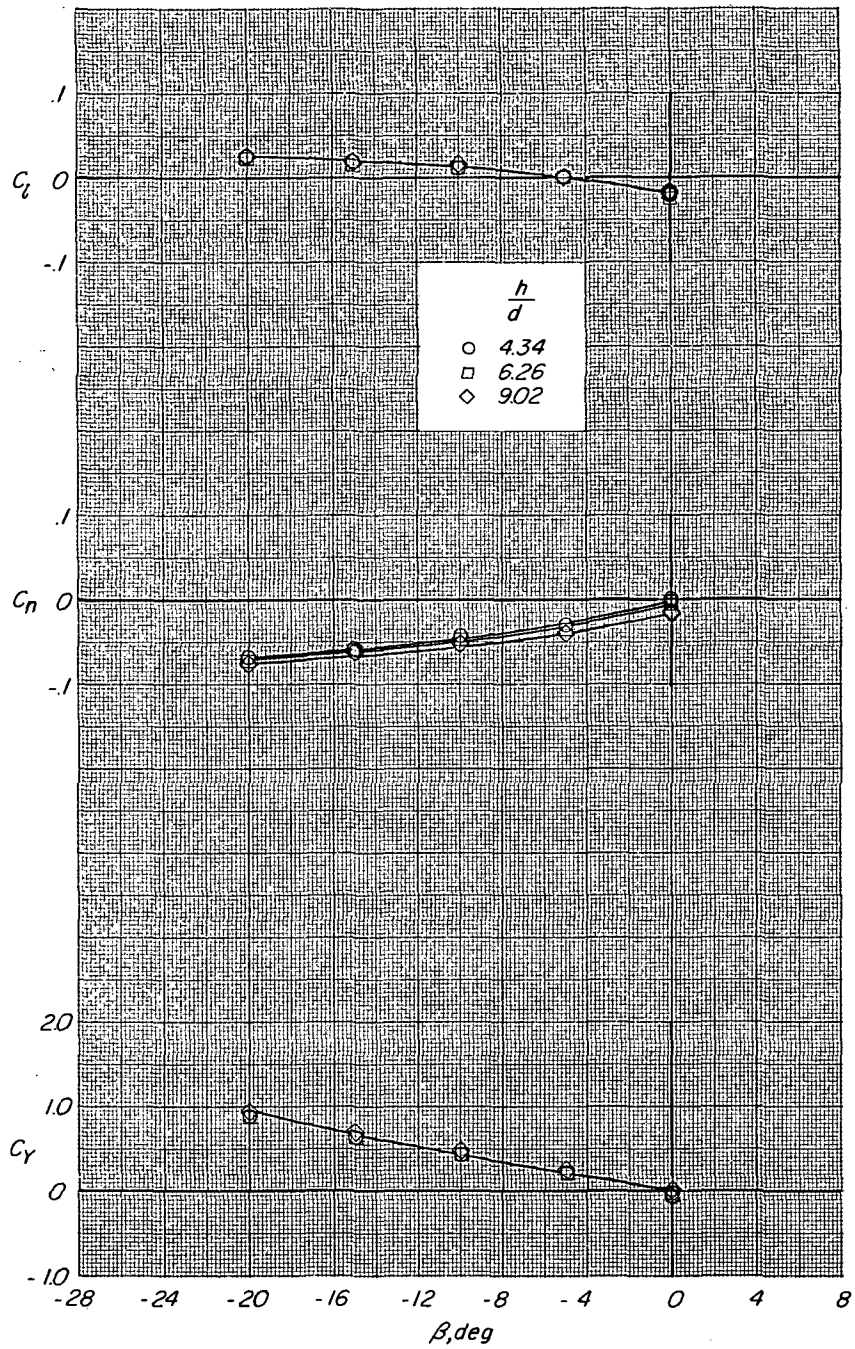

(a) Lateral-directional characteristics. $\delta_n = 10^0$.

Figure 21.- Aerodynamic characteristics in sideslip over moving ground plane. Four lift nozzles and two cruise nozzles; $\alpha = 0^0$; $C_T = 7.0$; $\delta_r = 0^0$.

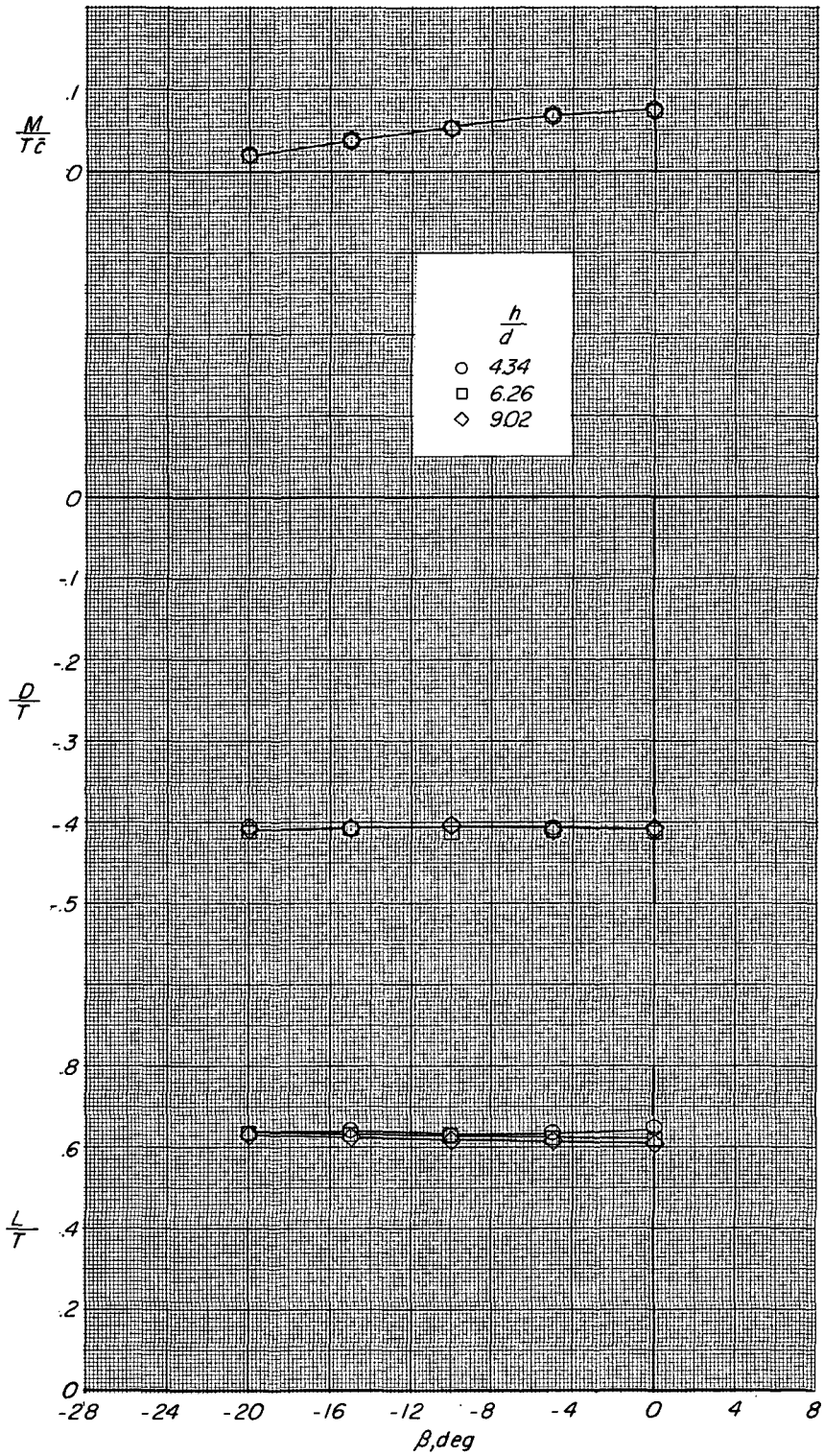

(b) Longitudinal characteristics. $\delta_n = 10^0$.

Figure 21.- Continued.

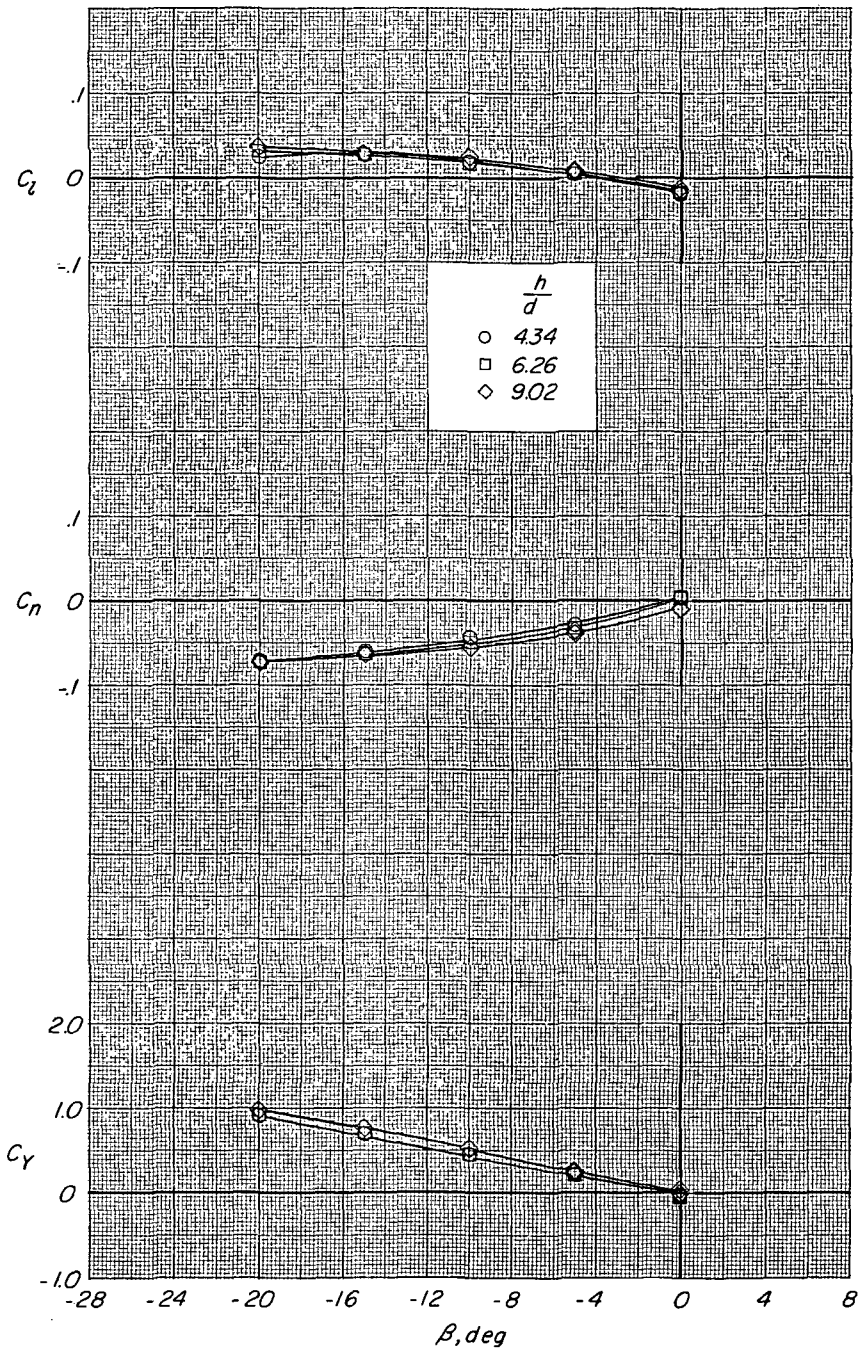

(c) Lateral-directional characteristics. $\delta_n = -10^o$.

Figure 21.- Continued.

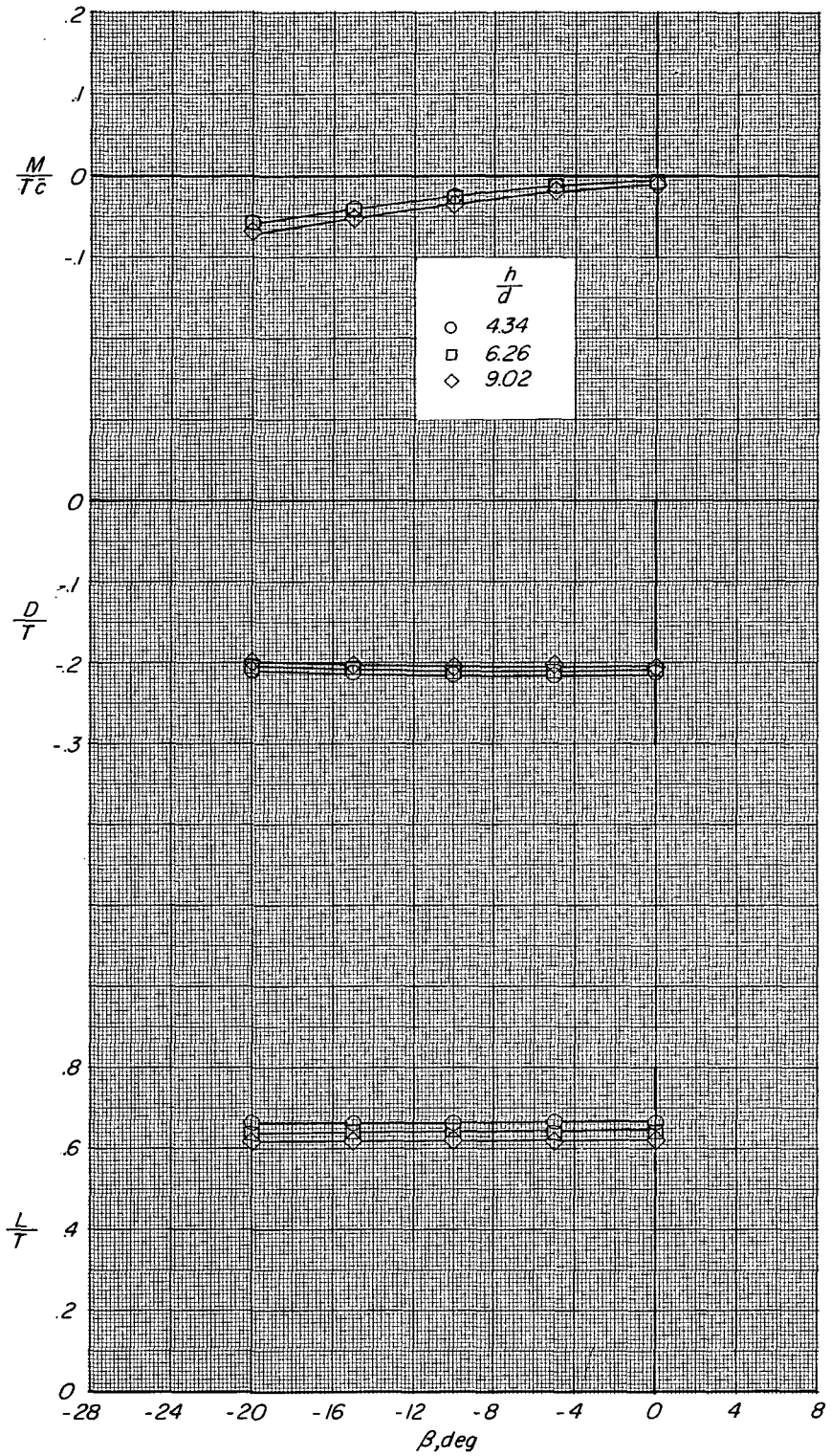

(d) Longitudinal characteristics. $\delta_n = -10^0$.

Figure 21.- Concluded.

NASA-Langley, 1969 — 1L-6368

NATIONAL AERONAUTICS AND SPACE ADMINISTRATION
WASHINGTON, D. C. 20546

OFFICIAL BUSINESS

FIRST CLASS MAIL

POSTAGE AND FEES PAI
NATIONAL AERONAUTICS
SPACE ADMINISTRATIO

POSTMASTER: If Undeliverable (Section
Postal Manual) Do Not F

"The aeronautical and space activities of the United States shall be conducted so as to contribute . . . to the expansion of human knowledge of phenomena in the atmosphere and space. The Administration shall provide for the widest practicable and appropriate dissemination of information concerning its activities and the results thereof."

—NATIONAL AERONAUTICS AND SPACE ACT OF 1958

NASA SCIENTIFIC AND TECHNICAL PUBLICATIONS

TECHNICAL REPORTS: Scientific and technical information considered important, complete, and a lasting contribution to existing knowledge.

TECHNICAL NOTES: Information less broad in scope but nevertheless of importance as a contribution to existing knowledge.

TECHNICAL MEMORANDUMS: Information receiving limited distribution because of preliminary data, security classification, or other reasons.

CONTRACTOR REPORTS: Scientific and technical information generated under a NASA contract or grant and considered an important contribution to existing knowledge.

TECHNICAL TRANSLATIONS: Information published in a foreign language considered to merit NASA distribution in English.

SPECIAL PUBLICATIONS: Information derived from or of value to NASA activities. Publications include conference proceedings, monographs, data compilations, handbooks, sourcebooks, and special bibliographies.

TECHNOLOGY UTILIZATION PUBLICATIONS: Information on technology used by NASA that may be of particular interest in commercial and other non-aerospace applications. Publications include Tech Briefs, Technology Utilization Reports and Notes, and Technology Surveys.

Details on the availability of these publications may be obtained from:

SCIENTIFIC AND TECHNICAL INFORMATION DIVISION

NATIONAL AERONAUTICS AND SPACE ADMINISTRATION

Washington, D.C. 20546